Modular Functionalization of Fluorescent Liposome Surfaces for Analytical Applications

Dissertation

zur Erlangung des Doktorgrades der Naturwissenschaften
(Dr. rer. nat.)
der Fakultät für Chemie und Pharmazie
der Universität Regensburg

vorgelegt von
Andreas Müller
aus Werneck

2015

The experimental part of this work was carried out between July 2010 and May 2014 under the supervision of Prof. Dr. Burkhard König at the Institute of Organic Chemistry, University of Regensburg.

Date of the Submission:	03.02.2015
Date of the Colloquium:	06.03.2015

Board of Examiners:	PD Dr. Sabine Amslinger	(Chair)
	Prof. Dr. Burkhard König	(1st Referee)
	Prof. Dr. Joachim Wegener	(2nd Referee)
	Prof. Dr. David Díaz Díaz	(Examiner)

Nur was wir glauben,

wissen wir gewiss.

(Wilhelm Busch)

TABLE OF CONTENTS

TABLE OF CONTENTS

CHAPTER I:

FUNCTIONALIZED VESICLES AS VERSATILE TOOLS FOR ANALYTICAL APPLICATIONS – A SHORT OVERVIEW

I.1 Functionalized Vesicles in Analytics

Liposomes and vesicles are self-assembled spherical bilayers composed of amphiphiles in aqueous solution (Figure 1.1). While the term "liposome" commonly implies membranes consisting of natural phospholipids, the term "vesicle" also comprises those supramolecular structures which are based on synthetic amphiphiles such as polymerizable diacetylenes.[1] The driving forces behind their formation are hydrophobic interactions of the unpolar alkyl chains in water. Due to their supramolecular nature and their modular construction principle, vesicles can be easily prepared and varied in their composition.

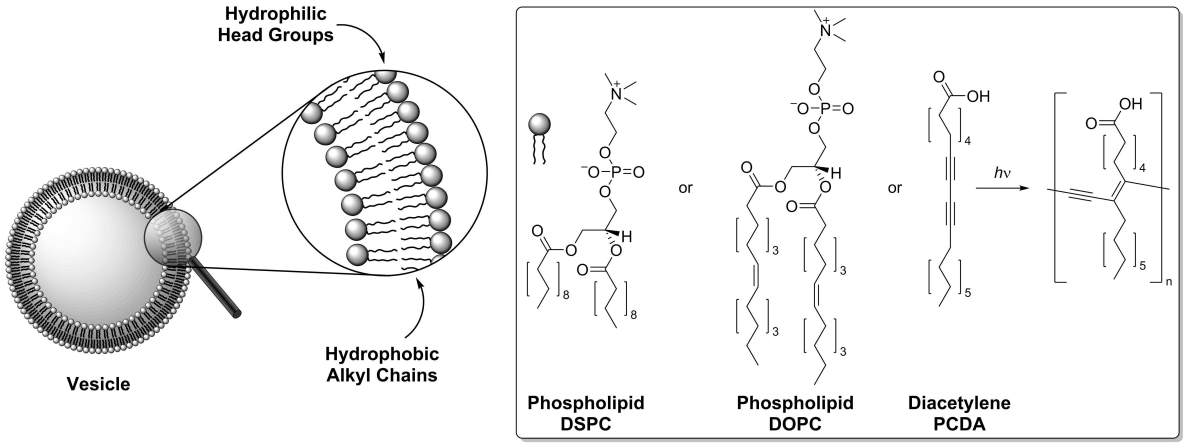

Figure 1.1: Construction principle of vesicles (left) and commonly employed membrane components (right).

The physical properties of the bilayers such as their phase behavior or the overall charge are basically determined by the structural characteristics of the utilized membrane components and thus can be optimally fine-tuned by careful choice of the individual building blocks. Moreover, vesicle membranes allow the incorporation of functional amphiphiles, which turns those self-assembled structures into capable candidates for nanomaterials with adjustable properties and functions. In this context, vesicles have gained increasing interest in the last few decades in the development of new analytical devices. Artificial liposomes can be functionalized with membrane-embedded receptors for specific binding to envisaged target molecules.[2] Remarkably, host–guest interactions at the vesicular surface can considerably benefit from the unique physico-chemical properties at the lipid–water interface.[3] Moreover, some characteristics of membranes such as their dynamicity, the two-dimensional confinement and organization of embedded amphiphiles and the formation of functional domains provide exceptional features and demarcate those systems from homogeneous solutions.

A fundamental requirement of vesicular sensors is the transformation of a microscopic binding event at the surface into an observable macroscopic signal. Numerous strategies have been established for that purpose and each of them has its particular advantages and limitations. Label-free formats rely on the readout of analyte recognition by physical methods such as surface plasmon resonance (SPR),[4] quartz crystal microbalance (QCM)[5] or atomic force microscopy (AFM).[6] However, these approaches require immobilization of the liposome bilayers on a solid support and need sophisticated and expensive technical instrumentation. Moreover, the sensitivities of these techniques are often insufficient for low molecular mass targets. Strategies based on, *e.g.*, electrochemical, colorimetric or fluorescent signals provide a more convenient sensing and can also be used for the detection of small molecules. Here, a close proximity of the recognition and the signaling units allowing the transduction of binding events is required. This can be achieved either by covalent attachment or non-covalently by taking advantage of the self-assembled nature of membranes. Some methods even allow the detection of receptor–target interactions by the naked eye. Vesicles composed of PCDA (10,12-pentacosadiyonic acid), for example, can be easily polymerized by UV light (Figure 1.1).[7] The conjugated π-electron system of the resulting polydiacetylene backbone exhibits light absorption in the visible spectral range and its color is responsive to external stimuli like binding of analytes to surface-exposed receptors. Better sensitivities are generally achieved by fluorescent methods. Our group demonstrated that a fluorescent moiety can be either covalently linked to membrane-receptors[8] or simply co-embedded into the bilayer.[9] A different signaling approach is based on competitive binding of indicator dyes and analytes. Displacement of the reporter molecules which are coordinated to membrane-embedded receptors by the targets can induce a change of their optical properties (so called indicator-displacement assay, IDA).[8,10] As vesicles enclose a large aqueous volume, they may also encapsulate reporter dyes in their interior compartment and thus provide signal amplification in heterogeneous sensing formats.[11] Among those, sandwich-hybridization or competitive assays in combination with immobilized receptors are commonly utilized.

Despite of the numerous promising developments with regard to the use of receptor-modified vesicles in analytics, the achievable complexity of artificial functionalized membranes is still rather limited.[2] Thus, we aimed to contribute to that field by investigations towards a flexible approach for the modification of vesicle membranes. The main objectives for the envisaged method were to be simple, highly modular and to allow the utilization of a broad variety of recognition units in a universal fashion.

I.2 Notes and Reference

[1] J. Voskuhl, B. J. Ravoo, "Molecular recognition of bilayer vesicles", *Chem. Soc. Rev.* **2009**, *38*, 495–505.

[2] B. Gruber, B. König, "Self-Assembled Vesicles with Functionalized Membranes", *Chem. Eur. J.* **2013**, *19*, 438–448.

[3] K. Ariga, H. Ito, J. P. Hill, H. Tsukube, "Molecular recognition: from solution science to nano/materials technology", *Chem. Soc. Rev.* **2012**, *41*, 5800–5835.

[4] a) R. J. Green, R. A. Frazier, K. M. Shakesheff, M. C. Davies, C. J. Roberts, S. J. B. Tendler, "Surface plasmon resonance analysis of dynamic biological interactions with biomaterials", *Biomaterials* **2000**, *21*, 1823–1835; b) K. Tawa, K. Morigaki, "Substrate-Supported Phospholipid Membranes Studied by Surface Plasmon Resonance and Surface Plasmon Fluorescence Spectroscopy", *Biophys. J.* **2005**, *89*, 2750–2758.

[5] M. C. Dixon, "Quartz Crystal Microbalance with Dissipation Monitoring: Enabling Real-Time Characterization of Biological Materials and Their Interactions", *J. Biomol. Tech.* **2008**, *19*, 151–158.

[6] a) E. I. Goksu, J. M. Vanegas, C. D. Blanchette, W.-C. Lin, M. L. Longo, "AFM for structure and dynamics of biomembranes", *Biochim. Biophys. Acta, Biomembr.* **2009**, *1788*, 254–266; b) K. E. Kirat, S. Morandat, Y. F. Dufrêne, "Nanoscale analysis of supported lipid bilayers using atomic force microscopy", *Biochim. Biophys. Acta, Biomembr.* **2010**, 1798, 750–765.

[7] a) S. Okada, S. Peng, W. Spevak, D. Charych, "Color and Chromism of Polydiacetylene Vesicles", *Acc. Chem. Res.* **1998**, *31*, 229–239; b) D. A. Jose, S. Stadlbauer, B. König, "Polydiacetylene-Based Colorimetric Self-Assembled Vesicular Receptors for Biological Phosphate Ion Recognition", *Chem. Eur. J.* **2009**, *15*, 7404–7412; c) D. A. Jose, B. König, "Polydiacetylene vesicles functionalized with N-heterocyclic ligands for metal cation binding", *Org. Biomol. Chem.* **2010**, *8*, 655–662.

[8] B. Gruber, S. Stadlbauer, K. Woinaroschy, B. König, "Luminescent vesicular receptors for the recognition of biologically important phosphate species", *Org. Biomol. Chem.* **2010**, *8*, 3704–3714.

[9] B. Gruber, S. Stadlbauer, A. Späth, S. Weiss, M. Kalinina, B. König, "Modular Chemosensors from Self-Assembled Vesicle Membranes with Amphiphilic Binding Sites and Reporter Dyes", *Angew. Chem. Int. Ed.* **2010**, *49*, 7125–7128; *Angew. Chem.* **2010**, *122*, 7280–7284.

[10] B. T. Nguyen, E. V. Anslyn, "Indicator–displacement assays", *Coord. Chem. Rev.* **2006**, *250*, 3118–3127.

[11] a) K. A. Edwards, A. J. Baeumner, "Liposomes in analyses", *Talanta* **2006**, *68*, 1421–1431; b) Q. Liu, B. J. Boyd, "Liposomes in biosensors", *Analyst* **2013**, *138*, 391–409.

CHAPTER II:

INVESTIGATIONS TOWARDS HYDROGEN BONDING AT VESICLE MEMBRANES

II.1 Introduction

Self-organization is one of the fundamental principles nature utilizes to create highly complex, multifaceted functional systems. The formation of supramolecular aggregates is based on the cooperative action of a multitude of weak interactions such as electrostatic attraction, hydrogen bonds, hydrophobic forces or π–π stacking.[1] A prominent example of a self-assembled biological structure is represented by the cell membrane. Its construction principle mainly relies on hydrophobic interactions of the unpolar phospholipid alkyl chains in aqueous media. Beyond that, non-covalent binding events at the surface of cells play a dominant role in biological processes such as cell adhesion or signal transduction.[2] Specific molecular recognition of the targets commonly involves hydrogen bonding to surface-exposed receptors, *e.g.*, carbohydrates or membrane proteins. The observed high selectivities originate from the pronounced directional and cooperative nature of hydrogen bonds. The binding strengths of the formed host–guest complexes are the result of a perfectly fine-tuned interplay of various synergistic parameters. Among them, not only the number of individual bonds is decisive but also the polarization of the involved hydrogen bond donor and acceptor functions and their specific sequence because of secondary attractive or repulsive interactions of adjacent binding units.[3] Additional electrostatic forces between charged entities often provide a considerable energetic contribution. As a result, the observed binding energies can cover the range between weak van der Waals interactions and covalent bonds with values from 0.5 to 40 kcal/mol.[4] Thus, hydrogen bonds can both stabilize static structures as well as mediate dynamic processes.

Importantly, not only the nature of a hydrogen bonding motif itself is crucial for the obtained binding strength of an interacting assembly but also its chemical context, *i.e.* for example, the polarity of the surroundings determined by the solvent system. Therefore, hydrogen bonding in aqueous media, as it applies for biological systems, is only possible if the entropically unfavorable loss of hydration is compensated by the enthalpy of the newly formed hydrogen bonds.[5] In spite of water molecules competing for hydrogen acceptor and donor sites through solvation, exposition of the binding partners at an interface of a hydrophobic phase to an aqueous environment can result in stable hydrogen bonding complexes due to unique physico-chemical properties in the transient region.[6] Surprisingly, the site of the molecular interaction does not necessarily have to be buried in the unpolar part of the interface. Quantum chemical modeling of host–guest binding energy profiles at

different distances from a lipid–water boundary revealed a significant impact of the low dielectric bilayer on interacting sites even positioned in the aqueous subphase.[7]

Since artificial phospholipid vesicles can be regarded as simple cell mimics,[8] investigations with functionalized vesicles might be helpful for a better knowledge of biological processes. *Vice versa*, elucidation of recognition processes at cell surfaces could expedite the development of potent analytical devices. Learning form the natural prototype, we recently accomplished the preparation of nanosized luminescent chemosensors by means of embedding of different functional amphiphiles into unilamellar liposome membranes.[9] Metal complexes were used as recognition elements, whereas fluorescent dyes served as reporter units to signal the binding of the targets to the vesicle surface. Despite of the simple and modular construction principle, a method which allows the modification of preformed, blank vesicles at the outer surface with different receptor units would provide an even higher flexibility in the preparation of novel nanoscopic sensors. Moreover, control over the two-dimensional receptor arrangement on the liposome surface is supposed to be more easily achievable by means of subsequent attachment at the phospholipid matrix. The realization of this goal is an essential requirement for the specific recognition of multivalent analytes. Therefore, our plan was to non-covalently functionalize vesicle surfaces equipped with membrane-anchored elements which can serve as universal "connectors" (Figure 2.1). The reversibility of the receptor fixation might then facilitate a dynamic structuring of their distribution by template molecules.

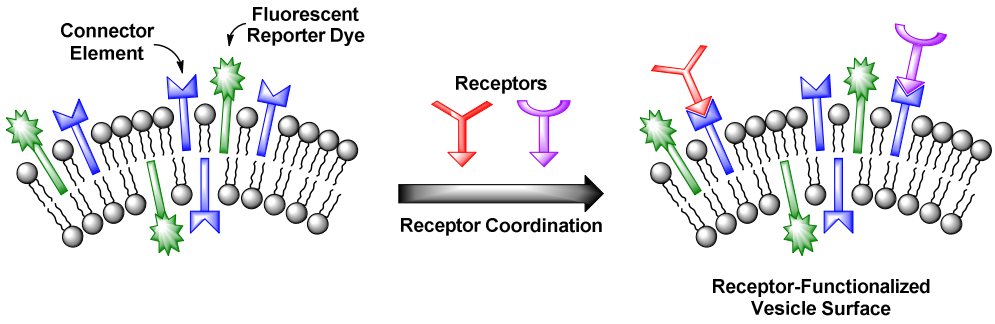

Figure 2.1: Intended approach: Receptor-functionalization of fluorescent vesicle surfaces *via* non-covalent interactions for the preparation of chemosensors.

Considering the exceptional physico-chemical properties at the vesicle–water interface, we aimed for utilizing hydrogen bonds for the post-functionalization of liposomes. Numerous studies demonstrated the feasibility of hydrogen bonding at air–water or lipid membrane–water interfaces.[6] Pioneering work in that field was achieved by Kitano and

Ringsdorf in 1985 by means of Langmuir monolayers prepared from nucleobase-containing lipids.[10] The authors observed a considerable impact on the surface pressure–area isotherms upon addition of the complementary nucleobases and attributed this to the specific formation of hydrogen bonding networks. A more direct evidence was provided by Kunitake *et al.* who evaluated the molecular recognition of aqueous thymine or thymidine by a monolayer of amphiphilic diaminotriazines at the air–water interface *via* FT-IR spectroscopy.[11] Lehn *et al.* reported on hydrogen bonding at vesicle surfaces.[12] It could be shown that mixtures of large unilamellar vesicles prepared from egg lecithin and 10 mol-% of lipids with modified head groups on basis of either barbituric acid or 2,4,6-triaminopyrimidine aggregate and even fuse. This behavior was ascribed to the formation of extended interfacial ribbon structures of the complementary, double-faced hydrogen bonding motifs. Additionally, the involvement of electrostatic interactions due to the generation of charged species by protonation / deprotonation processes was observed.

These literature reports initiated our investigations towards the utilization of hydrogen bonding with regard to non-covalent post-functionalization of vesicle surfaces. The primary aim of the presented study was to examine whether hydrogen bonding at membrane–water interfaces in general is efficient enough for the robust attachment of functional units.

II.2 Results and Discussion

II.2.1 Envisaged Hydrogen Bonding System

The use of a hydrogen bonding module based on melamine / barbituric acid was considered for the non-covalent modification of liposome surfaces due to the effortless synthetic accessibility of its single building blocks. As membrane-anchored binding motif, amphiphilic melamine **Mel-C_{18}** (Scheme 2.1) was envisaged, whereas a complementary barbiturate **RBar** can be modified at its nitrogen atom with a recognition unit of choice for particular analytical applications.

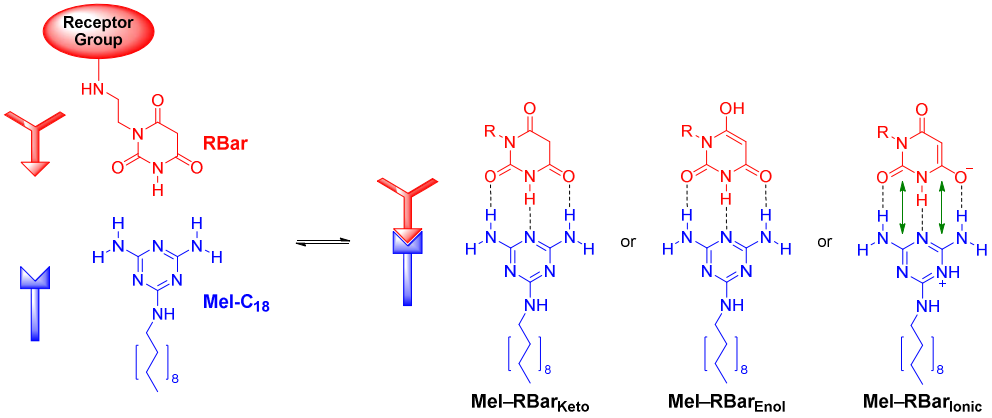

Scheme 2.1: Envisaged hydrogen bonding system for the post-functionalization of vesicles on basis of melamine and barbituric acid derivatives and possible binding modes of **Mel-C$_{18}$** with *N*-substituted barbiturates **RBar** (electrostatic interactions symbolized by double arrows).

Supposed that the aromatic structure of melamine derivative **Mel-C$_{18}$** depicted in Scheme 2.1 is the predominant tautomeric form,[13] three different binding modes for the complexation of **Mel-C$_{18}$** with *N*-substituted barbiturates **RBar** are conceivable. **RBar** can interact with receptor **Mel-C$_{18}$** either in its keto form (→ **Mel–RBar$_{Keto}$**) or in one of its enol forms (→ **Mel–RBar$_{Enol}$**). Considering the acidic properties of barbiturates, also a proton transfer from **RBar** to the weakly basic melamine **Mel-C$_{18}$** might be possible followed by complexation of the two generated ions (→ **Mel–RBar$_{Ionic}$**). The two neutral complexes **Mel–RBar$_{Keto}$** and **Mel–RBar$_{Enol}$** are assumed to possess similar affinity constants, whereas the zwitterionic aggregate **Mel–RBar$_{Ionic}$** is expected to gain a significant additional stabilization from the mutual electrostatic interactions.

II.2.2 Determination of the Binding Mode of Mel-C$_{18}$ with an *N*-Substituted Barbiturate in Organic Solution by ^{1}H-NMR Investigations

Our preliminary intension was to find out if electrostatic interactions caused by a proton transfer could be involved in the envisaged melamine–barbiturate system. The generation of charged species is observed, *e.g.*, for related diaminopyridine–barbiturate complexes in dichloromethane.[14] Thus, we first investigated the binding mode by ^{1}H-NMR measurements in organic medium. The amphiphilic melamine **Mel-C$_{18}$** was synthesized as described in the Experimental Part. For solubility reasons, we employed the 5-phenyl substituted barbiturate **BuPhBar** (see Scheme S2.2 in Experimental Part) as binding partner. Mixtures of **BuPhBar** with increasing amounts of **Mel-C$_{18}$** in $CDCl_3$ showed a significant downfield shift and broadening of the NH signal of **BuPhBar** as well as a downfield shift of

the amine protons of **Mel-C_{18}** compared to its uncomplexed form (see Figure S2.1 in Experimental Part). Moreover, a concentration dependency of the chemical shifts of the two-component system was found (see Figure S2.2). These observations indicate the participation of the respective protons in hydrogen bonding interactions. A gradual broadening and disappearance of the acidic CH function of the barbiturate moiety suggests a shift of the tautomeric equilibrium of **BuPhBar** towards the enol form. The steadiness of the signal changes, both in presence of substoichiometric and of excess amounts of **Mel-C_{18}**, and a downfield shift of the phenyl hydrogen atoms of **BuPhBar** do not hint at the occurrence of a proton transfer between the two species. Altogether, these observations show that a neutral complex according to the structure of **Mel–RBar$_{Enol}$** (Scheme 2.1) was formed under the applied conditions.

II.2.3 Investigation of Hydrogen Bonding Interactions of Mel-C_{18} with Barbiturates in Homogeneous Solutions by UV/Vis Titrations

As NMR techniques are less convenient for the investigation of hydrogen bonding at vesicle surfaces, we aimed to utilize an optical method for that purpose. Spange *et al.* developed the solvatochromic barbiturate **NiPhBar** (Scheme 2.2), whose absorption maximum in different solvents ranges from about 380 to 470 nm.[14] Several parameters influence the chromophoric properties of this dye. First, the equilibrium position of the different tautomers affects the intensity of light absorption. While the keto form is colorless, the two enol tautomers exhibit a yellow color due to the resulting electron donating ability of their barbiturate moiety which generates an electronic push–pull system along with the nitrophenyl group. The position of this tautomeric equilibrium is highly dependent on interactions with the solvent or with hydrogen bonding partners. Second, the electron donating strength of the enol forms and thus, the position of their absorption maximum is influenced by polarization of the barbiturate moiety through solvation or complexation. These characteristics make this dye a suitable tool for the investigation of hydrogen bonding interactions with suitable complementary partners. Studies demonstrated its ability to specifically discriminate between different pyridine derivatives and nucleobases. Due to the alkyl substituent at the nitrogen atom of **NiPhBar**, the scope of possible interactions is limited to targets with DAA and DAD motifs respectively (A = hydrogen bond acceptor and D = hydrogen bond donor).

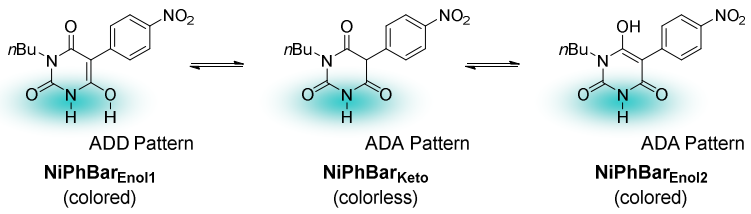

Scheme 2.2: Solvatochromic dye **NiPhBar** for the investigation of hydrogen bonding interactions and its keto–enol equilibrium.[14]

Before applying this dye for investigations on vesicular membranes, initial studies were performed in homogeneous solutions with increasing polarity in order to determine its optical response upon binding to **Mel-C$_{18}$**. UV/Vis titration measurements of **NiPhBar** with amphiphilic melamine **Mel-C$_{18}$** confirmed the conclusions drawn by the ^{1}H-NMR experiments in $CDCl_3$ described above. While pure **NiPhBar** in CH_2Cl_2 exists in the colorless keto form solely, its tautomeric equilibrium is shifted towards the yellow enol2 form by complexation with **Mel-C$_{18}$**. This behavior can be monitored by a strong increase of the dye's absorption maximum at 410 nm upon titration of 0–128 equivalents of melamine **Mel-C$_{18}$** (Figure 2.2). A binding affinity of lg $K_a \approx 3.4$ was obtained by non-linear curve fitting.

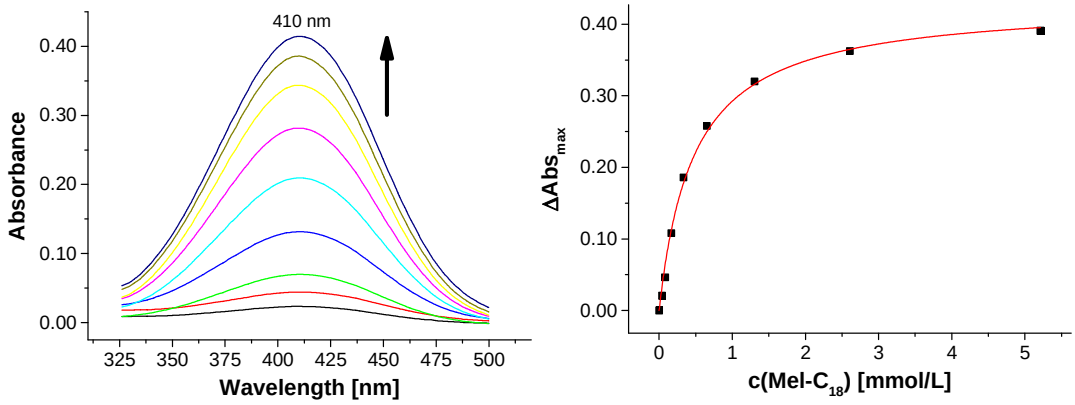

Figure 2.2: UV/Vis titration of barbiturate **NiPhBar** (41 μM) with melamine **Mel-C$_{18}$** (0–128 equivalents) in CH_2Cl_2.

A similar result was obtained in presence of small amounts of hydrogen bonding competitor MeOH (0.4 vol-%). Here, the enol tautomers of **NiPhBar** are slightly stabilized compared to a solution of **NiPhBar** in pure CH_2Cl_2 indicated by a small increase of the initial absorption maximum in Figure 2.3. Upon addition of an excess of **Mel-C$_{18}$**, the solvating MeOH molecules are gradually displaced by the melamine units resulting in a further increase of the absorption signal (Figure 2.3). The obtained binding affinity of lg $K_a \approx 3.3$ is not significantly lowered compared to that in the previous case by the small methanol content.

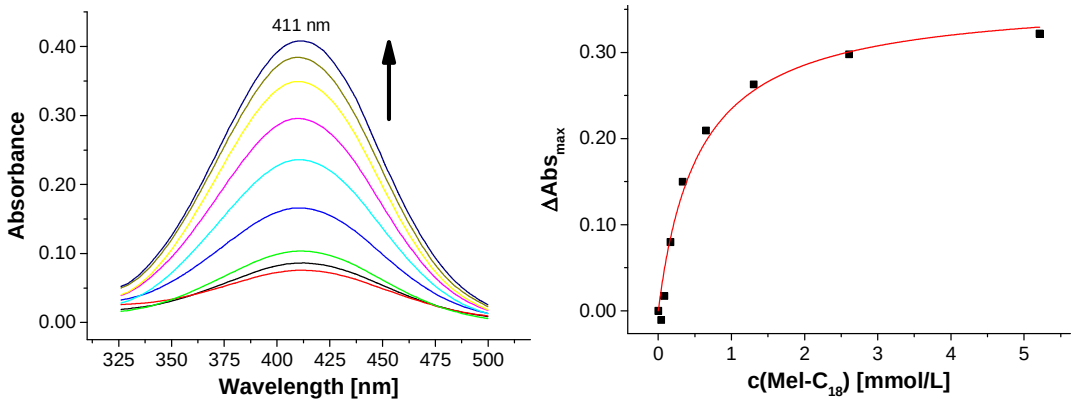

Figure 2.3: UV/Vis titration of barbiturate **NiPhBar** (41 μM) with melamine **Mel-C_{18}** (0–128 equivalents) in a solvent mixture of CH_2Cl_2 and 0.4 vol-% of MeOH.

On addition of a larger amount of MeOH (3.9 vol-%), already the uncomplexed dye **NiPhBar** features a high absorbance indicating the preference of its enol forms under those conditions (Figure 2.4). Noteworthy, the wavelength of the absorption maximum in this case exhibits a small bathochromic shift to 418 nm compared to that of the previous two titration series in less polar media (410 nm, Figures 2.2 and 2.3). This observation demonstrates the solvatochromic properties of the barbiturate dye and its sensitivity towards polarity changes in its environment. Displacement of the solvating methanol molecules by the complementary hydrogen bonding melamine is expected to affect the equilibrium of the **NiPhBar** tautomers as well as the polarization of the barbiturate group determining the position of the absorption maximum. However, upon addition of an excess of melamine **Mel-C_{18}**, neither a change of the absorption intensity nor a significant shift of the wavelength was observed (Figure 2.4). This shows that under the more polar conditions defined by the methanol content of 3.9 vol-%, hydrogen bonding between **Mel-C_{18}** and **NiPhBar** is presumably not occurring. Apparently, the enthalpy gain upon hydrogen bonding cannot compensate the loss of solvation energy of both binding partners in this case.

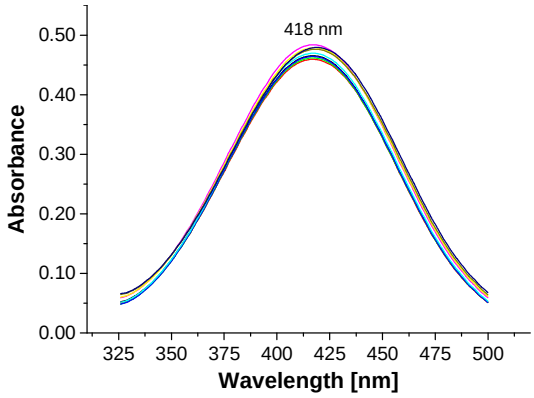

Figure 2.4: UV/Vis titration of barbiturate **NiPhBar** (41 μM) with melamine **Mel-C_{18}** (0–128 equivalents) in a solvent mixture of CH_2Cl_2 and 3.9 vol-% of MeOH.

II.2.4 Examination of Hydrogen Bonding on Vesicle Surfaces by UV/Vis Spectroscopy

It is supposed that the established buffer conditions for vesicle preparation (pH = 7.4) result in a partial deprotonation of the barbiturate moiety (pK_a of **NiPhBar** in bulk water: 1.9).[14] Due to the relatively weak basicity of melamine (pK_a of protonated melamine in bulk water: 5.0),[15] its protonation, however, is unfavored at that pH. Therefore, mutual electrostatic interactions between the two species, which would provide an additional stabilization of the hydrogen bonding complexes, are unlikely to occur in homogeneous aqueous solution. As exposure at vesicle surfaces might induce a shift of the respective pK_a values, no conclusions on the situation at the phospholipid–water interface can be drawn, though. For that reason, we next investigated if stable complex formation of **NiPhBar** with **Mel-C_{18}** is possible at vesicular surfaces. In case of hydrogen bonding taking place on the liposome membrane, a shift of the absorption maximum of the solvatochromic dye is expected due to the changed local polarity in that transient region.

We prepared small unilamellar DSPC vesicles with membrane-embedded **Mel-C_{18}** (9.0 mol-%) in HEPES buffer (25 mM, pH = 7.4) according to our established method.[9] However, on titration of the melamine-modified DSPC vesicles (0–3.2 equivalents of **Mel-C_{18}**) to barbiturate **NiPhBar**, no optical response – neither a shift of the wavelength nor a change of the absorption intensity – was observed *via* UV/Vis spectroscopy (Figure 2.5). That makes interactions of **NiPhBar** with **Mel-C_{18}** on the vesicle surface by hydrogen bonding seem improbable.

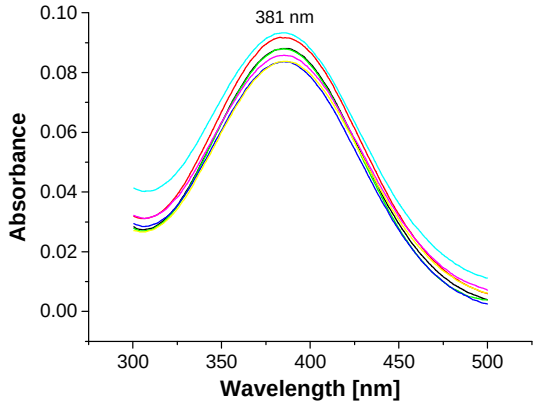

Figure 2.5: UV/Vis titration of solvatochromic barbiturate **NiPhBar** (20 μM) with vesicles containing membrane-embedded melamine **Mel-C_{18}** (0–3.2 equivalents) in aqueous HEPES buffer solution.

This finding was confirmed by size-exclusion chromatography (SEC) of the obtained mixture of vesicles and **NiPhBar**. After running the liposome dispersion through the separation gel, only the presence of the amphiphilic melamine **Mel-C_{18}** was detected by UV/Vis spectroscopy in the vesicle-containing eluate. This proves indeed its incorporation into the vesicle membrane; however, the absence of the signal of **NiPhBar** shows that the barbiturate was not robustly bound to the surface (see Figure S2.3 in Experimental Part). Consequently, the described experiments reveal that exposure of **Mel-C_{18}** at vesicle membranes is unlikely to result in the formation of stable complexes with barbiturates despite of literature reports on hydrogen bonding of melamine to barbituric acid derivatives at air–water boundaries.[16]

As an explanation, we assume a strong dependency of the type of interface on the strength of hydrogen bonding interactions. It is well documented that there is not only a considerable difference between the molecular level and interfaces in general concerning the modification of the physico-chemical properties of the aqueous subphase. In fact, also mesoscopic interfaces (such as of micelles or liposomes) differ substantially from macroscopic ones (*e.g.*, highly organized air–water systems) in this regard. This was shown by experimental investigations with a recognition motif for phosphates based on guanidinium.[17] While the respective binding constant in homogeneous solution is known to be as low as 1.4 M^{-1},[18] it is indeed enhanced to 10^2–10^4 M^{-1} at micelles and vesicular bilayers, but exhibits a remarkable increase at the air–water interface with affinity constants of 10^6–10^7 M^{-1}. Theoretical calculations suggest the importance of the size of the interface and its molecular smoothness with respect to the efficiency of molecular interactions.[19] As recognition processes can also benefit from electrostatic attraction of charged species,

modulation of the acido-basic properties of the involved binding partners is an important factor not to be ignored. In this context, studies revealed enormous differences in the impact of air–water interfaces on the pK_a shift of an embedded lysine derivative (4–5 units) compared to that of vesicle membranes (about 1 unit).[20] Moreover, a significant influence of the membrane curvature of small and large unilamellar vesicles on the pK_a values of phosphates was observed.[21] One has to conclude that there is without a doubt a remarkable qualitative difference between vesicle surfaces and air–water interfaces, which might explain the varying effectiveness of hydrogen bonding in those systems. However, their unusual physico-chemical properties in general are not fully understood yet and still remain under discussion.[22]

II.2.5 Multisite Recognition of Hexanucleotides on Vesicle Surfaces

One of the fundamental strategies nature applies to obtain high binding affinities in aqueous media is the utilization of multisite interactions. This can be observed, for example, in the base pairing of polynucleotides resulting in stable DNA double helices. Hydrogen bonding of nucleobases is not necessarily limited to interactions among each other, but can also involve artificial receptors with complementary binding patterns. Therefore, amphiphilic melamine **Mel-C$_{18}$** is supposed to be able to specifically discriminate between thymines and guanines (Figure 2.6) due to their ADA *versus* DDA motifs. In order to investigate if stable hydrogen bonding on vesicle surfaces can be achieved by means of multipoint interactions, we utilized a model system consisting of membrane-embedded **Mel-C$_{18}$** and thymidine hexanucleotide **TTTTTT**.

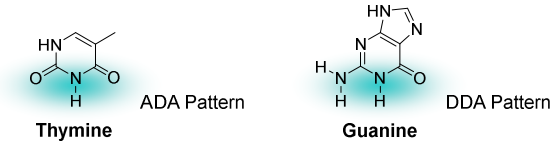

Figure 2.6: Nucleobases thymine and guanine.

An important requirement for the interaction of multivalent targets with multiple binding sites is the complementarity of the receptor entity. That means, the arrangement of the single recognition units must represent a more or less perfect imprint of the target molecule. Due to the two-dimensional confinement of embedded functional amphiphiles, phospholipid membranes provide an ideal scaffold for that purpose (Figure 2.7).[23]

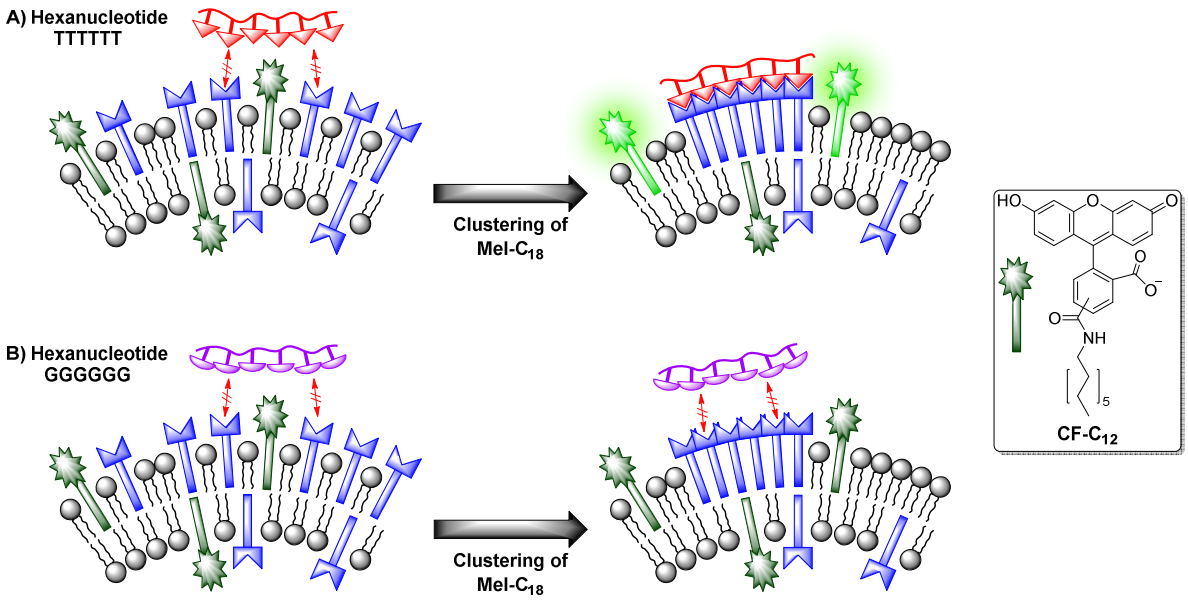

Figure 2.7: Top: Multisite binding of **TTTTTT** to membrane-embedded clusters of **Mel-C_{18}**. Bottom: Incompatibility of clustered and non-clustered **Mel-C_{18}** arrays for binding to **GGGGGG**. Right: Structure of the amphiphilic reporter dye **CF-C_{12}**.

The primary object of our research was to find out how the organization of the membrane receptors can be influenced in a way to allow multisite interactions. Previous studies in our group revealed that bivalent analyte binding can be induced by a dynamic assembly of membrane-embedded recognition units in fluid vesicle membranes.[24] As a result, an increase of the macroscopic binding constant by three orders of magnitude was achieved. Thus, we aimed to investigate whether this approach of dynamic receptor recruitment by cooperative interactions can also be applied for the hexavalent target **TTTTTT**, whose single thymine units exhibit only very low monovalent affinities to the membrane-embedded melamines in water. Due to the structural relationship of barbiturates and thymines, we also assume a similarity of their binding constants to melamines.

We prepared vesicles from the phospholipids DOPC and DSPC respectively and incorporated **Mel-C_{18}** (1.0 mol-%). The amphiphilic carboxyfluorescein **CF-C_{12}** (Figure 2.7, 5.0 mol-%) was co-embedded as reporter dye to signal the binding events at the surface in analogy to our previous investigations on vesicular chemosensors.[9] The two employed phospholipids are characterized by different aggregate states of their membranes at room temperature. While DOPC exhibits a phase transition temperature of –17 °C[25] providing a fluid-like liquid crystalline phase of the vesicle membrane, DSPC bilayers are in solid-like gel phase due to their phase transition temperature of 54 °C,[26] which prevents the lateral mobility of the embedded functional amphiphiles. Along with the statistical movement of the

melamines in a fluid membrane, the thymidine hexamer **TTTTTT** might be able to induce a clustering of **Mel-C_{18}** by cooperative binding with up to six units. The presence of the highly negatively charged oligonucleotide backbone at the vesicle surface and the altered lateral organization is supposed to affect a change of the fluorescent properties of the likewise negatively charged, membrane-embedded **CF-C_{12}** dyes.

Addition of **TTTTTT** to both vesicle solutions, however, did not reveal any changes of the fluorescence signal and no differences between DOPC and the DSPC membranes in their binding behavior were observed (Figure 2.8). As an explanation, we think that because of the very low monovalent binding constants of melamines to thymines at the aqueous interface, diffusion of the target from a membrane-embedded **Mel-C_{18}** molecule might be considerably faster than interaction with a second hydrogen bonding unit which comes into close proximity due to dynamic processes in the membrane. Thus, a threshold of the monovalent binding constants seems to exist for the multivalent target-induced dynamic assembly of receptors and underneath, recruitment of the recognition units is not possible.

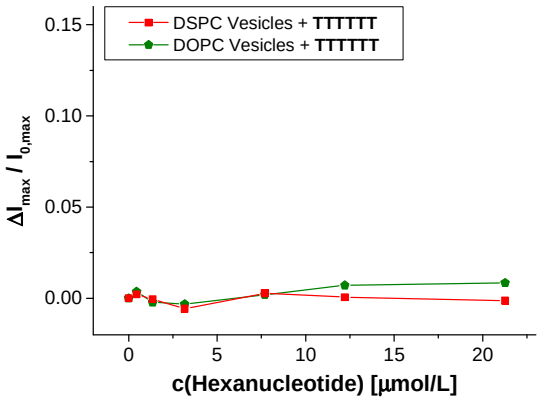

Figure 2.8: Fluorescence responses upon titration of the hexanucleotide **TTTTTT** to DSPC or DOPC vesicles modified with 1.0 mol-% of **Mel-C_{18}**.

Next, we prepared luminescent DOPC and DSPC vesicles with a tenfold higher concentration of embedded **Mel-C_{18}** (10 mol-%) and added again the hexanucleotide **TTTTTT**. Here, in contrast to the previous experiments, a significant difference between the two phospholipid membranes was observed: While DOPC vesicles did not show a fluorescence response of the embedded carboxyfluorescein **CF-C_{12}** (Figure 2.9, green pentagons), the DSPC vesicles exhibited a significant increase of the emission signal (Figure 2.9, red squares).

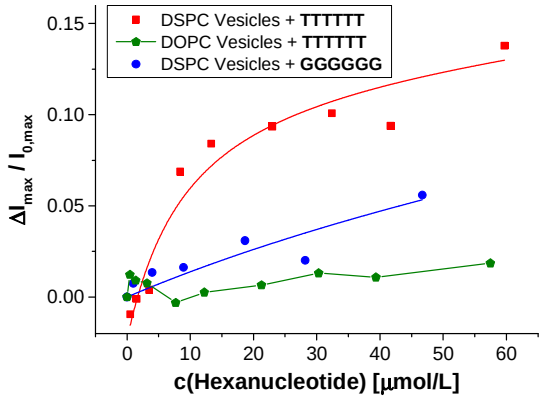

Figure 2.9: Fluorescence responses upon titration of the hexanucleotides **TTTTTT** or **GGGGGG** to DSPC or DOPC vesicles modified with 10 mol-% of **Mel-C$_{18}$**.

These findings can be explained by phase separation processes in the gel phase DSPC membranes due to packing considerations. While small concentrations (1.0 mol-%) of the embedded amphiphilic molecules result in a virtually statistical distribution and thus in a dilution of the melamines in the membrane, higher concentrations of incorporated amphiphiles (10 mol-%) probably lead to the formation of **Mel-C$_{18}$** domains. In these surface-exposed clusters, the melamine units are already preorganized for multivalent binding with the hexanucleotide **TTTTTT**. An apparent affinity constant of lg $K_a \approx 5.1$ was estimated by non-linear curve fitting. This result qualitatively confirms our previous studies on bivalent peptide binding on functionalized DSPC vesicles with a relatively high receptor content (10 mol-%).[24] Due to the fluidity of DOPC membranes at room temperature, the cluster formation is much less pronounced in that case, *i.e.*, the density of the embedded melamines in the membrane is only low.[27] Therefore, the formation of multisite complexes is unfavored.

A control experiment with the guanosine hexanucleotide **GGGGGG**, which possesses a mismatched hydrogen bonding pattern, with the modified DSPC vesicles showed a significantly lower response of the reporter dyes (Figure 2.9, blue dots). Thus, the higher observed fluorescence response in case of **TTTTTT** addition must be attributed to specific binding of its ADA hydrogen bonding units to membrane-embedded arrays of **Mel-C$_{18}$**. These results are in accordance with literature reports on hydrogen bonding-mediated vesicle aggregation of cyanuric acid- / melamine-functionalized vesicles.[27] It was demonstrated that in gel phase membranes prepared from DPPC, 20 mol-% of hydrogen bonding functions were sufficient to induce aggregation. Fluid membrane vesicles composed of egg phosphatidylcholine, however, required about 70 mol-% of embedded recognition units.[28] At significantly lower amounts, no aggregation was observed. Further investigations revealed

that forcing three hydrogen bonding groups into close proximity by covalent attachment at a single lipid molecule facilitates the recognition-based aggregation even at concentrations of 0.1–5.0 mol-% in fluid phospholipid membranes. According to the reported studies, rather the surface density of the recognition units is decisive than their lateral mobility for multisite hydrogen bonding on vesicle membranes. That means in turn that binding affinities can be easily adjusted by variation of the receptor concentration in the membrane. This principle is also found in nature where cells fine-tune biological responses dependent on the size of receptor–ligand clusters.[23a]

II.3 Conclusion

Our investigation revealed that the supposed unique physico-chemical properties at lipid–water interfaces on their own are not sufficient to result in stable monovalent melamine–barbiturate complexes at vesicle surfaces in aqueous solution. That means, 1:1 hydrogen bonding on liposome membranes is too inefficient to be utilized for the intended attachment of receptors. Furthermore, we found out that a proposed dynamic assembly of amphiphilic melamines embedded into fluid DOPC membranes cannot be induced by multivalent binding to thymidine hexamers. This is assumedly due to the very low binding affinity of a single melamine–thymine pair in water. However, it was shown that by the receptor concentrating effect of gel phase phospholipid bilayers, hydrogen bonding to multivalent targets can be achieved. Concentration-dependent phase separation processes in DSPC membranes are supposed to yield densely packed clusters of the embedded **Mel-C_{18}** amphiphiles. These preorganized arrays of recognition units allow multisite binding to the thymidine hexanucleotide **TTTTTT** with an apparent affinity constant of lg $K_a \approx 5.1$. For robust post-functionalization of vesicles with receptors, however, the observed complex stability might still be too low. As a possible solution, utilization of stronger binding modules which rely on more than three hydrogen bond donor–acceptor interactions and the combination of hydrogen bonding with electrostatic attraction could be envisaged. Based on these considerations, Schmuck *et al.* developed a zwitterionic hydrogen bonding motif containing six hydrogen bonds with estimated dimerization constants of around 10^{10} M^{-1} in DMSO and surprisingly high 170 M^{-1} in aqueous solution.[29] This example shows that by careful design of the binding units, stable monovalent hydrogen bonding complexes can in general be obtained even in water.

II.4 Experimental Part

II.4.1 General Methods and Material

General

Commercially available solvents of standard quality were used. Starting materials were purchased from either Acros or Sigma-Aldrich and used without any further purification. Phospholipids were obtained from Avanti Polar Lipids Inc. The hexanucleotides were synthesized by Jena Bioscience GmbH.

Thin layer chromatography (TLC) analyses were performed on pre-coated silica gel 60 F-254 with a 0.2 mm layer thickness (Pre-coated TLC-sheets ALUGRAM Xtra SIL G/UV_{254} from Macherey-Nagel). The detection was realized *via* UV light at 254 or 366 nm or by staining with $KMnO_4$. Flash column chromatography was performed on silica gel 60 (70–230 mesh) from Macherey-Nagel.

Melting Points

Melting points were determined on a Stanford Research Systems OptiMelt MPA100 with a heating rate of 2 °C/min.

NMR Spectra

For NMR spectroscopy, a Bruker Avance 300 (^{1}H: 300.1 MHz, ^{13}C: 75.5 MHz, T = 293 K) was used. All chemical shifts are reported in δ [ppm] (multiplicity, coupling constant *J*, number of protons, assignment) relative to the solvent residual peak as the internal standard ($CDCl_3$: ^{1}H: δ = 7.26 ppm, ^{13}C: δ = 77.16 ppm). The coupling constants are given in Hertz [Hz]. Abbreviations used for signal multiplicity: ^{1}H-NMR: s = singlet, d = doublet, t = triplet, q = quartet, m = multiplet, br = broad.

Mass Spectra

Mass spectra were measured on a ThermoQuest Finnigan TSQ 7000 mass spectrometer.

UV/Vis Measurements

Absorption spectroscopy was performed on a Varian Cary 50 Bio UV-visible spectrophotometer with temperature control using 10 × 10 mm Hellma quartz cuvettes at 21 °C.

Fluorescence Measurements

Fluorescence spectroscopy was carried out on a Varian Cary Eclipse fluorescence spectrophotometer with temperature control using 10 × 10 mm Hellma quartz cuvettes at 21 °C. Vesicles with embedded **CF-C$_{12}$** were excited at 495 nm. For better comparability of the different measurements, the relative fluorescence changes (ΔI_{max} / $I_{0,max}$) were calculated.

II.4.2 Synthesis

II.4.2.1 General Remarks

The amphiphilic carboxyfluorescein **CF-C$_{12}$**,[9] barbituric acid derivatives **BuPhBar**[30] and **NiPhBar**[30] were prepared according to previously reported procedures, the synthesis of **Mel-C$_{18}$** is described below.

II.4.2.2 Synthesis of N^2*-Octadecyl-1,3,5-triazine-2,4,6-triamine (**Mel-C$_{18}$**)*

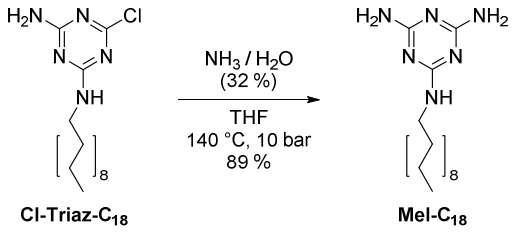

Scheme S2.1: Synthesis of amphiphilic melamine **Mel-C$_{18}$**.

Chlorotriazine **Cl-Triaz-C$_{18}$**[31] (142 mg, 0.36 mmol, 1.00 eq) was dissolved in THF (3.0 mL) and an aqueous solution of NH_3 (32 %, 4.35 mL, 72.0 mmol, 200 eq) was added. After stirring the reaction mixture for 5 h at 140 °C in an autoclave at 10 bar, the obtained white suspension was concentrated under reduced pressure. The resulting white residue was dissolved in CH_2Cl_2 (20 mL). Subsequently, the organic solution was washed with H_2O (10 mL) and brine (10 mL) and dried over Na_2SO_4. Evaporation of the solvent yielded the crude product as a white solid, which was subjected to column chromatography (SiO_2, MeOH/CH_2Cl_2 2:98 → 10:90) to give pure melamine **Mel-C$_{18}$** (121 mg, 0.32 mmol, 89 %).

R_f = 0.17 (MeOH/CH_2Cl_2 1:9). — MP: 96–97 °C. — ^{1}H-NMR ($CDCl_3$, 300 MHz): δ = 0.88

(t, J = 6.7 Hz, 3H, Me), 1.20–1.40 (m, 30H, $(CH_2)_{15}$), 1.53 (pseudo quint, J = 7.0 Hz, 2H, $NHCH_2CH_2$), 3.28–3.43 (m, 2H, $NHCH_2$), 4.60–4.90 (br m, 5H, 2 × NH_2, NH). — ^{13}C-NMR ($CDCl_3$, 75 MHz): δ = 14.28 (Me, octadecyl), 22.84 (CH_2, octadecyl), 27.02 (CH_2, octadecyl), 29.50 (CH_2, octadecyl), 29.51 (CH_2, octadecyl), 29.73 (CH_2, octadecyl), 29.81 (CH_2, octadecyl), 29.85 (br, CH_2, octadecyl), 32.08 (CH_2, octadecyl), 40.82 ($NHCH_2$, octadecyl), quaternary carbons were not detected. — MS (ESI^+): *m/z* (%) = 379.2 (100) $[M + H^+]^+$, 420.2 (38) $[M + H^+ + MeCN]^+$.

II.4.3 Preparation of Mel-C_{18}-Modified Vesicles

The melamine-modified vesicles were prepared analogously to formerly established protocols.[9] In a small glass vessel, stock solutions of the phospholipids DSPC or DOPC (2.00 mM in $CHCl_3$), **Mel-C_{18}** (1.00 mM in $CHCl_3$) and amphiphilic fluorophore **CF-C_{12}** (1.00 mM in $CHCl_3$) if luminescent vesicles required were mixed in appropriate volumes to yield the desired molar ratios of the membrane components (2.00–2.20 μmol in total). The organic solvent was removed at 75 °C and the remaining film of amphiphiles was dried in high vacuum. Aqueous HEPES buffer solution (25 mM, pH 7.4, 1.00 mL) was added to obtain a total amphiphile concentration of 2.00–2.20 mM. The sample was shaken for 15 min at room temperature (21 °C) in case of DOPC and at 75 °C for DSPC respectively resulting in a slightly turbid multilamellar vesicle suspension. A dispersion of unilamellar vesicles was obtained by extrusion through 100 nm pore size polycarbonate membranes with a LiposoFast liposome extruder from Avestin at room temperature or at 75 °C dependent on the phospholipid.

II.4.4 Determination of Binding Constants

On basis of the law of mass action and the assumption of a linear relationship between the concentration of the formed host–guest complex and the change of the UV/Vis absorption intensity or the fluorescence signal ΔI_{max}, the apparent affinity constants K_a were obtained by non-linear curve fitting according to the following expression:[32]

$$\Delta I_{max} = \varepsilon \frac{[A]_0 + [R]_0 + 1/K_a - \sqrt{([A]_0 + [R]_0 + 1/K_a)^2 - 4[A]_0[R]_0}}{2}$$

where $[A]_0$: total concentration of guest compound

$[R]_0$: total concentration of host compound

II.4.5 ^{1}H-NMR Binding Studies of Mel-C_{18} with BuPhBar

The ^{1}H-NMR investigations were performed in $CDCl_3$ as solvent. Stock solutions of **BuPhBar** (Scheme S2.2) and **Mel-C_{18}** in $CDCl_3$ were mixed together in different ratios and filled up with $CDCl_3$ to yield a total volume of 800 µL. The concentration of **BuPhBar** was kept constant at 3.80 mM, while that of **Mel-C_{18}** corresponded to 0–2.4 equivalents. Subsequently, the respective ^{1}H-NMR spectra (300 MHz) were measured (Figure S2.1). For a dilution experiment, the volume of a 1.0:0.5 mixture of **BuPhBar** and **Mel-C_{18}** was doubled by addition of $CDCl_3$ and the ^{1}H-NMR spectra before and after dilution were measured (Figure S2.2).

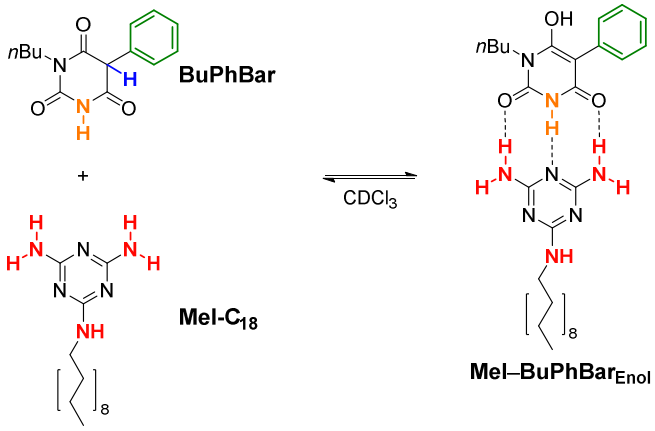

Scheme S2.2: Hydrogen bonding system employed for ^{1}H-NMR investigations. The color code refers to the signal assignments shown in Figure S2.1.

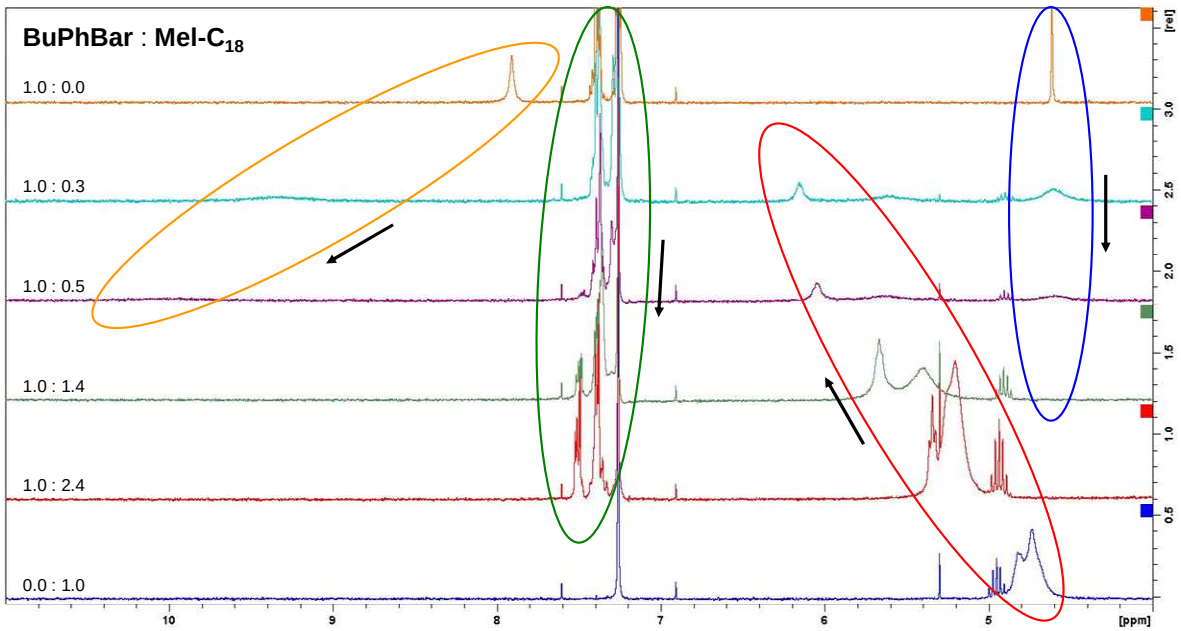

Figure S2.1: ^{1}H-NMR measurements of mixtures of **BuPhBar** and **Mel-C$_{18}$** in different ratios in $CDCl_3$; c(**BuPhBar**) = 3.80 mM. For the assignment of the protons, see the color code in Scheme S2.2.

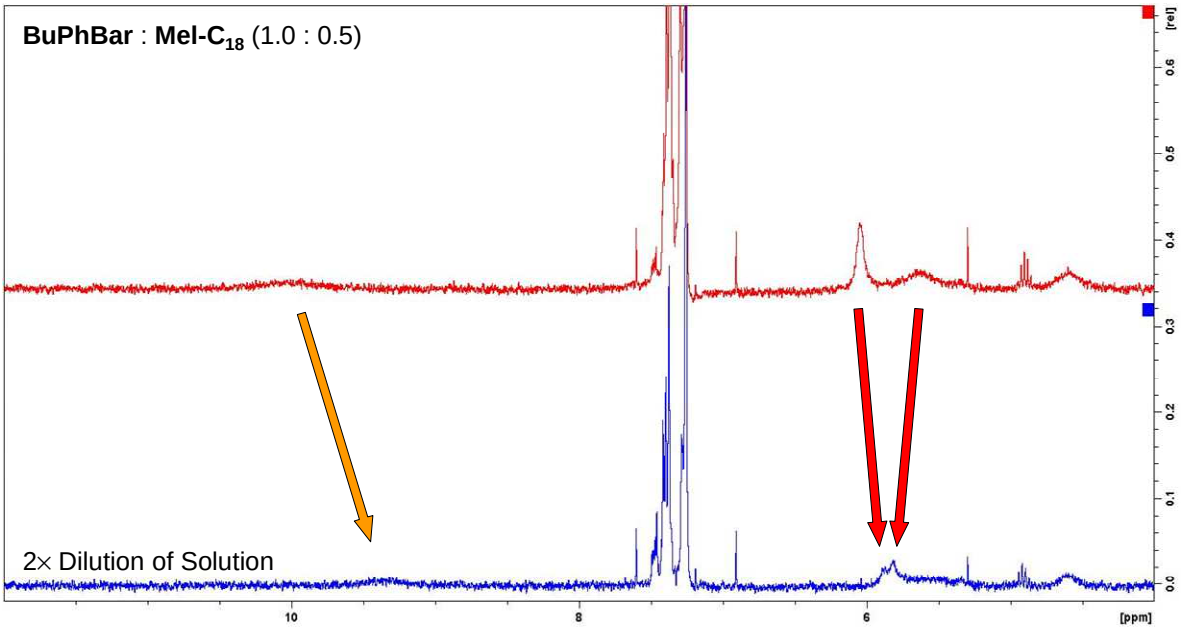

Figure S2.2: ^{1}H-NMR dilution experiment of a 1.0:0.5 mixture of **BuPhBar** and **Mel-C$_{18}$** in $CDCl_3$; c(**BuPhBar**) = 3.80 mM before dilution.

II.4.6 UV/Vis Binding Studies of Mel-C_{18} with NiPhBar

The UV/Vis titrations were performed using solvent mixtures of CH_2Cl_2 and MeOH (0 vol-%, 0.4 vol-% and 3.9 vol-%). To 1.00 mL of a stock solution of barbiturate **NiPhBar** (0.123 mM), aliquots (0–2.00 mL in total) of a melamine **Mel-C_{18}** stock solution (7.82 mM) corresponding to 0–128 equivalents were added. A constant concentration of **NiPhBar** (41 μM) for the UV/Vis absorption measurements was ensured by addition of an appropriate quantity of the solvent mixture to yield a total volume of 3.00 mL.

II.4.7 Examination of Hydrogen Bonding on Vesicle Surfaces by UV/Vis Spectroscopy

DSPC vesicles with 9.0 mol-% of embedded **Mel-C_{18}** were prepared (→ vesicles **V-Mel**). Aliquots (0–320 μL in total) of the vesicle solution corresponding to 0–64 nmol of receptor **Mel-C_{18}** were placed in a cuvette and filled up with HEPES buffer solution (25 mM, pH 7.4) to yield a total volume of 980 μL. In order to take the background absorption of the vesicles into account, difference UV/Vis absorption spectra before and after the addition of 20 μL of a stock solution of **NiPhBar** in HEPES buffer (1.00 mM) were recorded in each case (resulting concentration of **NiPhBar**: 20 μM).

II.4.8 Investigation of Vesicle Functionalization by Size-Exclusion Chromatography (SEC)

Sephadex LH-20 gel was swollen in HEPES buffer and placed in a small syringe (2.50 mL gel volume). Excessive buffer solution was removed by centrifugation at 4400 rpm for 30 s. A mixture of vesicles **V-Mel** (200 μL) with **NiPhBar** (40 μL of a 1.00 mM stock solution, 1.0 equivalent with respect to the amount of **Mel-C_{18}**) was then placed on top of the gel bed. The mini column was centrifuged at 4400 rpm for 15 s and the eluate was collected in an Eppendorf tube. The absorption spectrum of the mixture was recorded before and after SEC (Figure S2.3). For the UV/Vis measurements, the solutions were diluted with HEPES buffer to yield a total volume of 1.00 mL. In order to take the background absorption of the vesicles into account, the UV/Vis spectrum of blank DSPC vesicles of the same lipid concentration was measured and used as reference.

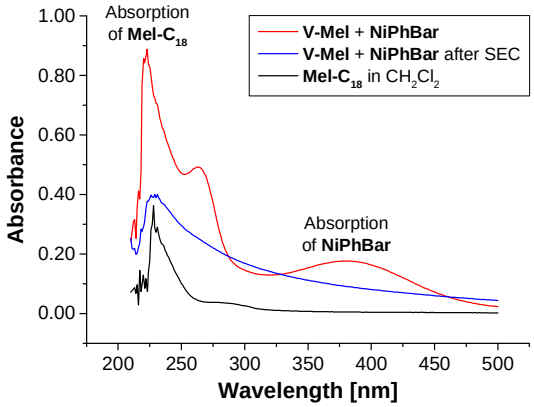

Figure S2.3: UV/Vis spectra of a) a mixture of **NiPhBar** (0.04 mM) and DSPC vesicles **V-Mel** loaded with 9.0 mol-% of **Mel-C_{18}** (corresponds to 0.04 mM) in HEPES buffer (red curve); b) the eluate after SEC of the mixture from a) (blue curve) – the reduced absorption intensity is probably due to dilution of the vesicle solution during SEC; c) pure melamine **Mel-C_{18}** in CH_2Cl_2 (0.02 mM, black curve).

II.4.9 Multisite Recognition of Hexanucleotides on Vesicle Surfaces

Luminescent, melamine-modified DSPC or DOPC vesicles containing 5.0 mol-% of reporter dye **CF-C_{12}** and 1.0 (a) or 10 mol-% (b) of melamine **Mel-C_{18}** were prepared. 100 (a) or 10 µL (b) of the freshly prepared vesicle solution were diluted 10-fold (a) or 100-fold (b) with HEPES buffer yielding a total volume of 1.00 mL and filled into a fluorescence cuvette. Aliquots (0.5–20 µL) of the stock solutions of hexanucleotides **TTTTTT** or **GGGGGG** in HEPES buffer (1.00 mM) were titrated to the corresponding vesicle solution and the fluorescence spectrum was measured after each addition. All fluorescence spectra were corrected for dilution.

II.5 Notes and Reference

[1] H.-J. Schneider, "Binding Mechanisms in Supramolecular Complexes", *Angew. Chem. Int. Ed.* **2009**, *48*, 3924–3977; *Angew. Chem.* **2009**, *121*, 3982–4036.

[2] H. Ringsdorf, B. Schlarb, J. Venzmer, "Molecular Architecture and Function of Polymeric Oriented Systems: Models for the Study of Organization, Surface Recognition, and Dynamics of Biomembranes", *Angew. Chem., Int. Ed. Engl.* **1988**, *27*, 113–158; *Angew. Chem.* **1998**, *100*, 117–162.

[3] a) L. J. Prins, D. N. Reinhoudt, P. Timmerman, "Noncovalent Synthesis Using Hydrogen Bonding", *Angew. Chem. Int. Ed.* **2001**, *40*, 2382–2426, *Angew. Chem.* **2001**, *113*, 2446–2492; b) T. Rehm, C. Schmuck, "How to achieve self-assembly in polar solvents based on specific interactions? Some general guidelines", *Chem. Commun.* **2008**, 801–813.

[4] G. R. Desiraju, "A Bond by Any Other Name", *Angew. Chem. Int. Ed.* **2011**, *50*, 52–59; *Angew. Chem.* **2011**, *123*, 52–60.

[5] For a further discussion on hydrogen bonding in aqueous solution, see: R. U. Lemieux, "How Water Provides the Impetus for Molecular Recognition in Aqueous Solution"; *Acc. Chem. Res.* **1996**, *29*, 373–380.

[6] a) C. M. Paleos, D. Tsiourvas, "Molecular Recognition of Organized Assemblies via Hydrogen Bonding in Aqueous Media", *Adv. Mater.* **1997**, *9*, 695–710; b) K. Ariga, T. Kunitake, "Molecular Recognition at Air–Water and Related Interfaces: Complementary Hydrogen Bonding and Multisite Interaction", *Acc. Chem. Res.* **1998**, *31*, 371–378; c) K. Ariga, J. P. Hill, "Monolayers at Air–Water Interfaces: From Origin-of-Life to Nanotechnology", *Chem. Rec.* **2011**, *11*, 199–211.

[7] a) M. Sakurai, H. Tamagawa, Y. Inoue, K. Ariga, T. Kunitake, "Theoretical Study of Intermolecular Interaction at the Lipid–Water Interface. 1. Quantum Chemical Analysis Using a Reaction Field Theory", *J. Phys. Chem. B* **1997**, *101*, 4810–4816; b) H. Tamagawa, M. Sakurai, Y. Inoue, K. Ariga, T. Kunitake, "Theoretical Study of Intermolecular Interaction at the Lipid–Water Interface. 2. Analysis Based on the Poisson-Boltzmann Equation", *J. Phys. Chem. B* **1997**, *101*, 4817–4825.

[8] J. Voskuhl, B. J. Ravoo, "Molecular recognition of bilayer vesicles", *Chem. Soc. Rev.* **2009**, *38*, 495–505.

[9] B. Gruber, S. Stadlbauer, A. Späth, S. Weiss, M. Kalinina, B. König, "Modular Chemosensors from Self-Assembled Vesicle Membranes with Amphiphilic Binding Sites and Reporter Dyes", *Angew. Chem. Int. Ed.* **2010**, *49*, 7125–7128; *Angew. Chem.* **2010**, *122*, 7280–7284.

[10] H. Kitano, H. Ringsdorf, "Surface Behaviors of Nucleic Acid Base-Containing Lipids in Monolayer and Bilayer Systems", *Bull. Chem. Soc. Jpn.* **1985**, *58*, 2826–2828.

[11] K. Kurihara, K. Ohto, Y. Honda, T. Kunitake, "Efficient, Complementary Binding of Nucleic Acid Bases to Diaminotriazine-Functionalized Monolayers on Water", *J. Am. Chem. Soc.* **1991**, 113, 5077–5079.

[12] a) V. Marchi-Artzner, L. Jullien, T. Gulik-Krzywicki, J.-M. Lehn, "Molecular recognition induced aggregation and fusion between vesicles containing lipids bearing complementary hydrogen bonding

head-groups", *Chem. Commun.* **1997**, 117–118; b) V. Marchi-Artzner, T. Gulik-Krzywicki, M.-A. Guedeau-Boudeville, C. Gosse, J. M. Sanderson, J.-C. Dedieu, J.-M. Lehn, "Selective Adhesion, Lipid Exchange and Membrane-Fusion Processes between Vesicles of Various Sizes Bearing Complementary Molecular Recognition Groups", *ChemPhysChem* **2001**, *2*, 367–376.

[13] I. M. Klotz, T. Askounis, "Absorption Spectra and Tautomerism of Cyanuric Acid, Melamine and Some Related Compounds", *J. Am. Chem. Soc.* **1947**, *69*, 801–803.

[14] I. Bolz, S. Spange, "An Enolisable Barbiturate with Adjustable Hydrogen-Bonding Structure for UV/Vis Detection of Nucleic Acid Bases and Related Compounds", *Chem. Eur. J.* **2008**, *14*, 9338–9346.

[15] Y. H. Jang, S. Hwang, S. B. Chang, J. Ku, D. S. Chung, "Acid Dissociation Constants of Melamine Derivatives from Density Functional Theory Calculations", *J. Phys. Chem. A* **2009**, *113*, 13036–13040.

[16] a) Q. Huo, L. Dziri, B. Desbat, K. C. Russell, R. M. Leblanc, "Polarization-Modulated Infrared Reflection Absorption Spectroscopic Studies of a Hydrogen-Bonding Network at the Air–Water Interface", *J. Phys. Chem. B* **1999**, *103*, 2929–2934; b) X. Kong, X. Du, "In Situ IRRAS Studies of Molecular Recognition of Barbituric Acid Lipids to Melamine at the Air–Water Interface", *J. Phys. Chem. B* **2011**, *115*, 13191–13198.

[17] M. Onda, K. Yoshihara, H. Koyano, K. Ariga, T. Kunitake, "Molecular Recognition of Nucleotides by the Guanidinium Unit at the Surface of Aqueous Micelles and Bilayers. A Comparison of Microscopic and Macroscopic Interfaces", *J. Am. Chem. Soc.* **1996**, *118*, 8524–8530.

[18] B. Springs, P. Haake, "Equilibrium Constants for Association of Guanidinium and Ammonium Ions with Oxyanions – The Effect of Changing Basicity of the Oxyanion", *Bioorg. Chem.* **1977**, *6*, 181–190.

[19] K. Kurihara, T. Kunitake , "Submicron-Range Attraction between Hydrophobic Surfaces of Monolayer-Modified Mica in Water", *J. Am. Chem. Soc.* **1992**, *114*, 10927–10933.

[20] K. Ariga, T. Nakanishi, J. P. Hill, M. Shirai, M. Okuno, T. Abe, J. Kikuchi, "Tunable p*K* of Amino Acid Residues at the Air–Water Interface Gives an L-zyme (Langmuir Enzyme)", *J. Am. Chem. Soc.* **2005**, *127*, 12074–12080.

[21] M. A. Swairjo, B. A. Seaton, M. F. Roberts, "Effect of vesicle composition and curvature on the dissociation of phosphatidic acid in small unilamellar vesicles – a ^{31}P-NMR study", *Biochim. Biophys. Acta, Biomembr.* **1994**, *1191*, 354–361.

[22] a) I. V. Stiopkin, C. Weeraman, P. A. Pieniazek, F. Y. Shalhout, J. L. Skinner, A. V. Benderskii, "Hydrogen bonding at the water surface revealed by isotopic dilution spectroscopy", *Nature* **2011**, *474*, 192–195; b) M. L. Berkowitz, R. Vácha, "Aqueous Solutions at the Interface with Phospholipid Bilayers", *Acc. Chem. Res.* **2012**, *45*, 74–82.

[23] a) E. L. Doyle, C. A. Hunter, H. C. Phillips, S. J. Webb, N. H. Williams, "Cooperative Binding at Lipid Bilayer Membrane Surfaces", *J. Am. Chem. Soc.* **2003**, *125*, 4593–4599; b) A. Grochmal, E. Ferrero, L. Milanesi, S. Tomas, "Modulation of In-Membrane Receptor Clustering upon Binding of Multivalent Ligands", *J. Am. Chem. Soc.* **2013**, *135*, 10172–10177.

[24] B. Gruber, S. Balk, S. Stadlbauer, B. König, "Dynamic Interface Imprinting: High-Affinity Peptide Binding Sites Assembled by Analyte-Induced Recruiting of Membrane Receptors", *Angew. Chem. Int. Ed.* **2012**, *51*, 10060–10063; *Angew. Chem.* **2012**, *124*, 10207–10210.

[25] R. N. A. H. Lewis, B. D. Sykes, R. N. McElhaney, "Thermotropic Phase Behavior of Model Membranes Composed of Phosphatidylcholines Containing Cis-Monounsaturated Acyl Chain Homologues of Studies Oleic Acid: Differential Scanning Calorimetric and ^{31}P NMR Spectroscopic Studies", *Biochemistry* **1988**, *27*, 880–887.

[26] M. Ueno, S. Katoh, S. Kobayashi, E. Tomoyama, S. Ohsawa, N. Koyama, Y. Morita, "Evaluation of Phase Transition Temperature of Liposomes by Using the Tautomerism of α-Benzoylacetoanilide", *J. Colloid Interface Sci.* **1990**, *134*, 589–592.

[27] M. Ma, A. Paredes, D. Bong, "Intra- and Intermembrane Pairwise Molecular Recognition between Synthetic Hydrogen-Bonding Phospholipids", *J. Am. Chem. Soc.* **2008**, *130*, 14456–14458.

[28] M. Ma, Y. Gong, D. Bong, "Lipid Membrane Adhesion and Fusion Driven by Designed, Minimally Multivalent Hydrogen-Bonding Lipids", *J. Am. Chem. Soc.* **2009**, *131*, 16919–16926.

[29] a) C. Schmuck, "Highly Stable Self-Association of 5-(Guanidiniocarbonyl)-1*H*-pyrrole-2-carboxylate in DMSO – The Importance of Electrostatic Interactions", *Eur. J. Org. Chem.* **1999**, 2397–2403; b) C. Schmuck, W. Wienand, "Highly Stable Self-Assembly in Water: Ion Pair Driven Dimerization of a Guanidiniocarbonyl Pyrrole Carboxylate Zwitterion", *J. Am. Chem. Soc.* **2003**, 125, 452–459.

[30] I. Bolz, C. Moon, V. Enkelmann, G. Brunklaus, S. Spange, "Probing Molecular Recognition in the Solid-State by Use of an Enolizable Chromophoric Barbituric Acid", *J. Org. Chem.* **2008**, *73*, 4783–4793.

[31] For the synthesis protocol and characterization data, see Chapter IV, compound **2**.

[32] For the derivation of the mathematical expression, see: A. E. Hargrove, Z. Zhong, J. L. Sessler, E. V. Anslyn, "Algorithms for the determination of binding constants and enantiomeric excess in complex host : guest equilibria using optical measurements", *New J. Chem.* **2010**, *34*, 348–354.

CHAPTER III:

PREPARATION OF LUMINESCENT CHEMOSENSORS BY POST-FUNCTIONALIZATION OF VESICLE SURFACES

This chapter was published in:

A. Müller, B. König, "Preparation of luminescent chemosensors by post-functionalization of vesicle surfaces", *Org. Biomol. Chem.* **2015**, *13*, 1690–1699. – Reproduced by permission of The Royal Society of Chemistry.

A. Müller performed the experimental work and wrote the manuscript. B. König supervised the project and is corresponding author.

III.1 Introduction

Molecular recognition at biomembranes is of fundamental importance for biological processes like cell recognition, adhesion, fusion or membrane transport phenomena. Since phospholipid vesicles can be considered as simple cell mimics, non-covalent interactions at the surface of receptor-functionalized synthetic liposomes resemble recognition events at membranes as they appear in nature.[1] Hence, the knowledge obtained from the investigation of artificial vesicular systems can help to gain improved insights into the correspondent processes in biology. Conversely, a better understanding of the natural prototypes can be exploited for the development of powerful devices for analytical applications. Various strategies have been established to transform the binding event at the vesicle membrane into an observable signal.[2] Fluorescent assays provide high sensitivities allowing the detection of analytes present in trace amounts, whereas colorimetric formats enable the analytic readout by the naked eye.[3] Typically, the signaling unit is in direct contact with the recognition element by either covalent attachment[4,5] or by non-covalent coordination as in indicator-displacement assays.[4,6] However, membranes are highly dynamic due to their supramolecular composition.[1] Based on this, our group recently reported on a novel strategy for the modular construction of chemosensors by means of unilamellar vesicular membranes, which serve as self-assembled supporting matrix for amphiphilic metal complex receptors and fluorescent reporter dyes.[7] Due to lateral phase separation, the co-embedded amphiphilic fluorophores and binding sites are expected to cluster on the surface resulting in fluorescence quenching of the amphiphilic dyes (Figure 3.1). Binding of analyte molecules to the surface-accessible receptors alters the physico-chemical properties in their microenvironment and thus induces a reorganization of the membrane components. These processes influence the optical properties of the co-embedded dyes, which in turn respond with a change of their emission intensity.

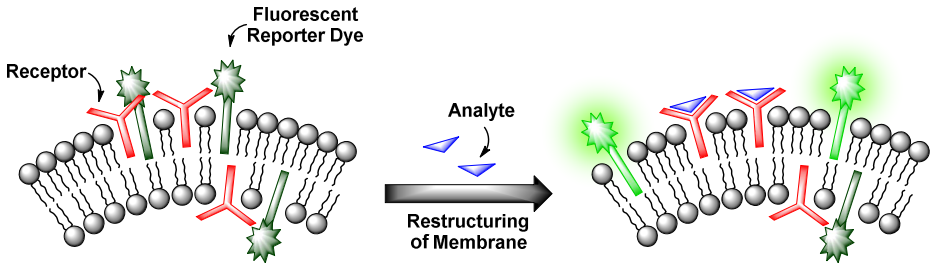

Figure 3.1: Sensing mechanism of receptor-functionalized fluorescent vesicles.

This co-embedding strategy allows an effortless preparation of sensor devices by simple mixing of different functional amphiphiles in aqueous solution. By careful variation of the binding and signaling units, their ratios and concentrations on the surface and by the choice of suitable phospholipids determining the physical properties of the membrane, vesicular sensors with specific characteristics can be designed. However, as the synthesis of the amphiphilic receptors can be quite tedious, the availability of suitable binding sites and hence the variety of addressable analytes is limited. Moreover, control over the two-dimensional receptor assembly for multipoint interactions on the surface is still a challenge.[8] Its accomplishment is an essential requirement for the highly selective recognition of multivalent analytes. In order to approach these issues, we developed a more universal method, which allows the facile preparation of vesicular chemosensors in a modular fashion by means of surface "post-functionalization" *via* click chemistry. The surface modification of preformed liposomes is an established method for the conjugation of various ligands ranging from sugars to peptides, proteins and antibodies and has found applications in, *e.g.*, the investigation of drug delivery systems.[9] We now combine this concept of vesicle post-modification with our co-embedding strategy of functional amphiphiles into phospholipid membranes. Only groups of the vesicle membranes which are exposed to the outer side are functionalized. The resulting asymmetric membrane composition represents a much better mimic of the bilayers appearing in nature. In view of more complex receptors of biological origin, we utilized a thiol–ene click reaction[10] due to the frequent occurrence of thiol groups in biomolecules. The reaction is fully biocompatible and does not, in contrast to the copper(I)-catalyzed azide–alkyne cycloaddition,[11] require a metal catalyst.

III.2 Results and Discussion

We first tested the applicability of the UV light-induced radical addition of thiols to electron-rich alkene moieties.[12] This type of reaction would implicate the possibility to externally trigger the functionalization process by controlled exposure to UV light. However, the envisaged photoreaction is at micromolar concentrations in aqueous solution not efficient (see Addendum to this Chapter for details). Thus, we focused on the widely used Michael addition of thiols to maleimides.[13] This reaction performs well over a large concentration range in aqueous media under benign conditions without the formation of byproducts and is commonly applied in bioconjugation.[10] We recently employed this method for the

construction of an aptamer-based biosensor by attachment of thiol-modified aptamers to membrane-embedded amphiphilic maleimide **Mal-C$_{16}$** (Figure 3.2).[14]

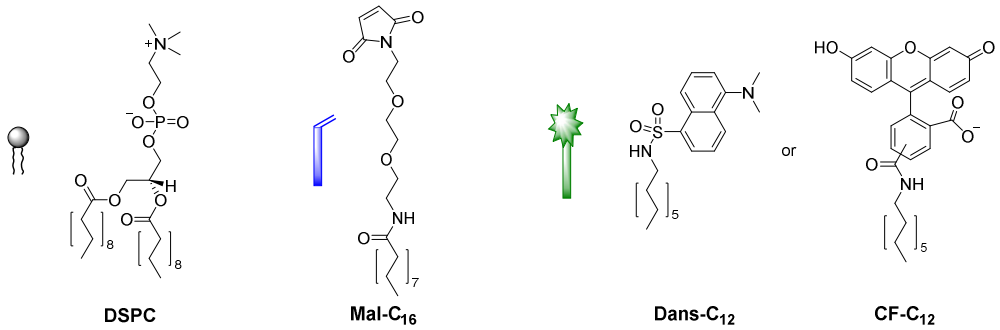

Figure 3.2: Structures of the functional amphiphiles used for vesicle preparation.

Here, we report on the development of the post-functionalization strategy of luminescent vesicle surfaces with receptor sites and demonstrate its facile and versatile applicability for the preparation of various sensors. As signaling units, either amphiphilic dansyl dye **Dans-C$_{12}$**[15] or carboxyfluorescein **CF-C$_{12}$** were incorporated into membranes of small unilamellar DSPC vesicles. Figure 3.3 depicts the different thiols which were used for our investigations. The syntheses of compounds **Mal-C$_{16}$**[14] and **CF-C$_{12}$**[7a] were previously reported by us, the preparation of **Cys-Trp** and **Zn-Cyclen$_2$** is described in the Experimental Part.

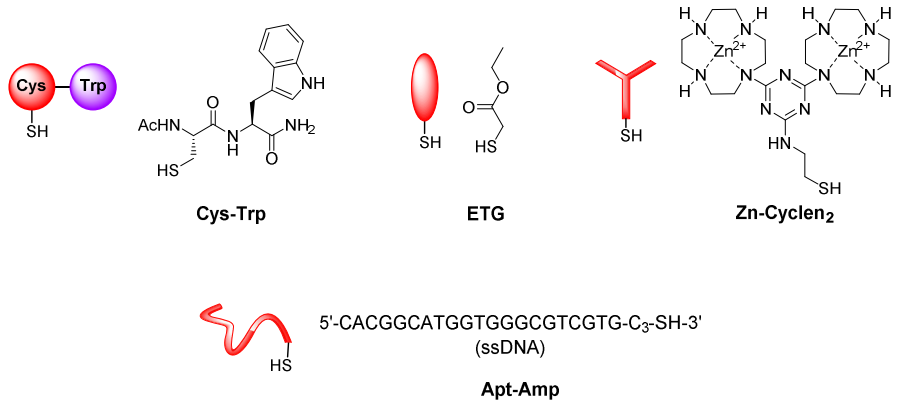

Figure 3.3: Thiols used for the post-functionalization of vesicle surfaces.

III.2.1 Optimization of the Post-Functionalization of Preformed Vesicles

The sensing mechanism of our vesicular sensors is based on the close spatial proximity of the binding sites to the membrane-embedded dyes. To test whether the

subsequently immobilized receptor molecules fulfill this condition, we developed an assay based on the distance-dependent Förster resonance energy transfer (FRET, Figure 3.4). As simple model system, we synthesized dipeptide **Cys-Trp** (Figure 3.3). The FRET partner of tryptophan, the amphiphilic dansyl dye **Dans-C_{12}** (Förster distance: 2.1 nm),[16] was co-embedded (5.0 mol-%) into the membrane of DSPC vesicles together with the attachment site for thiols **Mal-C_{16}** (5.0 mol-%). The preparation of the vesicles was performed in 25 mM HEPES buffer at a pH of 7.4 according to previously reported procedures (see Experimental Part for details). Extrusion through 100 nm polycarbonate membranes yielded vesicles **V-Dans** with a size distribution of around 130–150 nm (see Figure S3.1 in Experimental Part). The non-functionalized vesicles were stable and did not show significant aggregation after one day (see Figure S3.2 in Experimental Part).

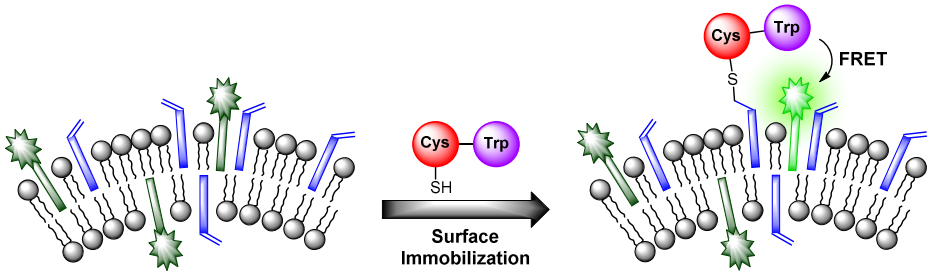

Figure 3.4: FRET assay proving the close spatial proximity of immobilized thiols to the membrane-embedded fluorophores.

Addition of **Cys-Trp** to **V-Dans** showed a time-dependent decrease of the tryptophan emission evidencing the fluorescence energy transfer and a considerable increase of the dansyl signal (Figure 3.5).

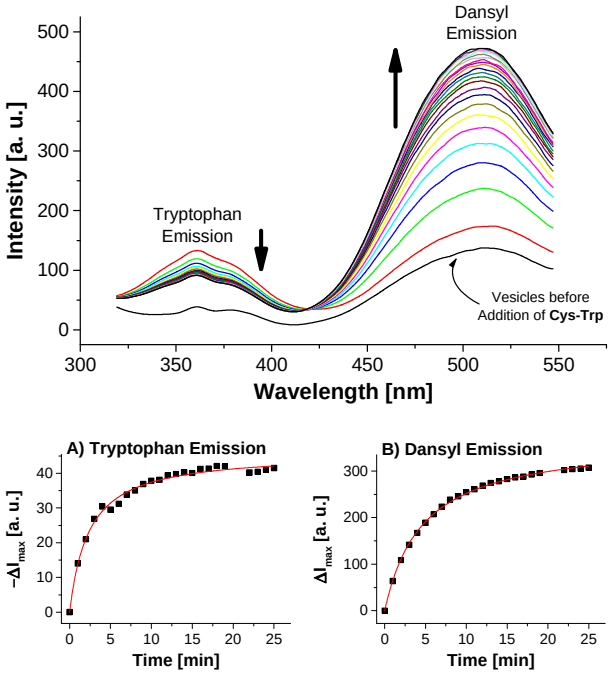

Figure 3.5: Top: Time-dependent fluorescence spectra of vesicles **V-Dans** after addition of 3.0 mol-% of peptide **Cys-Trp** (λ_{ex} = 280 nm). Bottom: Course of surface reaction as evidenced by the emission signals of either the tryptophan or dansyl dye.

Apart from the contribution of the resonance energy transfer from the tryptophan moiety, the extraordinarily strong increase of the dansyl signal must be attributed to two additional independent effects: (i) It is well documented that the fluorescence emission of dansyl dyes is quenched by adjacent maleimides *via* photoinduced electron transfer (PET), which proceeds from the excited state of the fluorophore to the maleimide.[17] After conjugation of thiols to the electron-deficient double bond of the maleimide π-system of **Mal-C_{16}**, this PET process is interrupted resulting in a dansyl fluorescence quantum yield enhancement. (ii) Furthermore, by the altered physico-chemical properties of the local environment upon surface functionalization, the optical properties of the membrane-embedded fluorophores change causing an increase in emission intensity. A fluorescence increase of **V-Dans** during the surface reaction with a non-tryptophan-containing thiol like **ETG** (ethyl thioglycolate, Figure 3.3) confirms this interpretation (see Figure S3.3 in Experimental Part). The observations clearly show that the thiol is covalently attached to the membrane-embedded maleimide **Mal-C_{16}** and the membrane-bound thiols in turn are in close proximity to the co-embedded fluorophores. Membranes without **Mal-C_{16}** show a much higher initial dansyl emission intensity and no time-dependent change of the emission signal of either fluorophores, the tryptophan or dansyl dye, occurred after addition of **Cys-Trp** (see

Figure S3.5 in Experimental Part). The same observation was made for vesicles **V-Dans** whose surface-accessible maleimides were saturated with **ETG** prior to the addition of **Cys-Trp** (see Figure S3.4 in Experimental Part). The experiments demonstrate that non-functionalized, maleimide-containing vesicles **V-Dans** can also be regarded as simple self-assembled sensors for thiols.[18]

In contrast to dansyl dyes, carboxyfluorescein derivatives do not show PET processes in presence of maleimides in the membrane. To further study the effect (ii), we prepared vesicles **V-CF** with embedded carboxyfluorescein **CF-C_{12}**, which showed a time-dependent increase of the fluorescence signal after addition of thiol **ETG** indicating membrane restructuring processes upon surface functionalization (see Figure S3.6 in Experimental Part). By non-linear curve fitting, the second-order rate constants of thiol–maleimide conjugations on the vesicle membranes were determined (Table 3.1). The rate constants are all in the same order of magnitude. Small deviations along with different combinations of employed thiol and membrane composition can be explained by the course of the thiol–maleimide addition *via* thiolate anions. Their concentration is directly related to the pH of the reaction medium and to the pK_a value of the corresponding thiol. These pK_a values in turn are influenced by both the chemical nature of the thiol and the physico-chemical properties in their environment, *i.e.*, by the individual properties of the particular vesicle–water interface.[19] Noteworthy, considerably basic conditions drastically enhance the nucleophilicity, however, also accelerate the oxidation of thiols to disulfides. Therefore, the pH value of 7.4 in our vesicular systems poses a good compromise between reaction rate and thiol stability. Compared to literature known rate constants from homogeneous systems (600–8850 M^{-1} s^{-1} at pH = 7.0),[20] the lower rate constants of about one order of magnitude at the liposomal surfaces are probably due to the lower diffusion rates of vesicles.[21]

Table 3.1: Rate constants for vesicle functionalization reactions based on the signal changes of the co-embedded fluorophores.

Entry	Vesicles	Thiol	k_{obs} [M^{-1} s^{-1}]
1	**V-Dans**	**Cys-Trp**	315
2	**V-Dans**	**ETG**	108
3	**V-CF**	**ETG**	455

III.2.2 Preparation of Chemosensors for Phosphates by Post-Functionalization of Vesicles with Zn-Cyclen$_2$

Next, we utilized the established conditions for the membrane attachment of thiolated species for the preparation of a simple chemosensor. As phosphates are ubiquitous in nature, they pose important targets for analytical devices. Recently, our group reported on the preparation of vesicular chemosensors for phosphates based on amphiphilic derivatives of bis-Zn^{2+}-cyclen complexes.[4,7a] Those receptors are known to bind to phosphates with nanomolar affinities.[22] To demonstrate the proof of principle of our post-functionalization approach and to show its applicability for sensor preparation in analogy to our previous investigations, we synthesized the thiolated bis-Zn^{2+}-cyclen receptor **Zn-Cyclen$_2$** (Figure 3.3) and immobilized it on maleimide-modified vesicles **V-CF**. For that purpose, we added a substoichiometric amount of the thiol (0.8 equivalents)[23] with respect to the surface-accessible concentration of **Mal-C$_{16}$** in order to avoid the separation of excess **Zn-Cyclen$_2$** after vesicle functionalization. Fluorescence measurements revealed a remarkable initial drop of the emission signal (see Figure S3.7 in Experimental Part) upon addition of **Zn-Cyclen$_2$** followed by a further time-dependent decrease of the fluorescence intensity indicating the progress of the surface reaction (Figure 3.6).

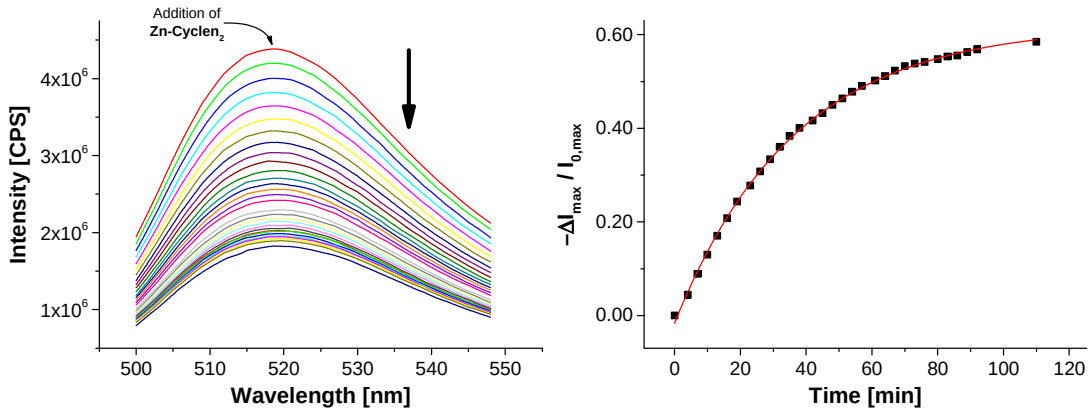

Figure 3.6: Time-dependent fluorescence response showing the functionalization progress of vesicles **V-CF** with 2.0 mol-% of **Zn-Cyclen$_2$**.

Compared to the surface reaction of vesicles **V-CF** with **ETG**, the functionalization with **Zn-Cyclen$_2$** was considerably slower (Table 3.2, entry 1). We explain this with the occurrence of multiple equilibria diminishing the concentration of free **Zn-Cyclen$_2$**: (i) The strong complexation abilities of thiol groups towards metal centers like zinc cations are supposed to result in intermolecular Zn^{2+}–SH coordination.[24] (ii) Furthermore, the

considerable instant quenching of the fluorescence signal after addition of the receptor indicates electrostatic interactions of the bis-Zn^{2+}-cyclen head groups with the negatively charged membrane-embedded carboxyfluorescein derivates. To further verify these assumptions, we varied the amount of receptor **Zn-Cyclen$_2$** since the proposed equilibria are expected to be shifted towards the coordinated species at higher concentrations of **Zn-Cyclen$_2$** (entries 2 and 4). Additionally, we performed the surface reaction in the presence of pyrophosphate (PP_i, entries 3 and 5) due to its ability to compete for the Zn^{2+}-centered coordination site of the receptor and thus to increase the concentration of free **Zn-Cyclen$_2$** thiol functions. The results presented in Table 3.2 show two obvious trends which confirm our hypothesis: An enhancement of the reaction rate in the presence of PP_i and a deceleration of the reaction along with higher thiol concentrations.

Table 3.2: Rate constants for the functionalization of vesicles **V-CF** with different amounts of **Zn-Cyclen$_2$** in absence or presence of PP_i (for fluorescence emission data, see Figures S3.7 and S3.8 in Experimental Part).

Entry	**Zn-Cyclen$_2$**[a]	PP_i[b]	k_{obs} [M^{-1} s^{-1}]
1	0.8 eq (2.0 mol-%)	–	82
2	1.0 eq (2.5 mol-%)	–	78
3	1.0 eq (2.5 mol-%)	2.0 eq	322
4	2.0 eq (5.0 mol-%)	–	31
5	2.0 eq (5.0 mol-%)	2.0 eq	202

[a] Equivalents with respect to surface-accessible amount of **Mal-C$_{16}$**.
[b] Equivalents with respect to total amount of **Zn-Cyclen$_2$**.

The addition of disulfide precursor of **Zn-Cyclen$_2$** (compound **7** in Scheme S3.2, Experimental Part) to **V-CF** leads to a strong decrease of the emission signal supporting the proposed coordinative interaction of the Zn^{2+}-complex with **CF-C$_{12}$**. However, as expected no further time-dependent decrease was observed due to the absence of free thiol groups required for the surface attachment (see Figure S3.9 in Experimental Part).

After completion of the functionalization process of **V-CF** with **Zn-Cyclen$_2$**, the obtained vesicles **V-CF-Zn** were ready for use as luminescent sensors for phosphate species. Titration of the analyte PP_i resulted in a strong increase of their fluorescence emission signal (Figure 3.7).

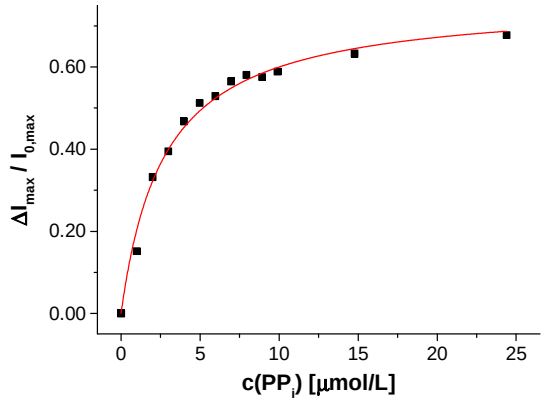

Figure 3.7: Fluorescence response upon titration of PP_i to functionalized vesicles **V-CF-Zn**.

For control experiments, non-functionalized vesicles were prepared by either omitting **Zn-Cyclen$_2$** or by addition of **Zn-Cyclen$_2$** to vesicles lacking the membrane-embedded attachment site **Mal-C$_{16}$**. Titration of PP_i did not show a significant response of the fluorescence signal in those cases (for titration data, see Figure S3.10 in Experimental Part). These results proved that the membrane attachment of the receptor molecules is an essential requirement for the sensing mechanism of the PP_i analyte molecules.

We examined different phosphate-containing analytes in their binding affinities to vesicles **V-CF-Zn** and found binding constants which are in good agreement with literature values demonstrating the proof of concept (Table 3.3). The absence of a fluorescence emission change upon titration of sulfate as a dianionic control analyte confirmed the specificity of **V-CF-Zn** towards phosphate anions.

Table 3.3: Binding affinities of **Zn-Cyclen$_2$**-functionalized vesicles **V-CF-Zn** to different analytes (for titration data, see Figure S3.11 in Experimental Part).

Entry	Analyte	lg K_a	Reference[a]
1	PP_i	6.3	6.2[7a]
2	D-Fructose 1,6 bisphosphate	6.0	6.1[4]
3	Phosphorylated hexapeptide **Pep-P-His** (Figure 3.8)	5.6	5.9[26a]
4	SO_4^{2-}	No response	–

[a] Refers to vesicular sensor systems obtained by co-embedding of amphiphilic bis-Zn^{2+}-cyclen receptors into the membrane.

Next, we investigated the dependency of the fluorescence response on the concentration of membrane-embedded fluorophores and immobilized receptor molecules (see

Figure S3.12 in Experimental Part). Best signal to noise ratios were obtained with increasing amounts of both dye and receptor. These results are consistent with our previous observations and support our mechanistic hypothesis of receptor–dye patches on the vesicle surface, which reorganize upon formation of receptor–analyte complexes.[7a]

III.2.3 Molecular Imprinting of Vesicle Surfaces

Our investigations with the **Zn-Cyclen$_2$** receptor revealed that the post-functionalization technique is well suited for the preparation of luminescent chemosensors in a modular fashion. Table 3.3 shows that the obtained binding constants of the different phosphates are almost equal. However, for the development of powerful analytical devices being able to discriminate between structurally related analytes, well-defined multipoint interactions between hosts and guests are essential. That means, the arrangement of the recognition elements on the vesicle surface must be complementary to the position of the binding units at the envisaged targets. Molecular imprinting is the classic technique in polymer science to achieve this aim.[25] In this connection, a molecule is utilized as a stamp to create its negative print in a suitable matrix. Recently, our group reported on two different strategies towards the preparation of highly specific, multi-receptor chemosensors. Both approaches are based on dynamic, template-guided recruitment of amphiphilic receptors on fluid vesicle membranes followed by fixation of the assemblies either by cooling the membrane down below the vesicular phase transition temperature[26a,b] or by photopolymerization of the membrane-embedded receptor arrays.[26c] A post-functionalization strategy can also be used for the molecular imprinting of defined two-dimensional receptor assemblies since the maleimide-decorated vesicles can be regarded as reactive matrices for template-assisted covalent functionalization. A fundamental prerequisite for that approach is the rigidity of the vesicle membrane preventing the lateral redistribution of the receptors after surface attachment. Hence, DSPC membranes with a phase transition temperature of 54 °C[27] represent an ideal scaffold for that purpose. Figure 3.8 illustrates the principle of molecular imprinting by vesicle post-functionalization. In detail, membrane-attached receptor–template complexes direct the surface fixation of additional receptor molecules by coordinative interactions in spatially defined arrangements. Subsequent separation of the templates leads to an imprinted vesicle surface with patterns of binding sites.

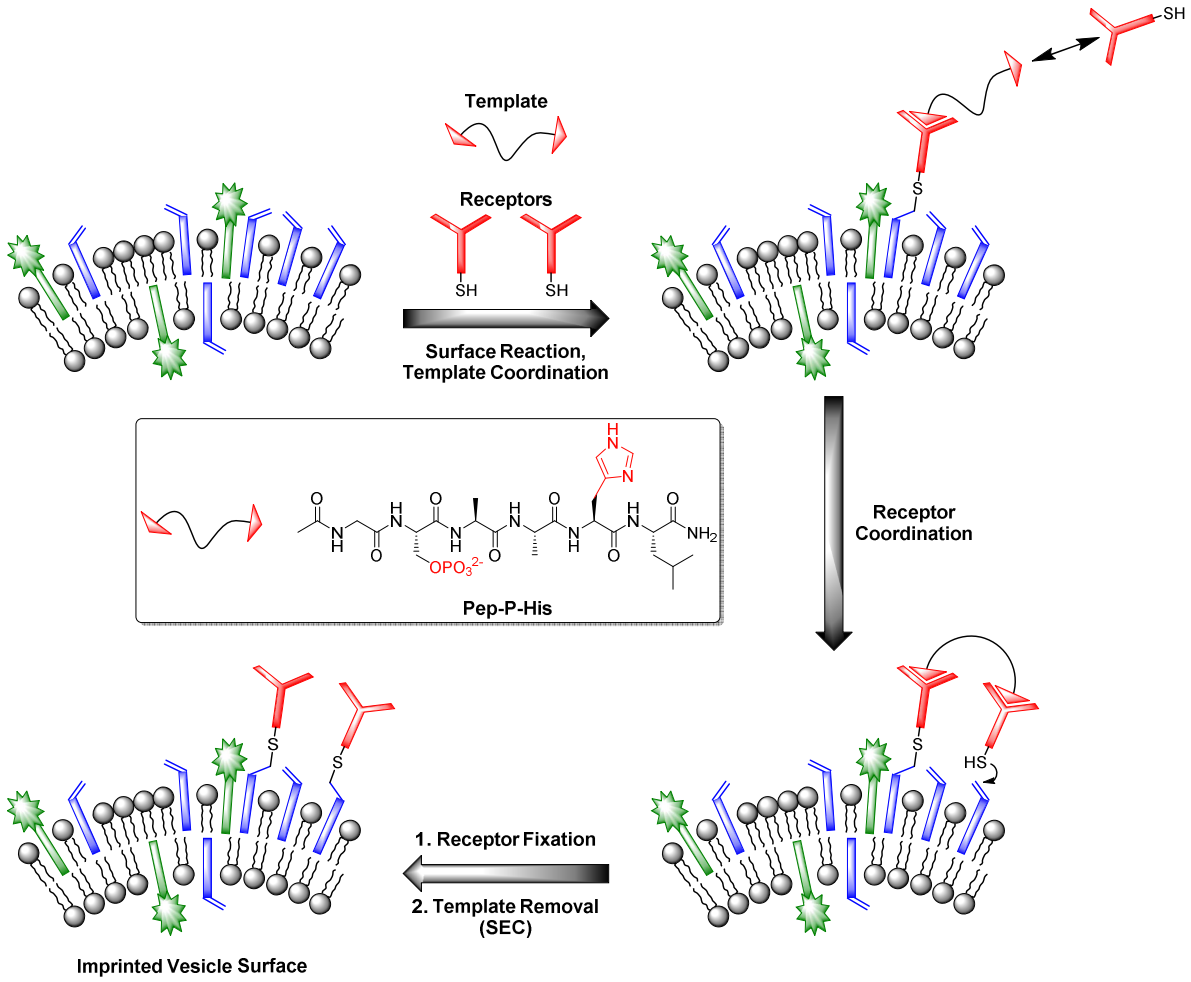

Figure 3.8: Principle of vesicle surface imprinting by template-assisted post-functionalization and bivalent peptide **Pep-P-His** used as model template.

Complex **Zn-Cyclen$_2$** is known to bind besides phosphates also to histidine moieties.[28] As template for our imprinting studies, we therefore utilized bivalent hexapeptide **Pep-P-His** (Figure 3.8) being able to form a ternary complex with two receptor molecules. We incubated a 1:2 mixture of the peptide and the thiolated receptor **Zn-Cyclen$_2$** with vesicles **V-CF** (0.4 equivalents of receptor with respect to surface-accessible maleimide) and removed the template molecules by size-exclusion chromatography (SEC) after completion of the surface functionalization. For comparison, vesicle surfaces were post-functionalized with **Zn-Cyclen$_2$** in absence of the bivalent peptide, but treated identically apart from that. Rebinding studies of the two obtained vesicle samples revealed a significantly different course of the fluorescence emission responses (Figure 3.9). While the imprinted vesicles displayed a fluorescence decrease upon titration of up to 0.5 equivalents of peptide **Pep-P-His**, the non-imprinted samples showed a steady increase. After further peptide addition, the

sign of the fluorescence signal change reversed in case of the imprinted vesicles and the curve progression approximated that of the non-imprinted ones.

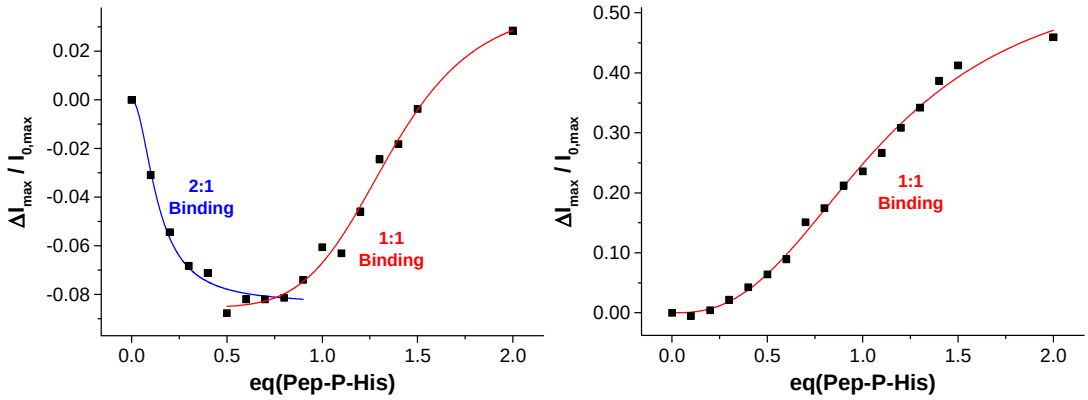

Figure 3.9: Rebinding isotherms of imprinted (left) and non-imprinted (right) vesicles **V-CF-Zn** upon addition of **Pep-P-His**.

This divergent behavior can be rationalized by different binding modes in the two cases. We hypothesize that the geometric confinement of the functional amphiphiles on the vesicle surface upon the formation of 2:1 complexes results in a further quenching of the co-embedded fluorophores. Gradual transition into 1:1 binding mode after addition of more than 0.5 equivalents of the peptide is assumed to provide a higher translational freedom of the membrane-embedded compounds leading to an emission intensity increase of the dye molecules.[29] Due to the superposition of two opposing effects in the case of imprinted vesicles, the overall fluorescence response is much lower compared to that of the non-imprinted samples. The macroscopic binding constants in the two cases obtained by Hill fitting of the titration curves are lg $K_a \approx 7.1$ for the imprinted vesicles (based on the addition of up to 0.8 equivalents of **Pep-P-His**) *versus* 5.1 for the control experiment.[30] However, due to the superposition of two diverging signal responses, the apparent affinity constant for the multipoint binding is likely to be underestimated.

Variation of the receptor concentration indicated that the success of vesicle surface patterning is dependent on the proportion of added receptor molecules and membrane-embedded maleimides. At an almost equimolar ratio (≈ 0.8 equivalents of receptor with respect to surface-accessible maleimide), the different binding behavior of imprinted and non-imprinted samples is much less pronounced (see Figure S3.13 in Experimental Part). We explain this result with the fact that here, approximately all surface-accessible maleimide molecules bear a receptor unit, *i.e.*, the receptor assembly simply reflects the random assembly of the membrane-embedded **Mal-C$_{16}$**. Thus, no external control over their spatial

distribution is possible and the receptors cannot attain an appropriate geometric arrangement for multipoint binding to the analyte. Conversely, when immobilizing the receptor in substoichiometric amounts, only membrane-embedded maleimides whose mutual distances are compatible to the formation of ternary receptor–template complexes are functionalized. The other maleimides remain unmodified and thereby do not impede the 2:1 binding on the vesicle surface.

III.2.4 Vesicle Functionalization with an Aptamer for Ampicillin

In living systems, multipoint interactions dominate the molecular recognition phenomena and provide for remarkably high specificities. Thus, to explore the full potential of our technique, we next extended the vesicular post-functionalization strategy to more complex binding units of biological origin. Among those, oligonucleotide-based aptamers represent one of the most exciting and promising class of receptors. Since they are developed by an evolutionary process of repeated selection and amplification steps, aptamers exhibit very high binding affinities and specificities to their targets ranging from small organics to proteins and pathogens.[31] In many cases, structurally related analytes can be discriminated on basis of subtle differences such as the presence or absence of methyl or hydroxyl groups. Compared to other biological recognition elements like antibodies, aptamers display some remarkable advantages including low immunogenicity, small size, easy production and modification by established solid-phase synthesis methods and therefore inexpensive commercial availability. Moreover, they are characterized by a high stability and convenient handling. Fluorescence-based methods for the detection of aptamer–target binding typically rely on covalent modification of the oligonucleotides with luminescent reporter moieties.[32] Another established technique involves hybridization of the aptamers with accordingly labeled complementary oligonucleotide strands and their subsequent displacement by the analyte molecules. This requirement of covalent attachment of fluorophores can make such assays laborious and costly. Label-free strategies on the other hand, *e.g.*, based on intercalation of a fluorescent dye into a double helix domain, are often limited in their applicability as they depend on particular properties of the aptamers such as specific folding modes upon complex formation with the target. In contrast to these analytical methods, the signaling mechanism of our vesicular sensors is generally supposed to originate rather from an analyte-induced redistribution of charges at the liposome–water interface than on defined

conformational changes of the recognition sites. Therefore, aptamer-functionalized vesicles with co-embedded reporter dyes potentially represent versatile systems for the detection of aptamer–target interactions. The modular nature of such aptasensors based on self-assembly and subsequent membrane modification allows for their easy preparation and facile optimization of their composition. Recently, we reported on the post-functionalization of luminescent vesicles with the thrombin-binding aptamer resulting in liposomal sensors, which signal the binding of the protein analyte to their surface.[14] To demonstrate the universal applicability of this approach for the preparation of various aptasensors, we utilized a DNA-based aptamer developed by Song *et al.* which specifically binds to the antibiotic ampicillin (Figure 3.10) with an affinity constant of lg $K_a \approx 8.0$.[33]

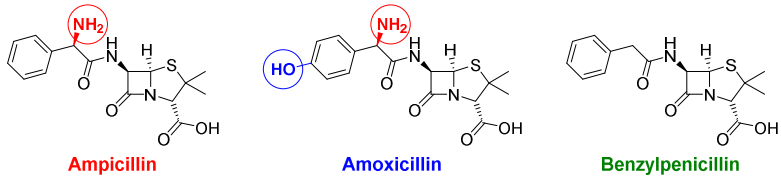

Figure 3.10: Structures of the antibiotic ampicillin and of related control antibiotics amoxicillin and benzylpenicillin; structural differences are marked with colored circles.

For the selection of the ampicillin aptamer, the authors used TRIS buffer with added salts (50 mM NaCl, 5 mM KCl, 5 mM $MgCl_2$). The presence of cations such as K^+ or Mg^{2+} is important to stabilize the folded analyte binding conformations of some aptamers. On the other hand, it is well explored that in particular bivalent cations can induce aggregation or even fusion of negatively charged vesicles (as it is the case for **V-CF**) by neutralizing their surface charge and thus by decreasing their electrostatic repulsion barrier.[34] In our case, it turned out that non-functionalized vesicles **V-CF** are indeed unstable and aggregate under the original buffer conditions. For that reason, we screened different buffer systems with respect to both vesicle stability and emission response of aptamer-functionalized vesicles after addition of ampicillin (see Experimental Part for details). Buffer systems without added salts did not result in significant fluorescence responses, whereas very high salt concentrations induced vesicle aggregation as determined by dynamic light scattering. HEPES buffer with added KCl (5 mM) and $MgCl_2$ (5 mM) represented the best compromise. The surface functionalization of maleimide-containing vesicles **V-CF** was performed with thiol-modified oligonucleotide **Apt-Amp** (Figure 3.3). A time-dependent change of the emission signal again displayed the progress of the aptamer-immobilization on the vesicular membrane (Figure 3.11).

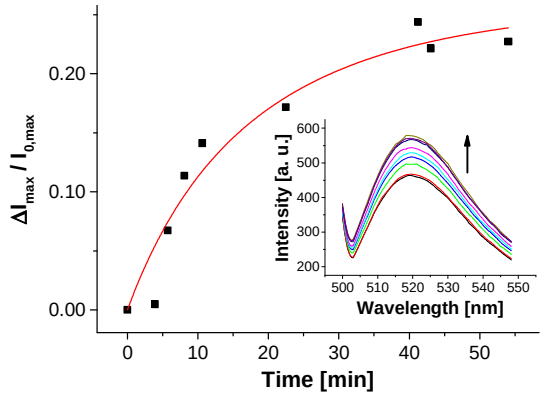

Figure 3.11: Fluorescence response showing the immobilization progress of vesicles **V-CF** with aptamer **Apt-Amp** (1.0 mol-%).

In contrast to the post-functionalization of **V-CF** with receptor **Zn-Cyclen$_2$**, the fluorescence signal increased during the surface reaction. We believe that the presence of the highly negatively charged oligonucleotides at the vesicle surface partially displaces the likewise negatively charged carboxyfluorescein molecules from the clusters of the functional amphiphiles. As a consequence, a reduction of the fluorophore self-quenching occurs. Binding of ampicillin to the surface-immobilized aptamers is thought to induce a more compact conformation of the aptamer strands. Therefore, a higher negative charge density at the vesicle membrane is generated, which in turn enforces more dye molecules to be squeezed out of their membrane domains. This process gives rise to a significant further increase of the emission signal (Figure 3.12).[35]

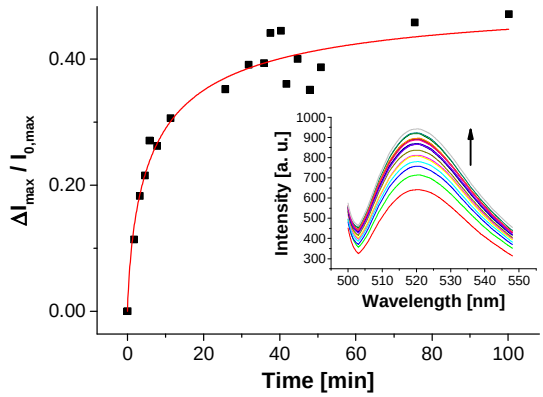

Figure 3.12: Time-dependent change of fluorescence emission of aptamer-functionalized vesicles **V-CF-Amp** (2.0 mol-% of **Apt-Amp**) after addition of ampicillin (0.40 μM).

The time-dependent fluorescence spectra depicted in Figure 3.12 show a rather slow emission response of **V-CF-Amp** upon addition of ampicillin. We assume that the aptamer-functionalized vesicles are more prone to salt-induced aggregation than the non-

functionalized ones due to their higher surface charge.[34] This assumption is supported by investigations of the vesicular size distribution, which revealed a significant cross linking of the vesicles after functionalization with the oligonucleotide (see Figure S3.15 in Experimental Part).[36] This process in turn reduces the accessibility of the surface-bound aptamers for ampicillin. Binding of the analyte molecules to their membrane receptors, however, seems to partially reverse the aggregation as indicated by a subsequent decrease of the size distribution maximum of the vesicles.[37]

Variation of the aptamer concentration and addition of ampicillin to the functionalized vesicles gave best emission responses of almost 50 % with 2.0 mol-% of oligonucleotides immobilized on the surface (Figure 3.13). These conditions having approximately equimolar amounts of the receptor molecules with respect to the membrane-embedded fluorophores on the outer vesicle provide highest sensitivities, which is in accordance with our results from **Zn-Cyclen$_2$**-functionalized vesicles.

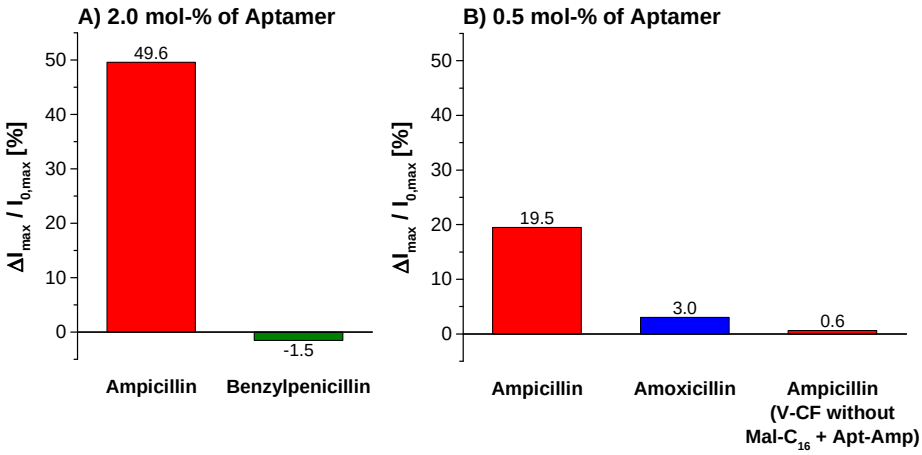

Figure 3.13: Comparison of relative fluorescence emission responses of **V-CF-Amp**, functionalized with different amounts of the aptamer, and of a mixture of maleimide-lacking vesicles **V-CF** and **Apt-Amp** after addition of ampicillin, benzylpenicillin or amoxicillin (0.40 μM in each case).

The specificity of the aptasensors **V-CF-Amp** towards ampicillin was illustrated by addition of the structurally related antibiotics benzylpenicillin or amoxicillin, which showed no significant fluorescence responses of the membrane-embedded carboxyfluorescein dyes (Figure 3.13). Vesicles lacking the amphiphilic attachment site for thiols **Mal-C$_{16}$** were prepared and incubated with the aptamer. Addition of ampicillin to that sample did not lead to a change of the emission. This observation proves that the analyte signaling depends on the interactions with the membrane-conjugated aptamers.

III.3 Conclusion

In summary, we have demonstrated that preformed, maleimide-decorated luminescent vesicles can be easily functionalized at the surface with different receptors by nucleophilic thiol addition. It was shown that the immobilized compounds may range from small organic molecules to peptides and metal complexes, such as bis-Zn^{2+}-cyclen, and to even more complex structures like oligonucleotides. The membrane-embedded fluorophores respond to the presence of the receptor units and to the formation of host–guest complexes on the vesicle surface with changing emission properties. We demonstrated potential applications of the concept including the detection of simple phosphates with surface-attached **Zn-Cyclen$_2$** or the specific sensing of ampicillin by an aptamer. Moreover, we showed that the post-functionalization strategy allows external control over the two-dimensional distribution of the receptors by assistance of multivalent templates. Here, significant differences between imprinted and non-imprinted samples were obtained in the fluorescence output of rebinding titrations. Due to the highly modular approach, our presented strategy allows an easy, fast and inexpensive access to a broad variety of supramolecular indicators with tailor-made properties. The non-functionalized vesicles can be prepared in advance. Since many heterobifunctional reagents for the *in situ* introduction of thiol groups to amines are commercially available (*e.g.*, Traut's reagent[38a] or SATA[38b]), our method is not only limited to thiol-containing host molecules, but can be readily extended to recognition elements based on other peptides, oligonucleotides or complex macromolecules. Hence, the development of novel customized bioanalytical devices may be facilitated.

III.4 Experimental Part

III.4.1 General Methods and Material

General

Commercially available solvents of standard quality were used. Starting materials and analytes (sodium pyrophosphate, D-fructose 1,6-bisphosphate, ampicillin, benzylpenicillin and amoxicillin) were purchased from either Acros or Sigma-Aldrich and used without any further purification. Phospholipids were purchased from Avanti Polar Lipids Inc. The hexapeptide **Pep-P-His** was obtained from GL Biochem Ltd. (Shanghai) and the thiolated aptamer **Apt-Amp** was synthesized by IBA GmbH (Göttingen).

Thin layer chromatography (TLC) analyses were performed on pre-coated silica gel 60 F-254 with a 0.2 mm layer thickness (Pre-coated TLC-sheets ALUGRAM Xtra SIL G/UV_{254} from Macherey-Nagel). The detection was realized *via* UV light at 254 or 366 nm or by staining with $KMnO_4$. Flash column chromatography was performed on silica gel 60 (70–230 mesh) from Macherey-Nagel.

Melting Points

Melting points were determined on a Stanford Research Systems OptiMelt MPA100 with a heating rate of 1–2 °C/min.

NMR Spectra

For NMR spectroscopy, a Bruker Avance 300 (^{1}H: 300.1 MHz, ^{13}C: 75.5 MHz, T = 293 K) or Bruker Avance 400 (^{1}H: 400.1 MHz, ^{13}C: 100.6 MHz, T = 293 K) was used. All chemical shifts are reported in δ [ppm] (multiplicity, coupling constant *J*, number of protons, assignment) relative to the solvent residual peak as the internal standard ($CDCl_3$: ^{1}H: δ = 7.26 ppm, ^{13}C: δ = 77.16 ppm; CD_3OD: ^{1}H: δ = 3.31 ppm, ^{13}C: δ = 49.00 ppm; CD_3CN: ^{1}H: δ = 1.94 ppm, ^{13}C: δ = 1.32 ppm). The coupling constants are given in Hertz [Hz]. Abbreviations used for signal multiplicity: ^{1}H-NMR: s = singlet, d = doublet, t = triplet, q = quartet, quint = quintet, dd = doublet of doublets, m = multiplet, br = broad. Assignments of the ^{13}C-NMR signals were made using DEPT technique (pulse angle: 135 °) and given as (+) for CH_3 or CH, (–) for CH_2 and (C_q) for a quaternary carbon.

Mass Spectra

Mass spectra were measured on a ThermoQuest Finnigan TSQ 7000 or an Agilent Q-TOF 6540 UHD mass spectrometer.

Fluorescence Measurements

Fluorescence spectroscopy was carried out on a Varian Cary Eclipse or a HORIBA FluoroMax-4 fluorescence spectrophotometer with temperature control using 10 × 4 mm Hellma quartz cuvettes at 21 °C. Vesicles containing **Dans-C_{12}** were excited at 280 nm, those with embedded **CF-C_{12}** at 495 nm. For better comparability of the different measurements, the relative fluorescence changes (ΔI_{max} / $I_{0,max}$) were calculated.

Dynamic Light Scattering (DLS)

Dynamic light scattering was performed on a Malvern Zetasizer Nano ZS at 25 °C using 1 cm disposable polystyrene cuvettes. Data analysis was performed using the Malvern Zetasizer software.

III.4.2 Synthesis

The amphiphiles **Mal-C_{16}**,[14] **Dans-C_{12}**[15] and **CF-C_{12}**[7a] were prepared according to previously reported procedures, the syntheses of **Cys-Trp** and of **Zn-Cyclen$_2$** are described below.

III.4.2.1 Synthesis of N-*Acetyl-L-cysteinyl-L-tryptophanamide (**Cys-Trp**)*

The synthesis of dipeptide **Cys-Trp** was carried out following a standard protocol for Fmoc-based solid-phase peptide synthesis (Scheme S3.1).[39] As solid phase, Fmoc-Rink-Amide-MBHA resin (200 mg, 0.106 mmol) was used. After precipitation in cold Et_2O, the peptide **Cys-Trp** was obtained as white solid (21 mg, 0.060 mmol, 57 %).

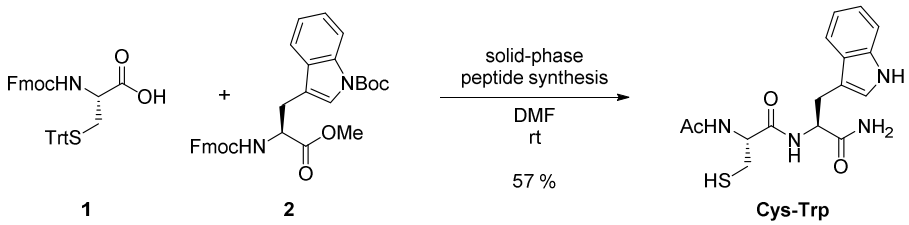

Scheme S3.1: Synthesis of dipeptide **Cys-Trp**.

R_f = 0.17 (MeOH/CH_2Cl_2 10:90). — ^{1}H-NMR (CD_3OD, 300 MHz): δ = 1.89 (s, 3H, Me), 2.66–2.82 (m, 2H, CH_2), 3.17–3.22 (m, 1H, C*H*H), 3.28–3.37 (m, 1H, CH*H*), 4.34–4.42 (m, 1H, CH), 4.63–4.72 (m, 1H, CH), 6.98–7.05 (m, 1H, CH, indole), 7.05–7.10 (m, 1H, CH, indole), 7.11 (s, 1H, CH, indole), 7.32 (d, J = 7.7 Hz, 1H, CH, indole), 7.62 (d, J = 7.7 Hz, 1H, CH, indole). — ^{13}C-NMR (CD_3OD, 75 MHz): δ = 22.37 (+, CH_3), 26.43 (–, CH_2), 28.66 (–, CH_2), 55.26 (+, CH), 57.44 (+, CH), 110.77 (C_q, indole), 112.32 (+, CH, indole), 119.40 (+, CH, indole), 119.94 (+, CH, indole), 122.49 (+, CH, indole), 124.70 (+, CH, indole), 128.81 (C_q, indole), 138.08 (C_q, indole), 172.22 (C_q=O), 173.85 (C_q=O), 176.57 (C_q=O). — HRMS (ESI$^+$): m/z = $[C_{16}H_{20}N_4O_3S + H^+]^+$ calculated 349.1329; found 349.1329.

III.4.2.2 Synthesis of ***Zn-Cyclen$_2$***

Starting from Boc-protected bis-cyclen **3**[40] (Scheme S3.2), dimer **5** was prepared by nucleophilic aromatic substitution with diamine **4**. Deprotection of **5** and coordination of **6** with Zn^{2+} yielded complex **7**. Due to its sensitivity towards oxidation, the thiol function was generated in the very last step of the synthesis by reduction of the disulfide bond providing **Zn-Cyclen$_2$**.

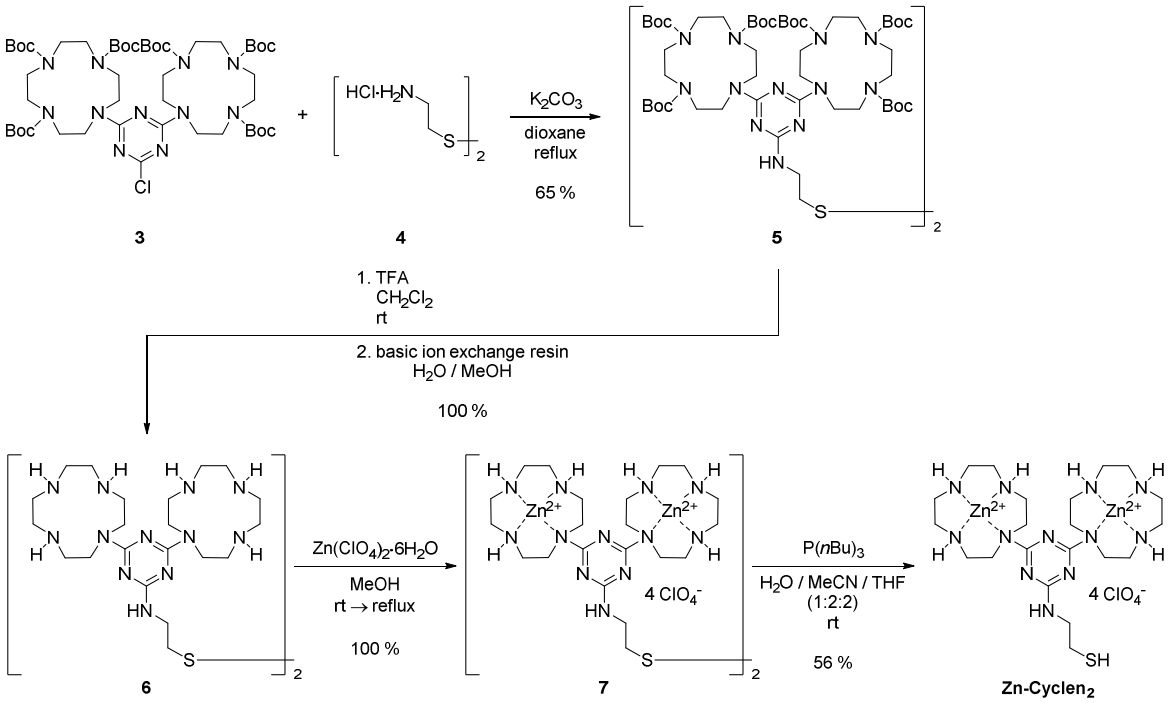

Scheme S3.2: Synthesis of thiolated bis-Zn^{2+}-cyclen complex **Zn-Cyclen$_2$**.

III.4.2.2.1 *N*,*N*′-(2,2′-Disulfanediylbis(ethane-2,1-diyl))bis(4,6-di(1,4,7,10-tetraazacyclododecan-1,4,7-tricarboxylic acid tri-*tert*-butyl ester-1-yl)-[1,3,5]-triazine-2-amine) (**5**)

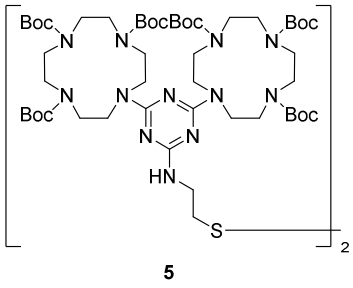

To a solution of bis-cyclen **3**[40] (300 mg, 0.284 mmol, 2.00 eq) and cystamine dihydrochloride (**4**, 32.0 mg, 0.142 mmol, 1.00 eq) in 1,4-dioxane (5.0 mL), potassium carbonate (193 mg, 1.42 mmol, 10.0 eq) was added. The reaction mixture was stirred at 120 °C for 14 h resulting in the formation of a fine white precipitate. Subsequently, the solvent was evaporated under reduced pressure and the obtained white residue was purified by column chromatography (SiO_2, EtOAc/PE 1:1) to yield disulfide **5** as white solid (203 mg, 0.093 mmol, 65 %).

R_f = 0.43 (EtOAc/PE 1:1). — MP: 126–132 °C. — ^{1}H-NMR ($CDCl_3$, 300 MHz): δ = 1.35 (br

s, 36H, 4 × Boc), 1.37 (s, 72H, 8 × Boc), 2.74 (t, J = 5.5 Hz, 4H, 2 × CH_2S), 3.03–3.73 (br m, 68H, 32 × CH_2, cyclen, 2 × NHCH_2), 4.91–5.40 (m, 2H, 2 × NH). ^{13}C-NMR ($CDCl_3$, 75 MHz): δ = 28.44 (+, Me, Boc), 28.47 (+, Me, Boc), 38.05 (–, $NHCH_2CH_2S$), 39.27 (–, $NHCH_2CH_2S$), 50.28 (–, br, CH_2, cyclen), 79.74 (C_qMe$_3$, Boc), 79.87 (C_qMe$_3$, Boc), 156.30 (br, C_q=O, Boc), 165.60 (C_q, triazine). — MS (ESI$^+$, CH_2Cl_2/MeOH + 10 mM NH_4OAc): *m/z* (%) = 1097.3 (100) $[M + 2H^+]^{2+}$, 2193.0 (11) $[M + H^+]^+$.

III.4.2.2.2 *N*,*N*′-(2,2′-Disulfanediylbis(ethane-2,1-diyl))bis(4,6-di(1,4,7,10-tetraazacyclododecan-1-yl)-[1,3,5]-triazine-2-amine) (**6**)

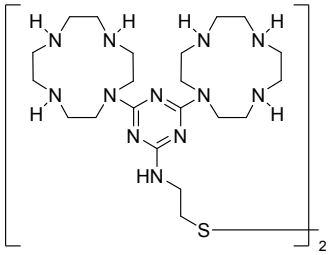

6

To a solution of disulfide **5** (190 mg, 0.087 mmol, 1.00 eq) in CH_2Cl_2 (6.0 mL), TFA (565 mg, 0.38 mL, 4.96 mmol, 57.0 eq) was added. The reaction mixture was stirred at rt (21 °C) for 17 h. The solvent was then removed under reduced pressure providing the TFA salt of **6** as yellowish oil. A strong basic ion exchange resin was swollen in H_2O/MeOH (1:1) for 15 min and washed neutral with H_2O. A column was charged with the swollen resin (2.10 mL, 1.89 mmol hydroxy equivalents at a given capacity of 0.9 mmol/mL, 22.0 eq). Subsequently, a solution of the TFA salt of **6** in H_2O/MeOH (10:1, 10 mL) was given onto the column and eluated with additional H_2O/MeOH (10:1, 10 mL). The eluate was lyophilized to yield tetra-cyclen **6** as light brown solid (86 mg, 0.087 mmol, 100 %).

MP: 120–125 °C. — ^{1}H-NMR (CD_3OD, 300 MHz): δ = 2.62–2.71 (m, 16H, 8 × CH_2, cyclen), 2.71–2.79 (m, 16H, 8 × CH_2, cyclen), 2.85–3.07 (m, 20H, 8 × CH_2, cyclen, 2 × CH_2S), 3.65 (t, J = 6.9 Hz, 4H, 2 × NHCH_2CH_2S), 3.69–3.81 (m, 16H, 8 × CH_2, cyclen). ^{13}C-NMR (CD_3OD, 75 MHz): δ = 39.55 (–, $NHCH_2CH_2S$), 41.08 (–, $NHCH_2CH_2S$), 46.55 (–, br, CH_2, cyclen), 47.08 (–, br, CH_2, cyclen), 49.26 (–, br, CH_2, cyclen), 49.33 (–, br, CH_2, cyclen), 166.98 (br, C_q, triazine), 167.98 (br, C_q, triazine). — MS (ESI$^+$): *m/z* (%) = 248.68 (100) $[M + 4H^+]^{4+}$, 331.24 (33) $[M + 3H^+]^{3+}$, 496.35 (6) $[M + 2H^+]^{2+}$.

III.4.2.2.3 *N*,*N*′-(2,2′-Disulfanediylbis(ethane-2,1-diyl))bis(4,6-di(1,4,7,10-tetraazacyclododecan-1-yl)-[1,3,5]-triazine-2-amine)-tetra-zinc(II)-octa-perchlorate (**7**)

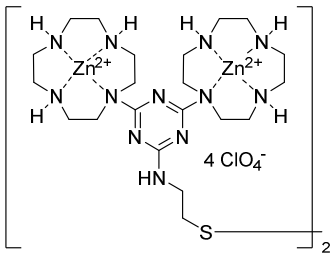

7

A solution of zinc(II) perchlorate hexahydrate (97 mg, 0.260 mmol, 4.20 eq) in MeOH (2.0 mL) was slowly added to a solution of tetra-cyclen **6** (61 mg, 0.062 mmol, 1.00 eq) in MeOH (3.5 mL) resulting in the formation of a white precipitate. The reaction mixture was stirred at rt (21 °C) for 20 h and then heated to 80 °C for further 17 h. The solvent was removed *in vacuo* providing compound **7** as yellowish residue (127 mg, 0.062 mmol, 100 %).

^{1}H-NMR (CD_3CN, 400 MHz): δ = 2.70–3.83 (br m, 72H, 32 × CH_2, cyclen, 2 × NHC*H*$_2$C*H*$_2$S), 3.94–4.10 (m, 4H, 4 × NH, cyclen), 4.23–4.42 (m, 8H, 8 × NH, cyclen), 6.52 (t, J = 5.7 Hz, 2H, 2 × N*H*CH_2CH_2S). ^{13}C-NMR (CD_3CN, 101 MHz): δ = 38.35 (–, $NHCH_2CH_2S$), 40.74 (–, $NHCH_2CH_2S$), 44.62 (–, br, CH_2, cyclen), 46.14 (–, br, CH_2, cyclen), 46.97 (–, br, CH_2, cyclen), 48.85 (–, br, CH_2, cyclen), 166.79 (C_q, triazine), 171.26 and 171.63 (C_q, triazine, tautomers). — MS (ESI^+, H_2O/MeCN): *m/z* (%) = 372.2 (34) $[M^{8+} + 4AcO^-]^{4+}$, 515.9 (100) $[M^{8+} + 5AcO^-]^{3+}$, 529.1 (85) $[M^{8+} + 4AcO^- + ClO_4^-]^{3+}$.

III.4.2.2.4 2-(4,6-Di(1,4,7,10-tetraazacyclododecan-1-yl)-1,3,5-triazin-2-ylamino)ethane-thiol-di-zinc(II)-tetra-perchlorate (**Zn-Cyclen$_2$**)

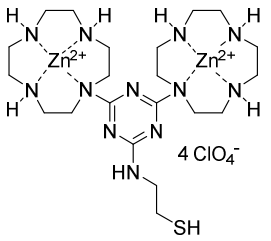

Zn-Cyclen$_2$

Disulfide **7** (51 mg, 0.025 mmol, 1.00 eq) was dissolved in a mixture of H_2O/MeCN/THF (1:2:2, 1.0 mL). The solution was degassed by bubbling nitrogen through it for 5 min. Tri-*n*-butylphosphine (18 mg, 0.088 mmol, 3.50 eq) was slowly added and the reaction mixture was

stirred at rt (21 °C) for 20 min. After evaporation of the solvents, the resulting residue was redissolved in MeCN (2.0 mL), H_2O (10 mL) was added and the aqueous mixture was extracted with CH_2Cl_2 (5 × 10 mL). Lyophilization of the aqueous phase yielded free thiol **Zn-Cyclen$_2$** as pale yellow solid (29 mg, 0.028 mmol, 56 %).

MP: > 150 °C (Decomposition). — ^{1}H-NMR (CD_3CN, 400 MHz): δ = 2.60–3.87 (br m, 36H, 16 × CH_2-cyclen, NHC*H*$_2$C*H*$_2$SH), 3.89–5.05 (br m, 6H, 6 × NH, cyclen), 5.70–6.30 (br m, 1H, N*H*CH_2CH_2SH). ^{13}C-NMR (CD_3CN, 101 MHz): δ = 42.99 (–, $NHCH_2CH_2SH$), 44.65 (–, $NHCH_2CH_2SH$), 46.18 (–, br, CH_2, cyclen), 46.52 (–, br, CH_2, cyclen), 46.76 (–, br, CH_2, cyclen), 47.09 (–, br, CH_2, cyclen), 166.92 (C_q, triazine), 171.26 and 172.25 (C_q, triazine, tautomers). — MS (ESI$^+$, H_2O/MeOH + 10 mM NH_4OAc): *m/z* (%) = 343.2 (18) $[M^{4+} - H^+ + AcO^-]^{2+}$, 373.1 (9) $[M^{4+} + 2AcO^-]^{2+}$.

III.4.3 General Methods for Vesicle Preparation and Characterization

III.4.3.1 Preparation of Functionalizable Luminescent Vesicles

The surface-reactive luminescent vesicles were prepared analogously to formerly established protocols.[7a,14,26c]

In a small glass vessel, stock solutions of DSPC (2.00 mM in $CHCl_3$, 900 µL), amphiphilic fluorophore **Dans-C$_{12}$** or **CF-C$_{12}$** (1.00 mM in $CHCl_3$, 100 µL) and **Mal-C$_{16}$** (1.00 mM in $CHCl_3$, 100 µL) were mixed to yield a molar ratio of DSPC / fluorophore / **Mal-C$_{16}$** = 90:5:5. The organic solvent was evaporated under a gentle stream of nitrogen and the remaining film of amphiphiles was dried in high vacuum. Aqueous HEPES buffer solution (25 mM, pH 7.4, 1.00 mL) was added to obtain a total amphiphile concentration of 2.00 mM. The sample was sonicated for 5 min at room temperature (21 °C) resulting in a slightly turbid multilamellar vesicle suspension. A dispersion of unilamellar vesicles was obtained by extrusion through 100 nm pore size polycarbonate membranes with a LiposoFast liposome extruder from Avestin at 60 °C.

*III.4.3.2 Post-Functionalization of Vesicle Surfaces with **Cys-Trp**, **ETG** or **Zn-Cyclen$_2$***

DSPC vesicles **V-Dans** or **V-CF** containing maleimide **Mal-C$_{16}$** (5.0 mol-%) and one of the amphiphilic fluorescent dyes **Dans-C$_{12}$** or **CF-C$_{12}$** (5.0 mol-% in each case) were prepared. 50–100 μL of the non-functionalized vesicle solution were diluted 5–10-fold with HEPES buffer (25 mM, pH 7.4, 1.00 mL) in a fluorescence cuvette. An appropriate volume of stock solutions of thiols **Cys-Trp** (1.00 mM), **ETG** (5.00 mM) or **Zn-Cyclen$_2$** (1.00 mM) in HEPES buffer was added yielding a thiol concentration of 2.0–7.5 mol-% with respect to the total concentration of the amphiphiles. The reaction mixture was left at room temperature (21 °C) and agitated from time to time. In order to monitor the functionalization process, fluorescence spectra of the vesicle solution were measured after certain time intervals. The surface functionalization reaction was completed after 0.5–2 h.

III.4.3.3 Imprinting of Vesicle Surfaces

For imprinting experiments, a stock solution of **Zn-Cyclen$_2$** (1.00 mM, 1.0–2.0 μL, equates to 1.0–2.0 mol-%) in HEPES buffer was added to a stock solution of the template **Pep-P-His** (1.00 mM, 0.5–1.0 μL, corresponds to 0.5 equivalents with respect to the receptor concentration). This mixture was then incubated with the vesicle dispersion **V-CF** (50 μL, diluted 10-fold with 450 μL of HEPES buffer) as described above. After completion of the functionalization reaction, the sample was subjected to size-exclusion chromatography (SEC, see below) in order to remove the template molecules. For control experiments with non-imprinted vesicles, the peptide **Pep-P-His** (same amount as above) was added to the vesicle solution after surface functionalization with **Zn-Cyclen$_2$** and likewise removed by SEC.

III.4.3.4 Size-Exclusion Chromatography (SEC) of Vesicles

Sephadex LH-20 gel was swollen in HEPES buffer and placed in a small syringe (1.25 mL gel volume). Excessive buffer solution was removed by centrifugation at 4400 rpm for 30 s. The vesicle solution (500 μL) was then placed on top of the gel bed. The mini column was centrifuged at 2000 rpm for 2 min and the eluate was collected in an Eppendorf tube.

III.4.3.5 Aptamer-Functionalization of Vesicle Surfaces

A stock solution of the thiolated aptamer **Apt-Amp** (0.10 mM, 2.5–10 μL, equates to 0.5–2.0 mol-%) was mixed with an aqueous solution of the disulfide reducing agent tris(2-carboxyethyl)phosphine hydrochloride[41] (TCEP, 1.00 mM, 1.25–5.0 μL, corresponds to 5.0 equivalents with respect to the amount of **Apt-Amp**) and left at room temperature (21 °C) for 20 min. This mixture was then added to 25 μL of the freshly prepared vesicle solution **V-CF**, diluted 20-fold with HEPES buffer yielding a total volume of 500 μL, in a fluorescence cuvette. The reaction mixture was left at room temperature and agitated from time to time. In order to monitor the functionalization process, fluorescence spectra of the vesicle solution were measured after certain time intervals. The surface functionalization reaction was completed after approximately 2 h. For determination of the fluorescence response in presence of the target, a stock solution of ampicillin or of control analytes (0.10 mM, 2.0 μL) in HEPES buffer was added and time-dependent fluorescence spectra were recorded until a stabilization of the emission signal was observed.

*III.4.3.6 Calculation of Concentration of Surface-Accessible **Mal-C$_{16}$***

With the assumption that the membrane-embedded maleimides **Mal-C$_{16}$** distribute equally between the outer and the inner surface of the vesicles with a radius of *r* nm and a bilayer thickness of 5 nm,[42] the concentration of surface-accessible maleimide was estimated according to the following equation:

$$[M]_{out} = \frac{r^2}{r^2 + (r-5)^2}[M]_{total}$$

III.4.3.7 Determination of Reaction Kinetics

Based on the integrated form for the second-order rate law and the assumption of a linear relationship between the concentration of the formed addition product *P* and the change of the fluorescence signal

$$\Delta I_{\max} = \varepsilon[P]_t = \varepsilon\left([T]_0 - [T]_t\right),$$

the apparent second-order rate constants k_{obs} were obtained by non-linear curve fitting of the time-dependent fluorescence data according to the following equation:

$$\Delta I_{max} = \varepsilon \frac{[T]_0[M]_0\left(e^{([T]_0-[M]_0)k_{obs}t}-1\right)}{[T]_0 e^{([T]_0-[M]_0)k_{obs}t}-[M]_0}$$

where t: reaction time

$[T]_0$: initial concentration of thiol

$[M]_0$: initial concentration of surface-accessible **Mal-C$_{16}$**

III.4.3.8 Determination of Binding Constants

A freshly prepared solution of receptor-functionalized vesicles **V-CF-Zn** (500–1000 μL) was filled into a fluorescence cuvette. Aliquots (0.5–5.0 μL) of the analyte stock solutions (0.20–1.00 mM) were added and the fluorescence spectrum was measured after each addition. All fluorescence spectra were corrected for dilution. Binding constants were obtained by non-linear curve fitting (ΔI_{max} *versus* total concentration of added analyte) using the mathematical expressions below.

III.4.3.8.1 Vesicular Sensor for Phosphates

On basis of the law of mass action and the assumption of a linear relationship between the concentration of the formed receptor–analyte complex and the change of the fluorescence signal ΔI_{max}, the apparent affinity constants K_a were obtained by non-linear curve fitting of the fluorescence titration data according to the following expression:[43]

$$\Delta I_{max} = \varepsilon \frac{[A]_0 + [R]_0 + 1/K_a - \sqrt{([A]_0 + [R]_0 + 1/K_a)^2 - 4[A]_0[R]_0}}{2}$$

where $[A]_0$: total concentration of analyte

$[R]_0$: total concentration of receptor

III.4.3.8.2 Imprinting Studies

For the estimation of the apparent binding constants K_a of the bivalent hexapeptide **Pep-P-His** by non-linear curve fitting, the following Hill equation was used:

$$\Delta I_{\max} = \frac{B_{\max}[A]_0^n}{1/K_a + [A]_0^n}$$

III.4.4 Dynamic Light Scattering of Vesicles

Vesicle size distributions were determined by dynamic light scattering. Figure S3.1 shows the typical size distribution of freshly extruded vesicles.

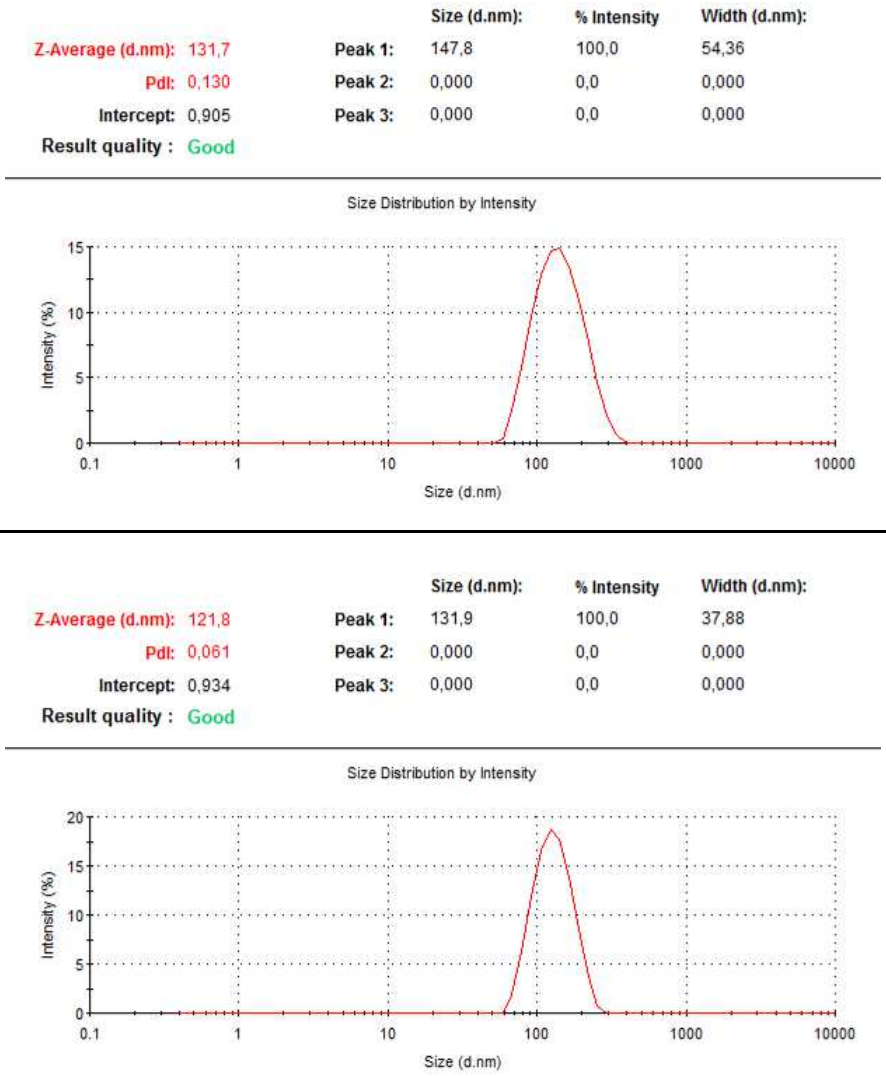

Figure S3.1: Typical size distribution of freshly prepared vesicles **V-Dans** (top) and **V-CF** (bottom).

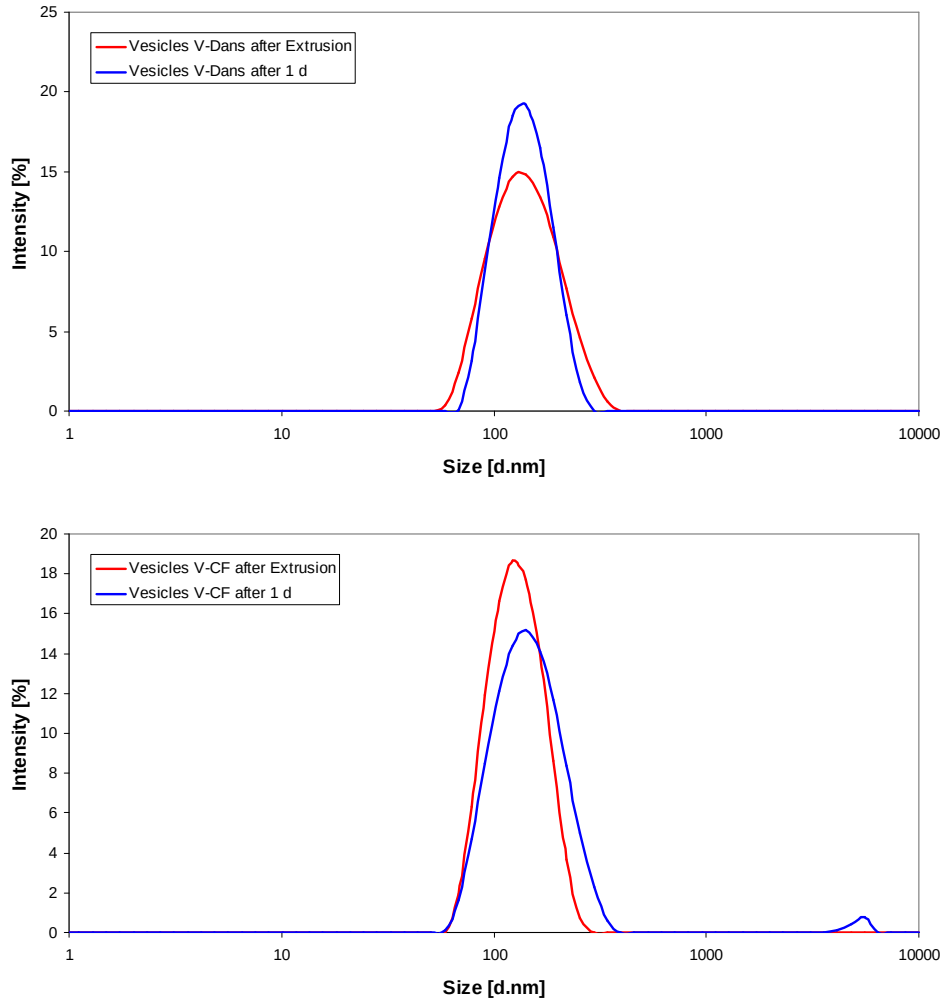

Figure S3.2: Comparison of size distribution of vesicles **V-Dans** (top) and **V-CF** (bottom) directly after extrusion (red curves) and after one day (blue curves).

III.4.5 Surface Functionalization of Vesicles with Cys-Trp or ETG

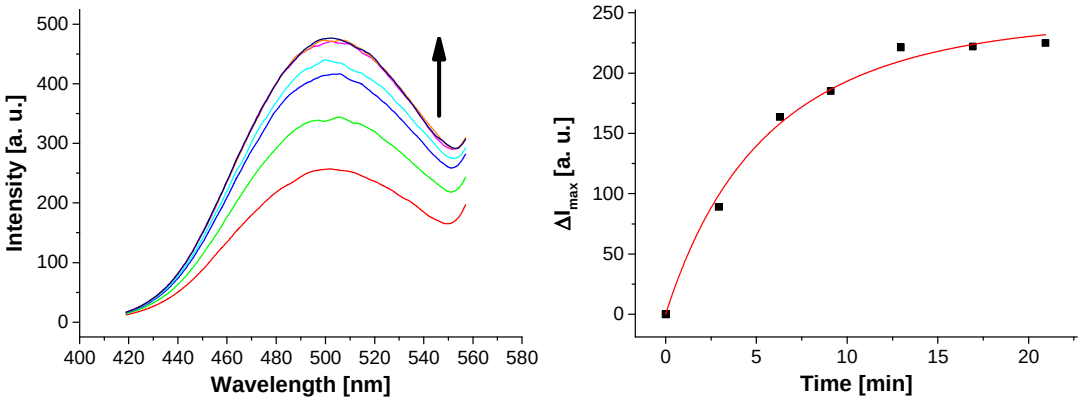

Figure S3.3: Time-dependent fluorescence spectra of vesicles **V-Dans** after addition of 7.5 mol-% of **ETG**; λ_{ex} = 280 nm.

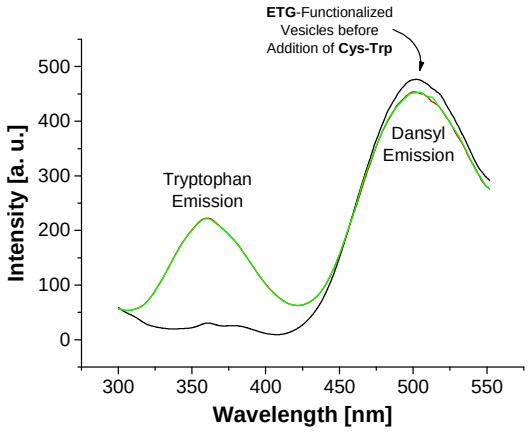

Figure S3.4: Time-dependent fluorescence spectra (0–7 min) after addition of 5.0 mol-% of peptide **Cys-Trp** to **ETG**-functionalized vesicles **V-Dans** from Figure S3.3; λ_{ex} = 280 nm.

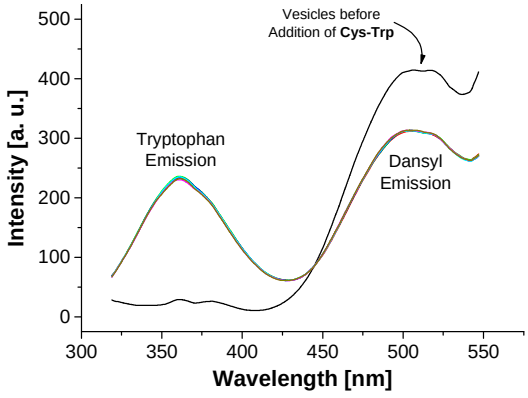

Figure S3.5: Time-dependent fluorescence spectra (0–17 min) of vesicles **V-Dans** lacking the maleimide **Mal-C_{16}** after addition of 7.5 mol-% of peptide **Cys-Trp**; λ_{ex} = 280 nm.

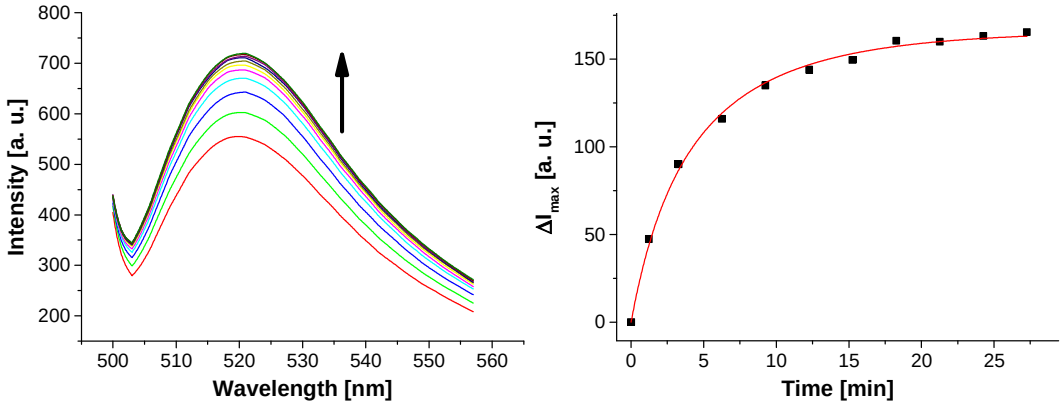

Figure S3.6: Time-dependent fluorescence spectra of vesicles **V-CF** after addition of 5.0 mol-% of **ETG**; λ_{ex} = 495 nm.

III.4.6 Post-Functionalization of Vesicles V-CF with Zn-Cyclen$_2$

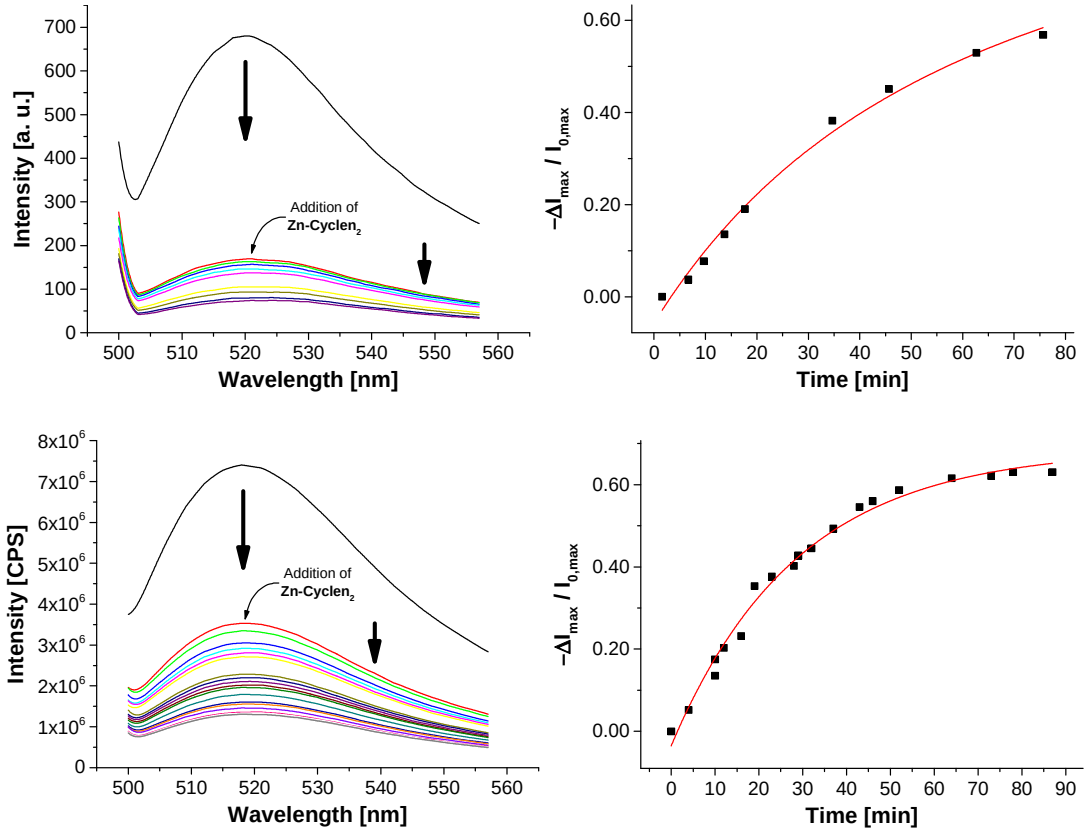

Figure S3.7: Functionalization progress of vesicles **V-CF** with **Zn-Cyclen$_2$** (top: 5.0 mol-%, bottom: 2.5 mol-%) in absence of PP_i; λ_{ex} = 495 nm.

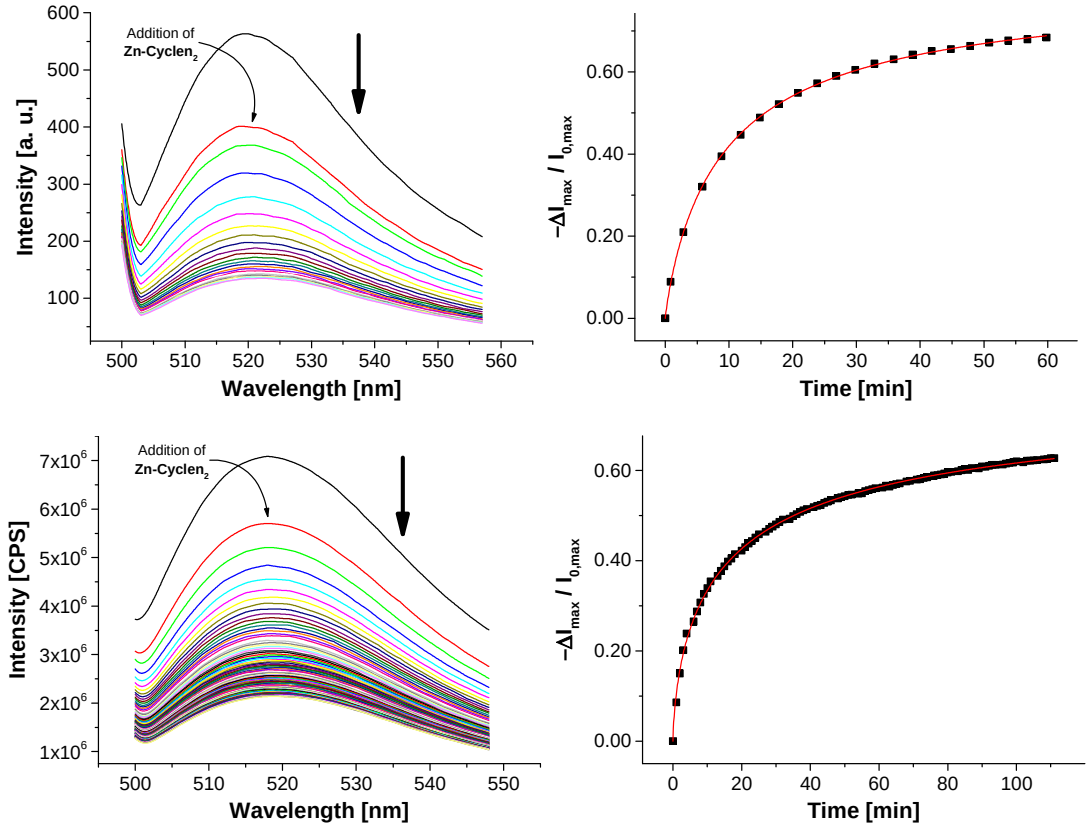

Figure S3.8: Functionalization progress of vesicles **V-CF** with **Zn-Cyclen$_2$** (top: 5.0 mol-%, bottom: 2.5 mol-%) in presence of PP_i (2.0 equivalents in each case with respect to **Zn-Cyclen$_2$**); λ_{ex} = 495 nm.

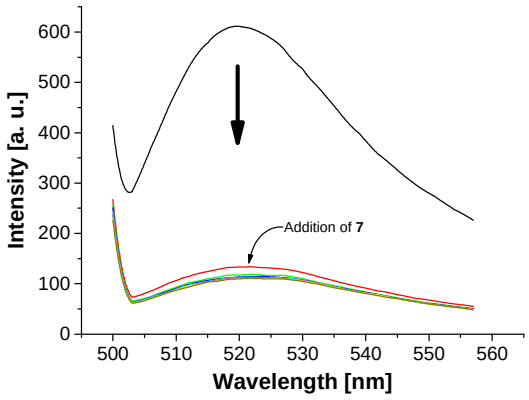

Figure S3.9: Time-dependent fluorescence response (0–15 min) of **V-CF** after addition of bis-Zn^{2+}-cyclen disulfide **7** (Scheme S3.2, 2.5 mol-%); λ_{ex} = 495 nm.

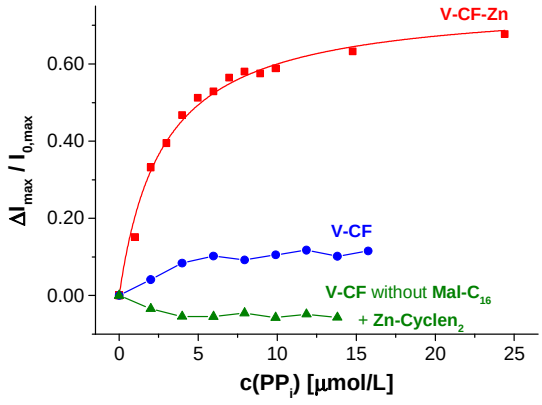

Figure S3.10: Fluorescence responses of functionalized vesicles **V-CF-Zn** (red squares), non-functionalized vesicles **V-CF** (blue dots) and **Mal-C_{16}**-lacking vesicles **V-CF** incubated with 1.5 mol-% of **Zn-Cyclen$_2$** (green triangles) upon titration with PP_i; λ_{ex} = 495 nm.

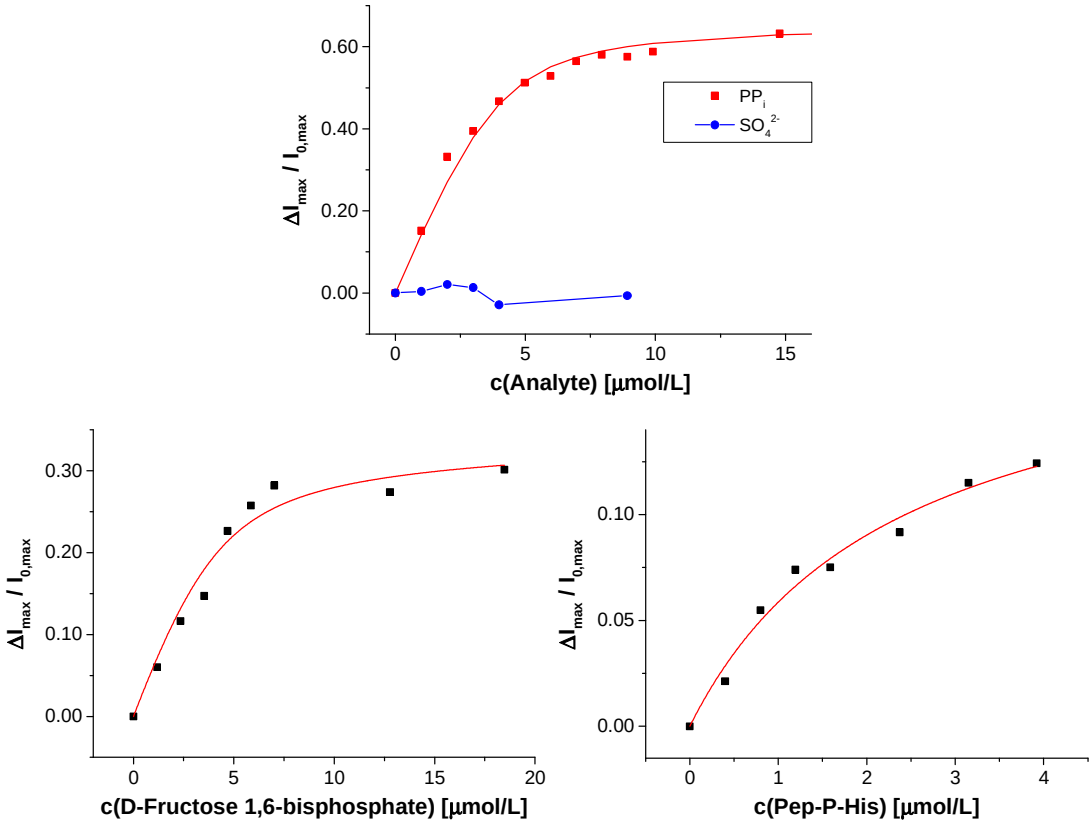

Figure S3.11: Binding isotherms of **V-CF-Zn** upon addition of different phosphates or Na_2SO_4; λ_{ex} = 495 nm.

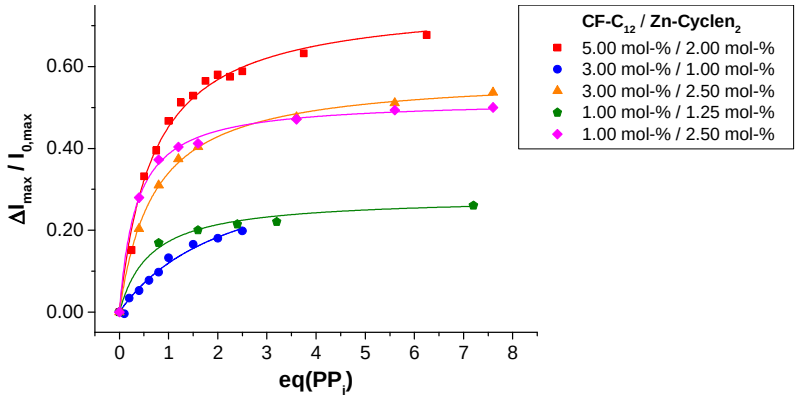

Figure S3.12: Dependency of the fluorescence response of **V-CF-Zn** after addition of PP_i on the dye and receptor concentrations on the vesicle surface; λ_{ex} = 495 nm.

III.4.7 Imprinting of Vesicle Surfaces with Bivalent Peptide Pep-P-His

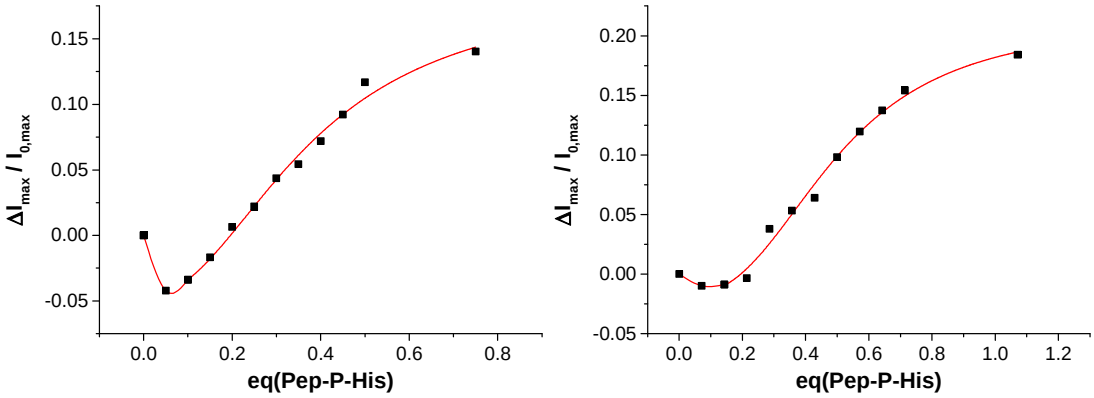

Figure S3.13: Rebinding isotherms of vesicles **V-CF** functionalized with 0.8 equivalents of **Zn-Cyclen$_2$** receptor (with respect to surface-accessible **Mal-C$_{16}$**) in presence (left) and absence (right) of the template **Pep-P-His**; λ_{ex} = 495 nm.

III.4.8 Vesicle Functionalization with an Aptamer for Ampicillin

III.4.8.1 Optimization of Buffer System

For the investigation of the stability of non-functionalized vesicles **V-CF**, we prepared vesicle solutions in different buffer systems and determined their size distribution by DLS directly after extrusion (Table S3.1).

Table S3.1: DLS measurement results of vesicles **V-CF** in different buffer systems.

Entry	Buffer	Added Salts	Z-Average [nm]	PDI	Peak 1 [nm]	Peak 2 [nm]
1	TRIS (20 mM, pH 8.0)	KCl (5 mM), $MgCl_2$ (5 mM)	208.4	0.274	257.3 (98.0 %)	4946 (2.0 %)
2	TRIS (20 mM, pH 8.0)	NaCl (50 mM), KCl (5 mM), $MgCl_2$ (5 mM)	208.3	0.655	128.9 (54.5 %)	1797 (45.5 %)
3	HEPES (25 mM, pH 7.4)	–	121.8	0.061	131.9 (100 %)	–
4	HEPES (25 mM, pH 7.4)	$MgCl_2$ (5 mM)	271.2	0.562	133.2 (41.7 %)	825.1 (58.3 %)
5	HEPES (25 mM, pH 7.4)	KCl (5 mM), $MgCl_2$ (5 mM)	185.6	0.212	213.9 (97.9 %)	4829 (2.1 %)
6	HEPES (25 mM, pH 7.4)	NaCl (50 mM), KCl (5 mM), $MgCl_2$ (5 mM)	755.3	0.861	505.6 (95.7 %)	5560 (4.3 %)

The best stability of vesicles was observed in HEPES buffer without added salts. Under those conditions however, no fluorescence response was observed after addition of ampicillin to aptamer-functionalized vesicles **V-CF-Amp** (Table S3.2). This result shows that the presence of certain cations is essential for the ability of the aptamer to bind to ampicillin. In buffer systems which resulted in significant aggregation of the vesicles, also non-specific fluorescence responses of aptamer-functionalized vesicles upon addition of the control analyte benzylpenicillin was obtained.

Table S3.2: Relative fluorescence response and specificity of **V-CF-Amp** after addition of ampicillin or benzylpenicillin (0.40 μM in each case).

Entry	Buffer	Added Salts	Ampicillin	Benzyl-penicillin
1	TRIS (20 mM, pH 8.0)	KCl (5 mM), $MgCl_2$ (5 mM)	3 %	n. d.
2	TRIS (20 mM, pH 8.0)	NaCl (50 mM), KCl (5 mM), $MgCl_2$ (5 mM)	17 %	6 %
3	HEPES (25 mM, pH 7.4)	–	3 %	n. d.
4	HEPES (25 mM, pH 7.4)	$MgCl_2$ (5 mM)	9 %	5 %
5	HEPES (25 mM, pH 7.4)	KCl (5 mM), $MgCl_2$ (5 mM)	50 %	–2 %
6	HEPES (25 mM, pH 7.4)	NaCl (50 mM), KCl (5 mM), $MgCl_2$ (5 mM)	no response	n. d.

n. d.: not determined

III.4.8.2 Variation of Aptamer Concentration on the Surface

For comparison to vesicles **V-CF** functionalized with 2.0 mol-% of the aptamer **Apt-Amp**, we also prepared vesicles with 0.5 mol-% of **Apt-Amp** on the surface and investigated their fluorescence response after addition of ampicillin (Figure S3.14).

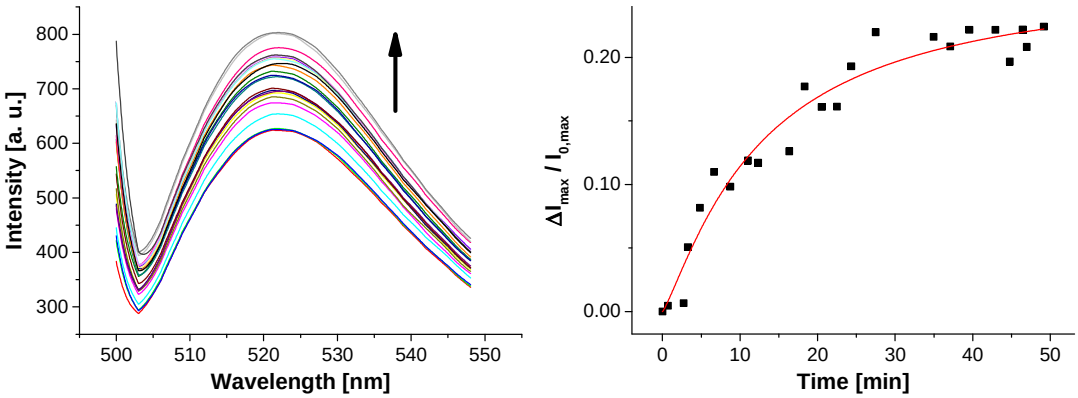

Figure S3.14: Time-dependent change of fluorescence emission of aptamer-functionalized vesicles **V-CF-Amp** (0.5 mol-% of **Apt-Amp**) after addition of ampicillin (0.40 μM); λ_{ex} = 495 nm.

III.4.8.3 Vesicle Size Distribution after Aptamer-Functionalization and Addition of Ampicillin

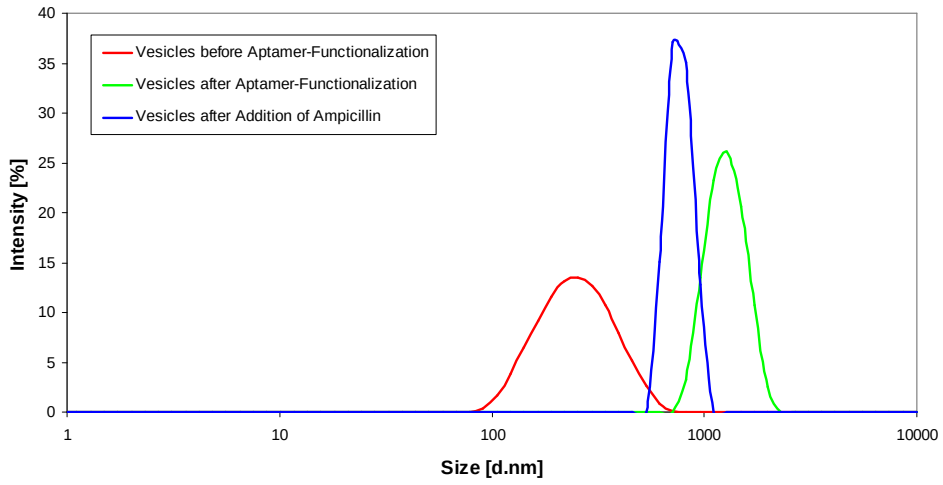

Figure S3.15: Comparison of vesicle size distribution before aptamer-functionalization of **V-CF** (red curve), after functionalization with **Apt-Amp** (green curve) and after addition of ampicillin to functionalized liposomes **V-CF-Amp** (blue curve).

III.5 Notes and Reference

[1] a) J. Voskuhl, B. J. Ravoo, "Molecular recognition of bilayer vesicles", *Chem. Soc. Rev.* **2009**, *38*, 495–505; b) K. Ariga, H. Ito, J. P. Hill, H. Tsukube, "Molecular recognition: from solution science to nano/materials technology", *Chem. Soc. Rev.* **2012**, *41*, 5800–5835.

[2] a) K. A. Edwards, A. J. Baeumner, "Liposomes in analyses", *Talanta* **2006**, *68*, 1421–1431; b) Q. Liu, B. J. Boyd, "Liposomes in biosensors", *Analyst* **2013**, *138*, 391–409.

[3] R. Martínez-Máñez, F. Sancenón, "Fluorogenic and Chromogenic Chemosensors and Reagents for Anions", *Chem. Rev.* **2003**, *103*, 4419–4476.

[4] B. Gruber, S. Stadlbauer, K. Woinaroschy, B. König, "Luminescent vesicular receptors for the recognition of biologically important phosphate species", *Org. Biomol. Chem.* **2010**, *8*, 3704–3714.

[5] T. W. Bell, N. M. Hext, "Supramolecular optical chemosensors for organic analytes", *Chem. Soc. Rev.* **2004**, *33*, 589–598.

[6] B. T. Nguyen, E. V. Anslyn, "Indicator–displacement assays", *Coord. Chem. Rev.* **2006**, *250*, 3118–3127.

[7] a) B. Gruber, S. Stadlbauer, A. Späth, S. Weiss, M. Kalinina, B. König, "Modular Chemosensors from Self-Assembled Vesicle Membranes with Amphiphilic Binding Sites and Reporter Dyes", *Angew. Chem. Int. Ed.* **2010**, *49*, 7125–7128; *Angew. Chem.* **2010**, *122*, 7280–7284; b) S. Banerjee, M. Bhuyan, B. König, "Tb(III) functionalized vesicles for phosphate sensing: membrane fluidity controls the sensitivity", *Chem. Commun.* **2013**, *49*, 5681–5683.

[8] a) M. Mammen, S.-K. Choi, G. M. Whitesides, "Polyvalent Interactions in Biological Systems: Implications for Design and Use of Multivalent Ligands and Inhibitors", *Angew. Chem. Int. Ed.* **1998**, *37*, 2754–2794; *Angew. Chem.* **1998**, *110*, 2908–2953; b) H. Jung, A. D. Robison, P. S. Cremer, "Multivalent ligand–receptor binding on supported lipid bilayers", *J. Struct. Biol.* **2009**, *168*, 90–94; c) A. Grochmal, E. Ferrero, L. Milanesi, S. Tomas, "Modulation of In-Membrane Receptor Clustering upon Binding of Multivalent Ligands", *J. Am. Chem. Soc.* **2013**, *135*, 10172–10177.

[9] a) L. Nobs, F. Buchegger, R. Gurny, E. Allémann, "Current Methods for Attaching Targeting Ligands to Liposomes and Nanoparticles", *J. Pharm. Sci.* **2004**, *93*, 1980–1992; b) V. P. Torchilin, "Recent advances with liposomes as pharmaceutical carriers", *Nat. Rev. Drug Discovery* **2005**, *4*, 145–160; c) F. S. Hassane, B. Frisch, F. Schuber, "Targeted Liposomes: Convenient Coupling of Ligands to Preformed Vesicles Using 'Click Chemistry'", *Bioconjugate Chem.* **2006**, *17*, 849–854; d) R. I. Jølck, L. N. Feldborg, S. Andersen, S. M. Moghimi, T. L. Andresen, "Engineering Liposomes and Nanoparticles for Biological Targeting", *Adv. Biochem. Engin./Biotechnol.* **2011**, *125*, 251–280.

[10] a) C. E. Hoyle, C. N. Bowman, "Thiol–Ene Click Chemistry", *Angew. Chem. Int. Ed.* **2010**, *49*, 1540–1573; *Angew. Chem.* **2010**, *122*, 1584–1617; b) C. E. Hoyle, A. B. Lowe, C. N. Bowman, "Thiol-click chemistry: a multifaceted toolbox for small molecule and polymer synthesis", *Chem. Soc. Rev.* **2010**, *39*, 1355–1387.

[11] V. D. Bock, H. Hiemstra, J. H. van Maarseveen, "Cu^{I}-Catalyzed Alkyne–Azide 'Click' Cycloadditions from a Mechanistic and Synthetic Perspective", *Eur. J. Org. Chem.* **2006**, 51–68.

[12] C. E. Hoyle, T. Y. Lee, T. Roper, "Thiol–Enes: Chemistry of the Past with Promise for the Future", *J. Polym. Sci., Part A: Polym. Chem.* **2004**, *42*, 5301–5338.

[13] a) B. Frisch, C. Boeckler, F. Schuber, "Synthesis of Short Polyoxyethylene-Based Heterobifunctional Cross-Linking Reagents. Application to the Coupling of Peptides to Liposomes", *Bioconjugate Chem.* **1996**, *7*, 180–186.; b) P. Schelte, C. Boeckler, B. Frisch, F. Schuber, "Differential Reactivity of Maleimide and Bromoacetyl Functions with Thiols: Application to the Preparation of Liposomal Diepitope Constructs", *Bioconjugate Chem.* **2000**, *11*, 118–123; c) R. J. Pounder, M. J. Stanford, P. Brooks, S. P. Richards, A. P. Dove, "Metal free thiol–maleimide 'Click' reaction as a mild functionalisation strategy for degradable polymers", *Chem. Commun.* **2008**, 5158–5160.

[14] A. Müller, B. König, "Vesicular aptasensor for the detection of thrombin", *Chem. Commun.* **2014**, *50*, 12665–12668; see also Chapter V.

[15] Y. Kitano, Y. Nogata, K. Matsumura, E. Yoshimura, K. Chiba, M. Tada, I. Sakaguchi, "Design and synthesis of anti-barnacle active fluorescence-labeled probe compounds and direct observation of the target region in barnacle cypris larvae for dimethyl-isocyanoalkyl compounds", *Tetrahedron* **2005**, *61*, 9969–9973.

[16] P. Wu, L. Brand, "Resonance Energy Transfer: Methods and Applications", *Anal. Biochem.* **1994**, *218*, 1–13.

[17] J. Guy, K. Caron, S. Dufresne, S. W. Michnick, W. G. Skene, J. W. Keillor, "Convergent Preparation and Photophysical Characterization of Dimaleimide Dansyl Fluorogens: Elucidation of the Maleimide Fluorescence Quenching Mechanism", *J. Am. Chem. Soc.* **2007**, *129*, 11969–11977.

[18] For examples of optical probes for thiol detection, see: X. Chen, Y. Zhou, X. Peng, J. Yoon, "Fluorescent and colorimetric probes for detection of thiols", *Chem. Soc. Rev.* **2010**, *39*, 2120–2135.

[19] M. P. Lutolf, N. Tirelli, S. Cerritelli, L. Cavalli, J. A. Hubbell, "Systematic Modulation of Michael-Type Reactivity of Thiols through the Use of Charged Amino Acids", *Bioconjugate Chem.* **2001**, *12*, 1051–1056.

[20] J. Li, Q. Xu, D. M. Cortes, E. Perozo, A. Laskey, A. Karlin, "Reactions of cysteines substituted in the amphipathic N-terminal tail of a bacterial potassium channel with hydrophilic and hydrophobic maleimides", *Proc. Natl. Acad. Sci. U. S. A.* **2002**, *99*, 11605–11610.

[21] P. Schelté, C. Boeckler, B. Frisch, F. Schuber, "Differential Reactivity of Maleimide and Bromoacetyl Functions with Thiols: Application to the Preparation of Liposomal Diepitope Constructs", *Bioconjugate Chem.* **2000**, *11*, 118–123.

[22] a) T. Koike, S. Kajitani, I. Nakamura, E. Kimura, M. Shiro, "The Catalytic Carboxyester Hydrolysis by a New Zinc(II) Complex with an Alcohol-Pendant Cyclen (1-(2-Hydroxyethyl)-1,4,7,10-tetraazacyclododecane): A Novel Model for Indirect Activation of the Serine Nucleophile by Zinc(II) in Zinc Enzymes", *J. Am. Chem. Soc.* **1995**, *117*, 1210–1219; b) E. Kimura, S. Aoki, T. Koike, M. Shiro, "A Tris(Zn^{II}-1,4,7,10-tetraazacyclododecane) Complex as a New Receptor for Phosphate Dianions in

Aqueous Solution", *J. Am. Chem. Soc.* **1997**, *119*, 3068–3076; c) S. Aoki, M. Zulkefeli, M. Shiro, M. Kohsako, K. Takeda, E. Kimura, "A Luminescence Sensor of Inositol 1,4,5-Triphosphate and Its Model Compound by Ruthenium-Templated Assembly of a Bis(Zn^{2+}-Cyclen) Complex Having a 2,2'-Bipyridyl Linker (Cyclen = 1,4,7,10-Tetraazacyclododecane)", *J. Am. Chem. Soc.* **2005**, *127*, 9129–9139.

[23] Considering a total concentration of **Mal-C_{16}** of 5.0 mol-% and therefore a surface-accessible concentration of approximately 2.5 mol-%, 0.8 equivalents of **Zn-Cyclen$_2$** equate to 2.0 mol-% relating to the total amphiphile concentration.

[24] S. Lacerda, M. P. Campello, I. C. Santos, I. Santos, R. Delgado, "Study of the cyclen derivative 2-[1,4,7,10-tetraazacyclododecan-1-yl]-ethanethiol and its complexation behaviour towards d-transition metal ions", *Polyhedron* **2007**, *26*, 3763–3773.

[25] G. Wulff, "Molecular Imprinting in Cross-Linked Materials with the Aid of Molecular Templates – A Way towards Artificial Antibodies", *Angew. Chem., Int. Ed. Engl.* **1995**, *34*, 1812–1832; *Angew. Chem.* **1995**, *107*, 1958–1979.

[26] a) B. Gruber, S. Balk, S. Stadlbauer, B. König, "Dynamic Interface Imprinting: High-Affinity Peptide Binding Sites Assembled by Analyte-Induced Recruiting of Membrane Receptors", *Angew. Chem. Int. Ed.* **2012**, *51*, 10060–10063; *Angew. Chem.* **2012**, *124*, 10207–10210; b) S. Balk, B. König, "Thermally induced molecular imprinting of luminescent vesicles", *J. Inclusion Phenom. Macrocyclic Chem.* **2015**, *81*, 135–139; c) S. Banerjee, B. König, "Molecular Imprinting of Luminescent Vesicles", *J. Am. Chem. Soc.* **2013**, *135*, 2967–2970.

[27] M. Ueno, S. Katoh, S. Kobayashi, E. Tomoyama, S. Ohsawa, N. Koyama, Y. Morita, "Evaluation of Phase Transition Temperature of Liposomes by Using the Tautomerism of α-Benzoylacetoanilide", *J. Colloid Interface Sci.* **1990**, *134*, 589–592.

[28] A. Grauer, A. Riechers, S. Ritter, B. König, "Synthetic Receptors for the Differentiation of Phosphorylated Peptides with Nanomolar Affinities", *Chem. Eur. J.* **2008**, *14*, 8922–8927.

[29] In our previously reported dynamic imprinting approaches,[26] we observed a steady increase of the signal in both cases, however, with the different binding affinities being reflected in different slopes of the binding isotherms. We explain this with the dynamic nature of the receptor recruitment process in that case providing a diverse arrangement of the fluorophore molecules relative to the receptor assemblies.

[30] The lower value of lg K_a in case of non-imprinted vesicles compared to that from Table 3.3 might be attributed to an incomplete separation of the template peptide by the SEC in that case. However, as the exactly identical conditions for SEC were applied for both the imprinted vesicles and the non-imprinted control solutions, the relative change of the binding affinities has to be considered.

[31] a) S. D. Jayasena, "Aptamers: An Emerging Class of Molecules That Rival Antibodies in Diagnostics", *Clin. Chem.* **1999**, *45*, 1628–1650; b) C. K. O'Sullivan, "Aptasensors – the future of biosensing?", *Anal. Bioanal. Chem.* **2002**, *372*, 44–48.

[32] a) E. J. Cho, J.-W. Lee, A. D. Ellington, "Applications of Aptamers as Sensors", *Annu. Rev. Anal. Chem.* **2009**, *2*, 241–264; b) R. E. Wang, Y. Zhang, J. Cai, W. Cai, T. Gao, "Aptamer-Based Fluorescent Biosensors", *Curr. Med. Chem.* **2011**, *18*, 4175–4184.

[33] K.-M. Song, E. Jeong, W. Jeon, M. Cho, C. Ban, "Aptasensor for ampicillin using gold nanoparticle based dual fluorescence-colorimetric methods", *Anal. Bioanal. Chem.* **2012**, *402*, 2153–2161.

[34] S. Nir, J. Bentz, J. Wilschut, N. Duzgunes, "Aggregation and fusion of phospholipid vesicles", *Prog. Surf. Sci.* **1983**, *13*, 1–124.

[35] The surface-immobilized **Zn-Cyclen$_2$** complexes, on the other hand, are supposed to electrostaticly interact with the membrane-embedded carboxyfluorescein molecules resulting in a partial quenching of their fluorescence emission.

[36] Vesicle aggregation based on specific intermolecular interactions between surface-attached oligonucleotides is unlikely due to the absence of complementary sequences in the immobilized aptamer required for hybridization.

[37] We did not face that aggregation behavior in our previously reported studies regarding the vesicular thrombin-aptasensor.[14] There, the presence of Mg^{2+} was not required for the conformational stabilization of the oligonucleotides. As a result, a dynamic and quick fluorescence response over a wide concentration range was observed.

[38] a) R. Jue, J. M. Lambert, L. R. Pierce, R. R. Traut, "Addition of Sulfhydryl Groups to *Escherichia coli* Ribosomes by Protein Modification with 2-Iminothiolane (Methyl 4-Mercaptobutyrimidate)", *Biochemistry* **1978**, *17*, 5399–5406; b) R. Julian, S. Duncan, P. D. Weston, R. Wrigglesworth, "A New Reagent Which May Be Used to Introduce Sulfhydryl Groups into Proteins, and its Use in the Preparation of Conjugates for Immunoassay", *Anal. Biochem.* **1983**, *132*, 68–73.

[39] For detailed synthesis protocols, see the Novabiochem® Catalog.

[40] D. S. Turygin, M. Subat, O. A. Raitman, V. V. Arslanov, B. König, M. A. Kalinina, "Cooperative Self-Assembly of Adenosine and Uridine Nucleotides on a 2D Synthetic Template", *Angew. Chem. Int. Ed.* **2006**, *45*, 5340–5344; *Angew. Chem.* **2006**, *118*, 5466–5470.

[41] C. C. Visser, L. H. Voorwinden, L. R. Harders, M. Eloualid, L. van Bloois, D. J. A. Crommelin, M. Danhof, A. G. de Boer, "Coupling of Metal Containing Homing Devices to Liposomes via a Maleimide Linker: Use of TCEP to Stabilize Thiol-groups without Scavenging Metals", *J. Drug Target.* **2004**, *12*, 569–573.

[42] a) J. F. Nagle, S. Tristram-Nagle, "Structure of lipid bilayers", *Biochim. Biophys. Acta, Rev. Biomembr.* **2000**, *1469*, 159–195; b) P. Balgavý, M. Dubničková, N. Kučerka, M. A. Kiselev, S. P. Yaradaikin, D. Uhríková, "Bilayer thickness and lipid interface area in unilamellar extruded 1,2-diacylphosphatidylcholine liposomes: a small-angle neutron scattering study", *Biochim. Biophys. Acta, Biomembr.* **2001**, *1512*, 40–52.

[43] F. H. Stootman, D. M. Fisher, A. Rodger, J. R. Aldrich-Wright, "Improved curve fitting procedures to determine equilibrium binding constants", *Analyst* **2006**, *131*, 1145–1151.

CHAPTER IV:

ADDENDUM TO CHAPTER III – INVESTIGATIONS TOWARDS RADICAL THIOL–ENE ADDITIONS ON VESICLE SURFACES

IV.1 Introduction: Radical Addition of Thiols to Alkenes

For our investigations towards the surface functionalization of preformed vesicles by means of click chemistry, the applicability of the radical thiol–ene addition was tested. Since this reaction can be induced by UV light, it offers the possibility to temporally trigger the functionalization process by controlled exposure to a light source. A further advantage compared to other click reactions is its feasibility without the need of potentially toxic metal catalysts. In general, this reaction is tolerant to the presence of oxygen, can be performed in aqueous media and yields the corresponding thioether almost quantitatively.[1] Dependent on the reaction conditions and the chemical structure of the employed thiol and alkene components, thiol–ene additions can be extremely rapid and complete in a time scale of seconds. The radical thiol–ene reaction proceeds *via* a typical chain process with initiation, propagation and termination steps (Scheme S4.1).[1,2]

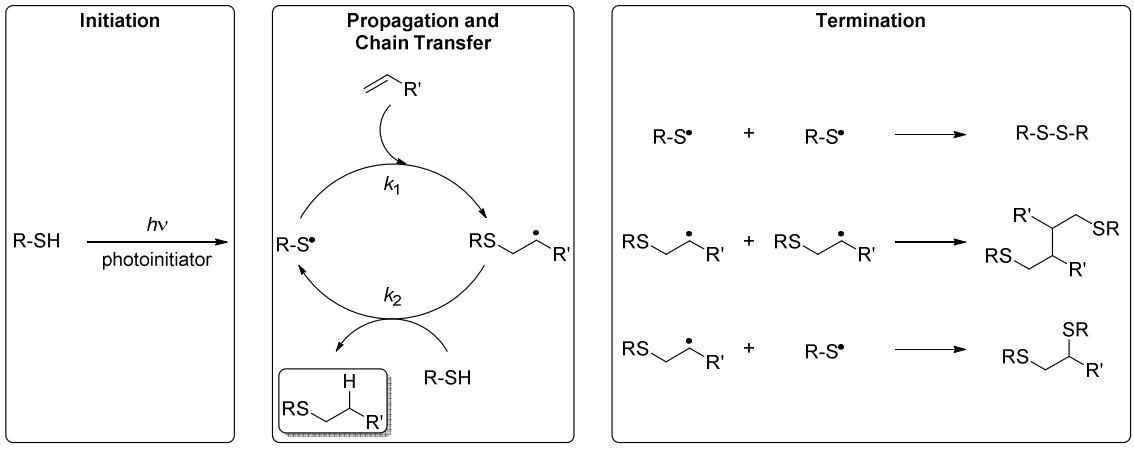

Scheme S4.1: Mechanism of the UV light-induced radical thiol–ene reaction.

Each of the single reaction steps influences the overall efficiency and therefore has to be taken into account for the optimization of the whole process. The generation of the reactive radicals can be induced by light of appropriate wavelength. Since thiol groups are able to absorb light in the UV range (at around 254 nm) followed by homolytic S–H cleavage, thiol–ene additions can be basically conducted by means of light-induced self-initiation, particularly in bulk systems. Better initiation efficiencies, however, are achieved by use of an external photoinitiator. Light-induced radical generation systems can be divided into two classes dependent on the mechanism of radical formation:[3] Norrish Type I photoinitiators undergo a homolytic bond cleavage (Scheme S4.2). Either or both of the formed radicals can then abstract a hydrogen atom from a thiol group. Norrish Type II systems initiate the thiol–ene

reaction by thiol-hydrogen abstraction in their excited state resulting in a thiyl radical and a non-reactive ketyl radical.

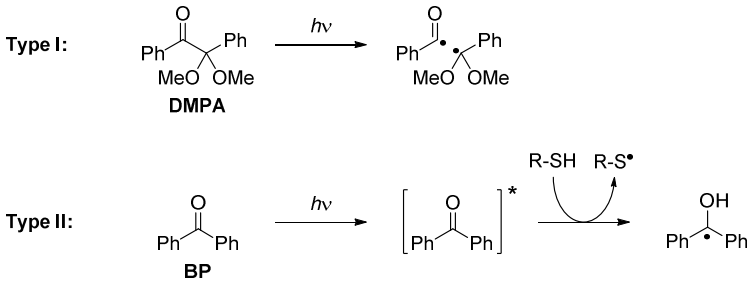

Scheme S4.2: **DMPA** and **BP** as examples for type I and II photoinitiators and mechanisms of UV light-induced radical formation.

In general, the efficiency of type I photoinitiators is higher compared to that of type II systems. The rate of the addition of the formed thiyl radicals to the alkene (k_1) relies on both the electrophilicity of the radical and the electron density of the envisaged carbon–carbon double bond. The rate of the chain transfer (k_2) in turn is dependent on the stability of the intermediate carbon-centered radical and thus its ability to abstract a hydrogen from another thiol. If these two steps in the reaction cycle are two slow compared to radical–radical recombinations, the formation of byproducts such as the disulfide can then dominate the overall process. Besides, disulfide formation can also occur *via* oxidation of the thiols by atmospheric oxygen.

For the applicability of the radial thiol–ene reaction in view of vesicular post-functionalization, the feasibility of this reaction type in aqueous solutions in the micromolar concentration range is a fundamental requirement. Therefore, we first attempted to find suitable reaction conditions in homogeneous solution within this limitation. As the reactivity at lipid–water interfaces can be different due to altered physico-chemical properties, the established conditions from homogenous media were examined for vesicular model systems in the next step. For our studies, the influence of several parameters such as light source and irradiation time, photoinitiator system, employed alkene component and presence of oxygen or of reducing agents was investigated.

IV.2 Experimental Part

IV.2.1 Materials and Syntheses

IV.2.1.1 Thiol Compounds

As simple model thiols for test reactions in homogeneous solution, cysteamine, cysteine and thioethylene glycol were used (Figure S4.1). Thiol-containing dansyl derivative **Dans-SH** served as fluorescent probe suitable for detection on TLC plates or for fluorescence spectroscopic analysis. Its synthesis was performed *via* the corresponding disulfide dimer starting from dansyl chloride according to the literature.[4] **Zn-Cyclen$_2$** was investigated as potential receptor unit for the preparation of vesicular phosphate sensors by means of post-functionalization.

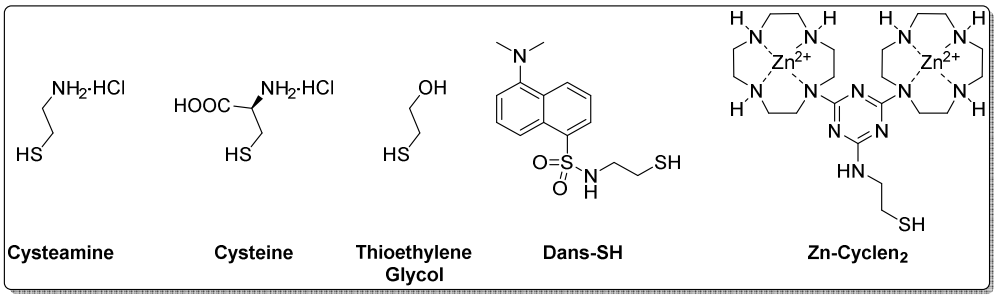

Figure S4.1: Different thiols used for model reactions.

IV.2.1.2 Amphiphilic Alkene Derivatives

Since the efficiency of the radical thiol–ene addition is highly dependent on the nature of the ene component, various amphiphilic alkenes (Scheme S4.3) were synthesized and tested. While butenyl ether **Ene4-C$_{18}$** is characterized by a higher electron density at the C–C double bond compared to that of allyl ether **Ene3-C$_{18}$**, **Norb-C$_{18}$** exhibits a considerable bond angle distortion resulting in a high ring strain which is relieved after hydrothiolation.[2]

Compound **1**[5] was synthesized following a literature protocol. Chlorotriazine **2** was obtained by nucleophilic substitution with aqueous ammonia. Further substitution of the remaining chlorine atom in **2** with different alcohols **3a–c** yielded amphiphilic alkenes **Ene3-C$_{18}$**, **Ene4-C$_{18}$** and **Norb-C$_{18}$**.

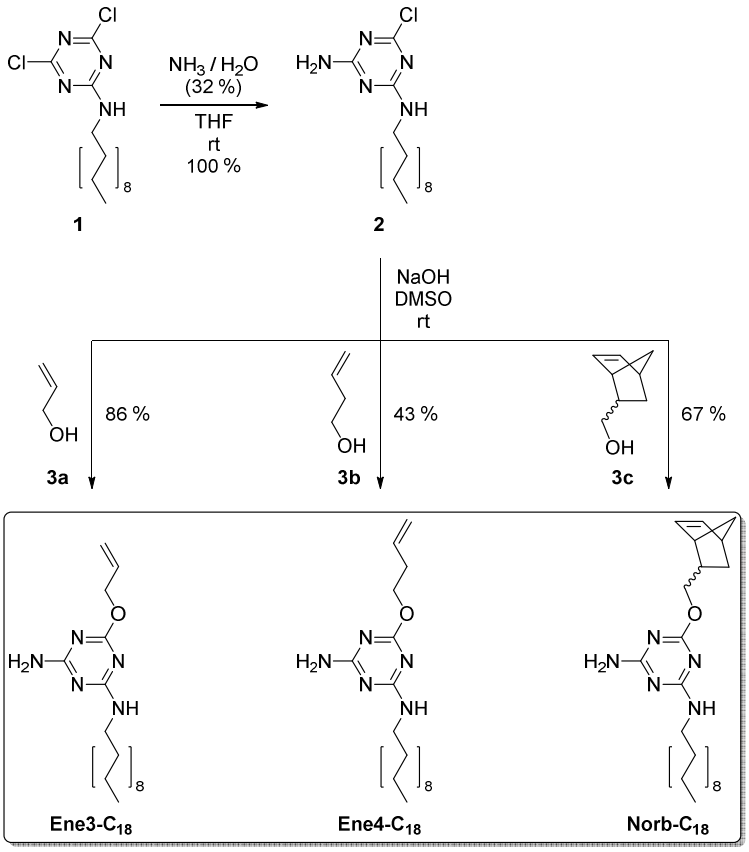

Scheme S4.3: Synthesis of amphiphilic alkenes used for radical thiol–ene model reactions.

IV.2.1.2.1 6-Chloro-N^2-octadecyl-1,3,5-triazine-2,4-diamine (**2**)

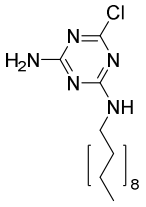

Dichlorotriazine **1** (6.18 g, 14.8 mmol, 1.00 eq) was dissolved in THF (60 mL) and an aqueous solution of NH_3 (32 %, 5.10 mL, 84.4 mmol, 5.70 eq) was slowly added at such a rate maintaining a reaction temperature of 21–25 °C. During the reaction, a white precipitate formed. After stirring for 24 h at rt (21 °C), the reaction mixture was concentrated under reduced pressure at ambient temperature. The resulting residue was suspended in H_2O (90 mL) and the insoluble white solid was filtered off, washed with H_2O (30 mL) and dried *in vacuo*. The crude product (5.90 g, 14.8 mmol, 100 %) was pure enough to be used for the next step without further purification.

R_f = 0.35 (EtOAc/PE 2:3). — MP: 110–115 °C. — ^{1}H-NMR ($CDCl_3$, 300 MHz): δ = 0.87 (t, J = 6.7 Hz, 3H, Me), 1.17–1.39 (m, 30H, $(CH_2)_{15}$), 1.55 (pseudo quint, J = 6.7 Hz, 2H, $NHCH_2CH_2$), 3.29–3.46 (m, 2H, $NHCH_2$), 5.09–5.64 (br m, 2H, NH_2), 5.64–5.80 (m, 1H, NH). — ^{13}C-NMR ($CDCl_3$, 75 MHz): δ = 14.29 (+, Me, octadecyl), 22.85 (–, CH_2, octadecyl), 26.91 (–, CH_2, octadecyl), 29.40 (–, CH_2, octadecyl), 29.52 (–, CH_2, octadecyl), 29.69 (–, CH_2, octadecyl), 29.73 (–, CH_2, octadecyl), 29.82 (–, CH_2, octadecyl), 29.85 (–, CH_2, octadecyl), 32.08 (–, CH_2, octadecyl), 41.12 (–, br, $NHCH_2$, octadecyl), 166.06 (C_q, triazine), 167.19 (C_q, triazine), 169.24 (C_q, triazine). — MS (ESI^+): *m/z* (%) = 398.2 (100) $[M + H^+]^+$, 439.2 (98) $[M + H^+ + MeCN]^+$.

IV.2.1.2.2 6-(Allyloxy)-N^2-octadecyl-[1,3,5]-triazine-2,4-diamine (**Ene3-C$_{18}$**)

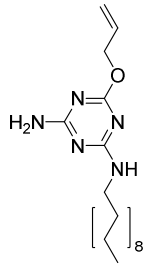

Ene3-C$_{18}$

Sodium hydroxide (30 mg, 0.75 mmol, 1.50 eq) was dissolved in hot allyl alcohol (**3a**, 145 mg, 2.51 mmol, 5.00 eq). Subsequently, a solution of chlorotriazine **2** (200 mg, 0.50 mmol, 1.00 eq) in DMSO (1.0 mL) was added. The reaction mixture was stirred at rt (23 °C) for 46 h. To the cloudy orange solution, H_2O (10 mL) was added. The resulting aqueous suspension was extracted with CH_2Cl_2 (5 × 10 mL). The combined organic solutions were dried over Na_2SO_4 and evaporated to give a yellowish oil, which was dissolved in a small amount of EtOH. Addition of H_2O resulted in a pale yellow precipitate, which was filtered off, washed with H_2O and subjected to column chromatography (SiO_2, EtOAc/PE 1:2) to yield pure alkene **Ene3-C$_{18}$** as white solid (179 mg, 0.43 mmol, 86 %).

R_f = 0.33 (EtOAc/PE 1:1). — MP: 73–75 °C. — ^{1}H-NMR ($CDCl_3$, 300 MHz): δ = 0.87 (t, J = 6.7 Hz, 3H, Me), 1.16–1.49 (m, 30H, $(CH_2)_{15}$), 1.54 (pseudo quint, J = 6.8 Hz, 2H, $NHCH_2CH_2$), 3.28–3.43 (m, 2H, $NHCH_2$), 4.77 (dd, J = 17.2, 4.6 Hz, 2H, OCH_2), 5.10–5.25 (m, 2H, NH_2), 5.22 (d, J = 10.7 Hz, 1H, =C*H*H), 5.28 (t, J = 5.8 Hz, 1H, NH), 5.35 (d, J = 17.3 Hz, 1H, =CH*H*), 5.91–6.12 (m, 1H, C*H*=CH_2). — ^{13}C-NMR ($CDCl_3$, 75 MHz): δ =

14.26 (+, Me, octadecyl), 22.82 (–, CH_2, octadecyl), 26.99 (–, CH_2, octadecyl), 29.47 (–, CH_2, octadecyl), 29.49 (–, CH_2, octadecyl), 29.71 (–, CH_2, octadecyl), 29.74 (–, CH_2, octadecyl), 29.80 (–, CH_2, octadecyl), 29.83 (–, CH_2, octadecyl), 32.06 (–, CH_2, octadecyl), 40.98 (–, br, $NHCH_2$, octadecyl), 67.19 and 67.56 (–, OCH_2, tautomers), 117.56 and 117.99 (–, $=CH_2$), 132.95 (+, =CH), 167.54 (C_q, triazine), 168.04 and 168.62 (C_q, triazine, tautomers), 170.55 and 171.06 (C_q, triazine, tautomers). — HRMS (ESI^+): *m/z* = $[C_{24}H_{45}N_5O + H^+]^+$ calculated 420.3697; found 420.3706.

IV.2.1.2.3 6-(But-3-enyloxy)-N^2-octadecyl-[1,3,5]-triazine-2,4-diamine (**Ene4-C_{18}**)

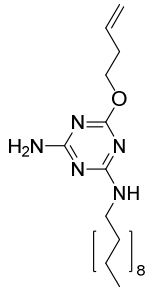

Ene4-C_{18}

Sodium hydroxide (42 mg, 1.06 mmol, 1.50 eq) was dissolved in hot 3-buten-1-ol (**3b**, 252 mg, 3.52 mmol, 5.00 eq). Subsequently, a solution of chlorotriazine **2** (280 mg, 0.70 mmol, 1.00 eq) in DMSO (1.5 mL) was added. The reaction mixture was stirred at rt (21 °C) for 20 h, heated to 80 °C for 10 min to dissolve the formed precipitate and then stirred at rt again for 4 d. To the cloudy orange solution, H_2O (20 mL) was added. The resulting aqueous suspension was acidified with HCl (37 %) and extracted with CH_2Cl_2 (5 × 20 mL). The combined organic solutions were dried over Na_2SO_4 and evaporated to give a yellowish oil, which was dissolved in a small amount of EtOH. Addition of H_2O resulted in a brownish precipitate, which was filtered off, washed with H_2O and subjected to column chromatography (SiO_2, EtOAc/PE 1:3 → 1:1) to yield pure alkene **Ene4-C_{18}** as white solid (130 mg, 0.30 mmol, 43 %).

R_f = 0.29 (EtOAc/PE 1:1). — MP: 74–76 °C. — ^{1}H-NMR ($CDCl_3$, 300 MHz): δ = 0.85 (t, J = 6.6 Hz, 3H, Me), 1.14–1.35 (m, 30H, $(CH_2)_{15}$), 1.51 (pseudo quint, J = 6.5 Hz, 2H, $NHCH_2CH_2$), 2.38–2.53 (m, 2H, OCH_2CH_2), 3.25–3.40 (m, 2H, $NHCH_2$), 4.14–4.36 (m, 2H, OCH_2), 5.04 (d, J = 10.7 Hz, 1H, =C*H*H), 5.10 (d, J = 17.8 Hz, 1H, =CH*H*), 5.50–5.71 (m, 2H, NH_2), 5.71–5.94 (m, 2H, $CH=CH_2$, NH). — ^{13}C-NMR ($CDCl_3$, 75 MHz): δ = 14.19 (+,

Me, octadecyl), 22.76 (–, CH_2, octadecyl), 26.96 (–, CH_2, octadecyl), 29.44 (–, CH_2, octadecyl), 29.68 (–, CH_2, octadecyl), 29.70 (–, CH_2, octadecyl), 29.74 (–, CH_2, octadecyl), 29.78 (–, CH_2, octadecyl), 31.99 (–, CH_2, octadecyl), 33.35 (–, OCH_2CH_2), 40.87 (–, br, $NHCH_2$, octadecyl), 65.74 and 65.98 (–, OCH_2, tautomers), 117.13 (–, $=CH_2$), 134.29 (+, =CH), 167.32 (C_q, triazine), 167.85 and 168.54 (C_q, triazine, tautomers), 170.54 and 171.04 (C_q, triazine, tautomers). — MS (ESI^+): *m/z* (%) = 434.3 (100) $[M + H^+]^+$.

IV.2.1.2.4 6-(Bicyclo[2.2.1]hept-5-en-2-ylmethoxy)-N^2-octadecyl-[1,3,5]-triazine-2,4-diamine (**Norb-C_{18}**)

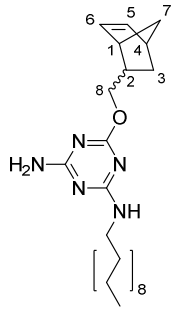

Norb-C_{18}

Chlorotriazine **2** (300 mg, 0.75 mmol, 1.00 eq) and sodium hydroxide (84 mg, 2.11 mmol, 2.80 eq) were suspended in DMSO (2.0 mL). Subsequently, 5-norbornene-2-methanol (**3c**, mixture of *endo* and *exo*, 279 mg, 2.26 mmol, 3.00 eq) was added. The reaction mixture was heated to 60 °C for 10 min and then stirred at rt (21 °C) for 17 h. Stirring was continued at 60 °C for further 22 h. To the obtained cloudy yellowish solution, H_2O (20 mL) was added. The resulting aqueous suspension was acidified with HCl (37 %) and extracted with CH_2Cl_2 (6 × 20 mL). The combined organic solutions were dried over Na_2SO_4 and evaporated to give a brownish oil, which was purified by column chromatography (EtOAc/PE 1:3 → 3:1) yielding norbornene derivative **Norb-C_{18}** (*endo* and *exo*) as white solid (245 mg, 0.50 mmol, 67 %).

R_f = 0.24 (EtOAc/PE 1:1). — MP: 96–100 °C. — ^{1}H-NMR ($CDCl_3$, 300 MHz): δ = 0.49–0.62 (m, 0.6H, 3-H, *endo*), 0.83 (t, J = 6.4 Hz, 3H, Me), 0.93–1.08 (m, 0.4H, 3-H, *exo*), 1.09–1.36 (m, 31.4H, $(CH_2)_{15}$, 3′-H, *exo*, 7-H, *exo*, 7-H, *endo*), 1.36–1.44 (m, 1H, 7′-H, *exo*, 7′-H, *endo*), 1.44–1.56 (m, 2H, $NHCH_2CH_2$), 1.73–1.91 (m, 1H, 2-H, *exo*, 3′-H, *endo*), 2.36–2.56 (m, 0.6H, 2-H, *endo*), 2.72–2.84 (m, 1.4H, 1-H, *exo*, 1-H, *endo*, 4-H, *exo*), 2.89–2.99 (m, 0.6H, 4-

H, *endo*), 3.20–3.41 (m, 2H, NHC*H*$_2$), 3.64–3.85 (m, 0.6H, 8-H, *endo*), 3.88–4.18 (m, 1H, 8′-H, *endo*, 8-H, *exo*), 4.18–4.39 (m, 0.4H, 8′-H, *exo*), 5.58–5.79 (m, 3H, NH, NH$_2$), 5.85–5.98 (m, 0.8H, 5-H, *exo*, 6-H, *exo*), 5.99–6.07 (m, 0.6H, 6-H, *endo*), 6.07–6.15 (m, 0.6H, 5-H, *endo*). — ^{13}C-NMR ($CDCl_3$, 75 MHz): δ = 14.16 (+, Me, octadecyl), 22.72 (–, CH_2, octadecyl), 26.94 (–, CH_2, octadecyl), 29.05 (–, br, CH_2, norbornene), 29.41 (–, CH_2, octadecyl), 29.67 (–, CH_2, octadecyl), 29.70 (–, CH_2, octadecyl), 29.74 (–, CH_2, octadecyl), 31.96 (–, CH_2, octadecyl), 37.93 (+, CH, norbornene), 38.16 (+, CH, norbornene), 40.80 and 40.88 (–, $NHCH_2$, octadecyl, tautomers), 41.63 (+, CH, norbornene), 42.26 (+, CH, norbornene), 43.67 (+, CH, norbornene), 43.87 (+, CH, norbornene), 44.98 (–, CH_2, norbornene), 49.43 (–, CH_2, norbornene), 69.99 and 70.11 (–, 8-CH_2, tautomers), 70.69 and 70.77 (–, 8-CH_2, tautomers), 132.45 (+, =CH, norbornene), 136.44 (+, =CH, norbornene), 136.72 (+, =CH, norbornene), 137.39 (+, =CH, norbornene), 167.33 (C_q, triazine), 167.93 and 168.51 (C_q, triazine, tautomers), 170.56 and 171.07 (C_q, triazine, tautomers). — MS (ESI$^+$): *m/z* (%) = 486.3 (100) $[M + H^+]^+$.

IV.2.1.3 Photoinitiators

For our investigations, 2,2-dimethoxy-2-phenylacetophenone (**DMPA**, Figure S4.2), lithium phenyl-2,4,6-trimethylbenzoylphosphinate (**LAP**,[6] both type I) and benzophenone (**BP**, type II) were tested as photoinitiators. **LAP** was synthesized according to a literature procedure,[7] while **BP** and **DMPA** were commercially available.

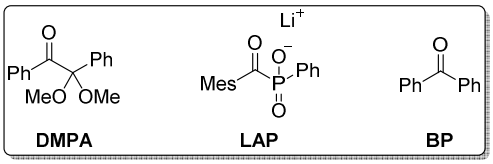

Figure S4.2: Employed photoinitiators **DMPA**, **LAP** and **BP**.

IV.2.2 General Procedure for the Thiol–Ene Addition

Optimization of the thiol–ene reaction was performed both in homogeneous solution and on vesicle surfaces. For test reactions in homogeneous aqueous systems, stock solutions of the alkene derivatives were made in EtOH due to their low solubility in water. For investigations

on vesicle surfaces, DSPC vesicle solutions containing 15 mol-% of the amphiphilic alkene were prepared (total amphiphile concentration: 2.00 mM). Appropriate volumes of the stock solutions of the alkene component or of alkene-decorated vesicles respectively, thiol and photoinitiator were mixed and diluted with aqueous HEPES buffer. The resulting concentrations of thiol or alkene were in the range of 0.1–100 mM. The photoinitiator **LAP** was added in quantities corresponding to 0.5–5.0 equivalents, whereas saturated aqueous solutions of unknown concentrations were employed in case of **DMPA** or **BP** due to their low solubility in water. The irradiation was performed with a 4 W UV hand lamp designed for TLC plate visualization or with a set of four 9 W black light fluorescent tubes with an emission maximum at 366 nm in each case.

IV.2.3 Methods for Evaluating the Thiol–Ene Reaction Progress

The efficiency of the reaction was determined either directly by monitoring the consumption of starting material or the formation of the addition product or indirectly by investigation of the properties of the post-functionalized vesicles.

IV.2.3.1 Colorimetric Monitoring of Thiol Consumption by Ellman's Method

5,5'-Dithiobis(2-nitrobenzoic acid) (**DTNB**, Scheme S4.4) reacts fast and quantitatively with any thiol forming a mixed disulfide and releasing a strongly colored thiolate dianion (Ellman's method).[8] The extinction value of the absorption maximum of the colored species (412 nm) is thus directly proportional to the concentration of free thiols. For this purpose, 20 µL of a 2.00 mM stock solution of **DTNB** in phosphate buffer (100 mM containing 1.00 mM of EDTA, pH 8.0) was added to 200 µL of the reaction solution, diluted with aqueous buffer to yield a total volume of 1.00 mL and left for 10 min. The thiol consumption was qualitatively observed by the naked eye or followed quantitatively by UV/Vis absorption spectroscopy.

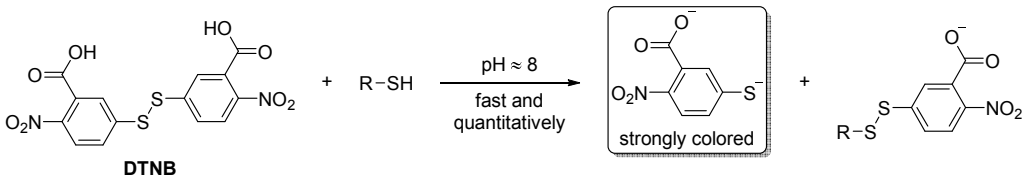

Scheme S4.4: Colorimetric detection of thiols with **DTNB** according to Ellman.[8]

IV.2.3.2 Monitoring of Starting Material Consumption by TLC

The aqueous reaction mixtures were extracted with EtOAc and the organic phase was run on TLC (EtOAc/PE 1:1). Consumption of the substoichiometric component of the starting material (either thiol or alkene), formation of the addition product or of the disulfide byproduct was qualitatively followed in case of non-charged species (*e.g.*, **Dans-SH**: R_f = 0.59 in EtOAc/PE 1:1; disulfide of **Dans-SH**: R_f = 0.38 in EtOAc/PE 1:1).

*IV.2.3.3 Quantification of Surface-Immobilized Fluorophore **Dans-SH***

Membrane-embedded amphiphilic alkenes were functionalized with **Dans-SH**. The vesicle solution was subsequently subjected to size-exclusion chromatography (SEC) to remove all fluorophore molecules which are not covalently bound to the vesicle surface. The fluorescence emission intensity of the vesicle solutions after SEC provided an indicator for the success of the surface reaction.

*IV.2.3.4 Quantification of Surface-Immobilized Receptor **Zn-Cyclen$_2$***

Preformed, alkene-modified vesicles were functionalized with **Zn-Cyclen$_2$**. The vesicle solution was then subjected to SEC twice to remove all solutes which are not covalently attached at the vesicle membrane. The resulting solution was subsequently titrated to an aqueous solution of coumarin methyl sulfonate (**CMS**, 5.0 μM), which is known to form a non-fluorescent complex with bis-Zn^{2+}-cyclen complexes.[9] The obtained emission quenching curves are thus dependent on the total amount of membrane-bound receptor molecules. As reference, DSPC vesicles with 5.0 mol-% of membrane-embedded **Zn-Cyclen$_2$-C$_{18}$**[10] (Figure

S4.3) were prepared (→ vesicles **V-Zn-C_{18}**).

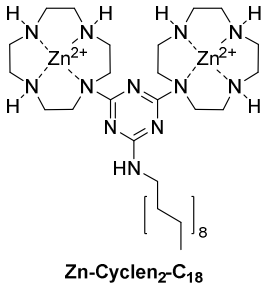

Figure S4.3: Amphiphilic bis-Zn^{2+}-cyclen complex[10] for the preparation of functionalized reference vesicles.

IV.3 Summary of Results

IV.3.1 Investigation of Various Parameters Influencing the Radical Thiol–Ene Addition

a) Influence of the Photoinitiator

Experiments without photoinitiator did not show conversion of the thiols, whereas reactions performed in presence of a photoactive radical generator yielded mixtures of the addition product and the undesired disulfide after exposure to UV light. Besides, the photoinitiator **BP** resulted in lower reaction efficiencies and therefore, longer irradiation times for the conversion of the starting material were required than with photoinitiators **DMPA** or **LAP**. In case of **LAP**, higher concentrations could be applied due to its increased water solubility compared to that of **DMPA** or **BP**. Higher quantities of the photoinitiator in turn resulted in enhanced efficiencies of the radical addition.

b) Influence of the UV Light Source and Irradiation Time

Irradiation with a 4 W TLC lamp only provided full conversion of the starting material in a time scale of minutes when higher concentrations of thiols and alkenes (≈ 100 mM) were employed. At lower concentrations, long irradiation times (≈ 2 h) were required. However, stronger irradiation energies (set of four 9 W lamps) resulted in higher efficiencies of the thiol–ene reaction. Under those conditions, the complete consumption of the starting material at concentrations of around 10 mM could be observed after 10 min.

c) Influence of the Alkene Moiety

Investigations in homogeneous solution did not reveal a significant dependence of the overall thiol–ene addition efficiency on the employed amphiphilic alkene **Ene3-C$_{18}$**, **Ene4-C$_{18}$** or **Norb-C$_{18}$**.

d) Influence of the Concentration of Starting Material

Particularly at low concentrations of the starting material (≈ 0.1 mM), a considerable formation of disulfide was observed. Therefore, for full conversion of the employed alkene, a high excess of thiol was needed (≈ 10 equivalents). This can be explained with the fact that in this concentration range, the quantity of the thiol approaches that of the dissolved oxygen, which facilitates the oxidation reaction (solubility of oxygen at ambient conditions in water: 0.28 mM).[11]

e) Influence of the Presence of Oxygen or of Reducing Agents

The formation of the disulfide at low concentrations of the starting material (≈ 0.1 mM) was remarkably suppressed either by use of degassed HEPES buffer (by freeze-pump-thaw technique) as reaction medium or by addition of tri-*n*-butylphosphine or tris(2-carboxyethyl)phosphine hydrochloride (TCEP) as disulfide reducing agents.[12]

IV.3.2 Functionalization of Vesicle Surfaces with Zn-Cyclen$_2$

DSPC vesicles containing 15 mol-% of amphiphilic alkene were post-functionalized with the phosphate-binding receptor group **Zn-Cyclen$_2$** (1.3 equivalents with regard to the surface-accessible amount of the alkene) applying varying reaction conditions. The success of the surface reaction was quantified by the extent of **CMS** fluorescence quenching upon titration of the resulting **Zn-Cyclen$_2$**-functionalized vesicles. Figures S4.4 and S4.5 show that the obtained **CMS** emission response curves in case of the post-functionalized vesicles do not exceed that of the reference vesicles **V-Zn-C$_{18}$** (5.0 mol % of membrane-embedded receptor **Zn-Cyclen$_2$-C$_{18}$**). That means, by taking the alkene content of 15 mol-% in the membrane into account, not more than one third of the surface-accessible olefin units were functionalized under those conditions. The influence of the irradiation time and energy (Figure S4.4) and of the employed membrane-embedded alkene (Figure S4.5) is in line with

the qualitative results outlined in the previous section.

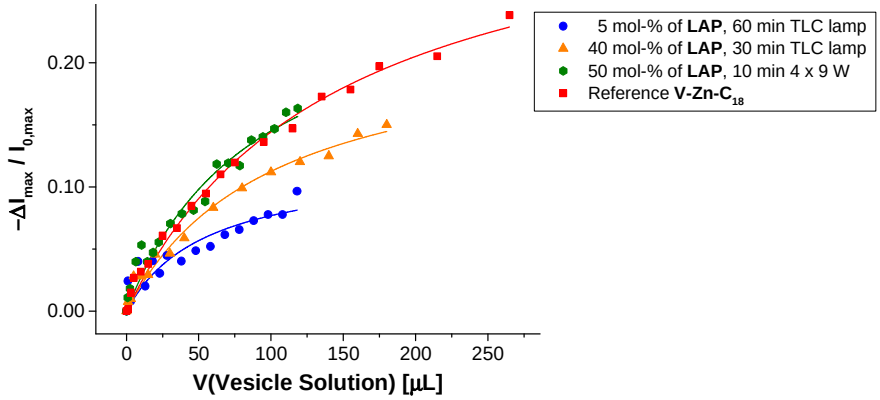

Figure S4.4: **CMS** fluorescence quenching upon addition of DSPC vesicles (15 mol-% of **Ene3-C$_{18}$** as alkene component embedded) which were post-functionalized with **Zn-Cyclen$_2$** under different conditions and of reference vesicles **V-Zn-C$_{18}$** (red squares).

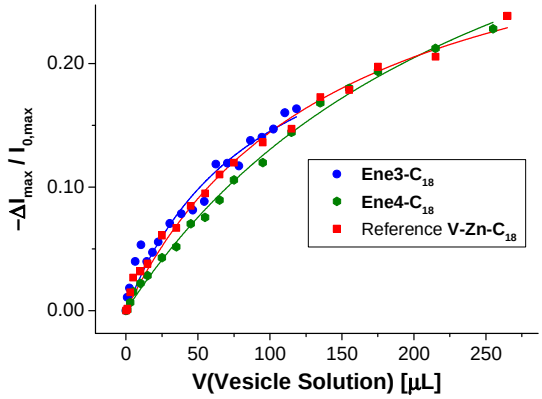

Figure S4.5: **CMS** fluorescence quenching upon addition of DSPC vesicles (15 mol-% of either **Ene3-C$_{18}$** or **Ene4-C$_{18}$** as alkene component embedded) which were post-functionalized with **Zn-Cyclen$_2$** (photoinitiator **LAP**, irradiation with a set of four 9 W lamps for 10 min) and of reference vesicles **V-Zn-C$_{18}$** (red squares).

IV.3.3 Influence of UV Light Irradiation on Membrane-Embedded Fluorophores

The previous experiments demonstrated that for satisfactory conversion of the starting material, about 10 min of UV light irradiation with a set of four 9 W lamps was required. Under those conditions, however, considerable photobleaching of the amphiphilic carboxyfluorescein **CF-C$_{12}$**, which is commonly employed as reporter dye for signaling of receptor–target interactions on vesicle surfaces, was observed (Figure S4.6).

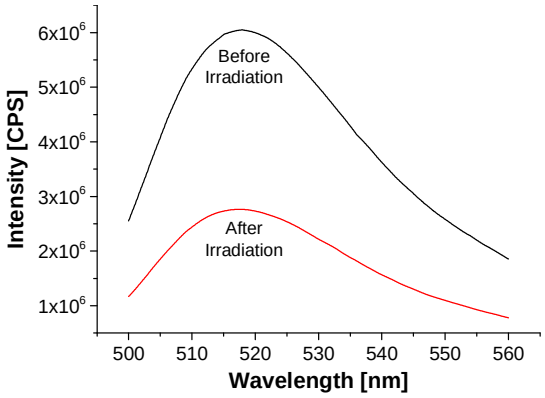

Figure S4.6: Photobleaching of amphiphilic carboxyfluorescein **CF-C_{12}** (10 μM in HEPES buffer containing catalytic amounts of **DMPA**) after irradiation at 366 nm with a set of four 9 W lamps for 10 min.

IV.4 Conclusion

It was found that the radical addition of thiols to alkenes in aqueous micromolar solutions is subject to several restrictions. The following conditions are required for the complete conversion of the alkenes into the corresponding thioether products:

- excess of the thiol component (≈ 10 equivalents) due to the formation of the disulfide byproduct
- high quantities of photoinitiator (≈ 5 equivalents)
- relatively long irradiation with UV light (≈ 10 min with a set of four 9 W lamps)

One can conclude that the specified conditions do not fulfill the criteria for click reactions. As a consequence, the applicability of this reaction type for the post-functionalization of vesicle surfaces is very limited. The requirement of a thiol excess makes the reaction uneconomic. An additional purification step of the post-functionalized vesicles by SEC would be necessary to remove thiols which are not bound to the surface as well as disulfide byproducts. Moreover, the observed photobleaching of the membrane-embedded reporter fluorophore restricts the feasibility of this method for the preparation of luminescent sensors.

IV.5 Comparison with Nucleophilic Thiol–Ene Reaction

As alternative thiol-based click reaction for the surface modification of preformed vesicles, we tested the nucleophilic addition of thiols to electron poor C–C double bonds (Scheme S4.5). Maleimides are generally very susceptible to Michael addition reactions of nucleophiles due to their olefinic bond which is conjugated with two electron withdrawing carbonyl groups.

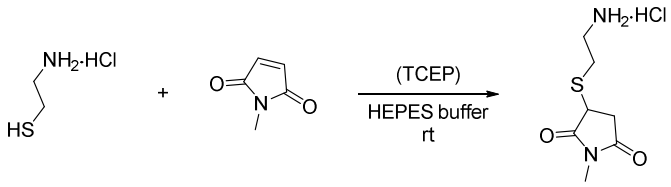

Scheme S4.5: Model system to test the nucleophilic thiol–ene reaction.

Investigations on basis of the model system (Scheme S4.5) revealed a smooth and quick performance of that reaction type even at 0.1 mM concentrations of the starting material without observed formation of byproducts. Here, equimolar ratios of both components were sufficient for the effective thiolation of the maleimide in a time range of 15–30 min. The presence of catalytic amounts of TCEP can be beneficial as it is able both to reduce potentially formed disulfide and to act as a catalyst for the Michael addition.[1,12]

IV.6 Notes and Reference

[1] A. B. Lowe, "Thiol–ene 'click' reactions and recent applications in polymer and materials synthesis", *Polym. Chem.* **2010**, *1*, 17–36.

[2] C. E. Hoyle, T. Y. Lee, T. Roper, "Thiol–Enes: Chemistry of the Past with Promise for the Future", *J. Polym. Sci., Part A: Polym. Chem.* **2004**, *42*, 5301–5338.

[3] M. Uygun, M. A. Tasdelen, Y. Yagci, "Influence of Type of Initiation on Thiol–Ene 'Click' Chemistry", *Macromol. Chem. Phys.* **2010**, *211*, 103–110.

[4] C. Robinson, R. F. Hartman, S. D. Rose, "Emollient, humectant, and fluorescent α,β-unsaturated thiol esters for long-acting skin applications", *Bioorg. Chem.* **2008**, *36*, 265–270.

[5] L. Tei, M. Benzi, F. Kielar, M. Botta, C. Cavallotti, G. B. Giovenzana, S. Aime, "Synthesis and Relaxometric Properties of Gadolinium(III) Complexes of New Triazine-Based Polydentate Ligands", *Helv. Chim. Acta* **2009**, *92*, 2414–2426.

[6] Abbreviated **LAP** for lithium acylphosphinate according to the literature.

[7] B. D. Fairbanks, M. P. Schwartz, C. N. Bowman, K. S. Anseth, "Photoinitiated polymerization of PEG-diacrylate with lithium phenyl-2,4,6-trimethylbenzoylphosphinate: polymerization rate and cytocompatibility", *Biomaterials* **2009**, *30*, 6702–6707.

[8] G. L. Ellman, "Tissue Sulfhydryl Groups", *Arch. Biochem. Biophys.* **1959**, *82*, 70–77.

[9] B. Gruber, S. Stadlbauer, K. Woinaroschy, B. König, "Luminescent vesicular receptors for the recognition of biologically important phosphate species", *Org. Biomol. Chem.* **2010**, *8*, 3704–3714.

[10] D. S. Turygin, M. Subat, O. A. Raitman, V. V. Arslanov, B. König, M. A. Kalinina, "Cooperative Self-Assembly of Adenosine and Uridine Nucleotides on a 2D Synthetic Template", *Angew. Chem. Int. Ed.* **2006**, *45*, 5340–5344; *Angew. Chem.* **2006**, *118*, 5466–5470.

[11] B. B. Benson, D. Krause, "The concentration and isotopic fractionation of oxygen dissolved in freshwater and seawater in equilibrium with the atmosphere", *Limnol. Oceanogr.* **1984**, *29*, 620–632.

[12] J. A. Burns, J. C. Butler, J. Moran, G. M. Whitesides, "Selective Reduction of Disulfides by Tris(2-carboxyethyl)phosphine", *J. Org. Chem.* **1991**, *56*, 2648–2650.

CHAPTER V:

VESICULAR APTASENSOR FOR THE DETECTION OF THROMBIN

This chapter was published in:

A. Müller, B. König, "Vesicular aptasensor for the detection of thrombin", *Chem. Commun.* **2014**, *50*, 12665–12668. – Reproduced by permission of The Royal Society of Chemistry.

A. Müller performed the experimental work and wrote the manuscript. B. König supervised the project and is corresponding author.

V.1 Introduction

The last two decades have seen considerable progress in the design of biopolymer-based receptors for high-affinity and -specificity analyte binding. The first reports on the evolutionary selection of RNA molecules binding to specific ligands in 1990[1] laid the foundation for the development of numerous nucleic acid aptamers. A broad variety of ligands were targeted ranging from small organic molecules[2a] to proteins[2b] and pathogens,[2c] and the technique was applied in environmental and food analytics.[3] With an increasing number of available aptamers, suitable methods for transforming the microscopic binding event into a macroscopic signal were established.[4] Fluorescence-based[5a] and electrochemical[5b] detection methods are among the most important ones due to their high sensitivities. They both typically rely on covalent modification of the aptamers with a luminescent or an electroactive moiety. Another commonly used technique is based on hybridization of the aptamers with antisense oligonucleotides whose displacement by the target analytes induces a fluorescent or electrical response.[6] The requirement of covalent reporter attachment at the aptamer or the need of accordingly labeled complementary oligonucleotide strands can make such assays laborious and costly. For that reason, label-free strategies were investigated, but their general applicability is often limited as they rely on specific structural characteristics of the applied aptamers such as certain folding modes upon binding to the target. Formation of a double helix domain, for example, allows the intercalation of a suitable dye accompanied by a change of its emission properties.[7] Previously, our group reported on the modular construction of luminescent chemosensors by means of unilamellar vesicular membranes as self-assembled supporting frames for metal complex receptors and fluorescent reporter sites.[8] This strategy facilitates an effortless sensor preparation based on self-assembly by simple mixing of different functional amphiphiles in aqueous solution. As a consequence, our method allows an easy variation of the sensor composition, *i.e.*, of the binding and signaling units, their ratios and concentration on the surface and the physical properties of the supporting vesicle membranes determined by the nature of the phospholipids.[9] We now expand the pool of available binding sites to more complex structures based on molecules of biological origin. As a model system, we immobilized the very well established thrombin-binding 15-mer DNA aptamer[10] on fluorescent phospholipid vesicle surfaces. DNA-decorated liposomes have been used as signal amplification tags,[11] for controlled liposome adhesion or fusion[12] and for specific cell

targeting with regard to drug delivery.[13] Moreover, the conjugated polymeric backbone of oligonucleotide-functionalized polydiacetylene vesicles was utilized as colorimetric sensing matrix for target detection.[14] These reports prompted us to combine the concept of liposome-anchored aptamers with our strategy of non-covalent receptor and fluorophore co-embedding into phospholipid membranes.

V.2 Results and Discussion

As attachment site for thiol-modified aptamers, we incorporated the amphiphilic maleimide **Mal-C$_{16}$** (Figure 5.1, 5.0 mol-%) into membranes of small unilamellar DSPC vesicles. Amphiphilic pyrene **Pyr-C$_{18}$** (→ vesicles **V-Pyr**) or rhodamine **Rho-C$_{18}$**[15] (→ vesicles **V-Rho**) were co-embedded as reporter dyes (1.0–5.0 mol-%). The synthesis of **Mal-C$_{16}$** is described in the Experimental Part, preparation of **Pyr-C$_{18}$** was performed by *in situ* click reaction of commercially available *N*-(1-pyrenyl)maleimide and 1-octadecanethiol. The vesicle preparation was performed in 25 mM HEPES buffer at pH = 7.4 according to previously reported procedures (see Experimental Part for details).

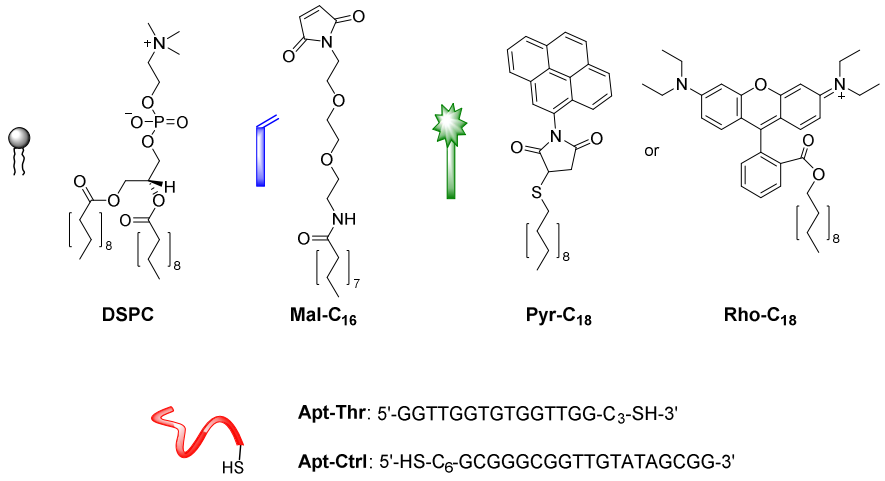

Figure 5.1: Structures of the functional amphiphiles used for vesicle preparation and of the immobilized aptamers.

Next, we functionalized the vesicle membrane covalently with the aptamer by nucleophilic thiol–maleimide addition. After addition of thiolated **Apt-Thr** (0.4–0.5 equivalents with respect to the total amount of **Mal-C$_{16}$**) to **V-Pyr**, we observed a time-dependent decrease of the fluorescence signal indicating the reaction progress on the vesicle surface. Phase separation processes in the membrane result in high local concentrations of the embedded functional amphiphiles as it is evidenced by the presence of the pyrene excimer

signal of **V-Pyr** at 470 nm (Figure 5.2A, inset). We assume that the surface-anchored oligonucleotides strongly impact the physical properties at the membrane interface by their high negative charge and steric demand. This local interference results in a partial fluorescence emission quenching of the nearby pyrene aggregates (Figure 5.3, top). Moreover, it is well documented that nucleotides are able to quench the fluorescence of fluorophores such as pyrene[16] or rhodamine[17] derivatives by photoinduced electron transfer. We believe that this mechanism also contributes to the observed effect in our case. Rhodamine-modified liposomes **V-Rho** exhibit a similar behavior during functionalization with the aptamer **Apt-Thr** (Figure 5.2B).

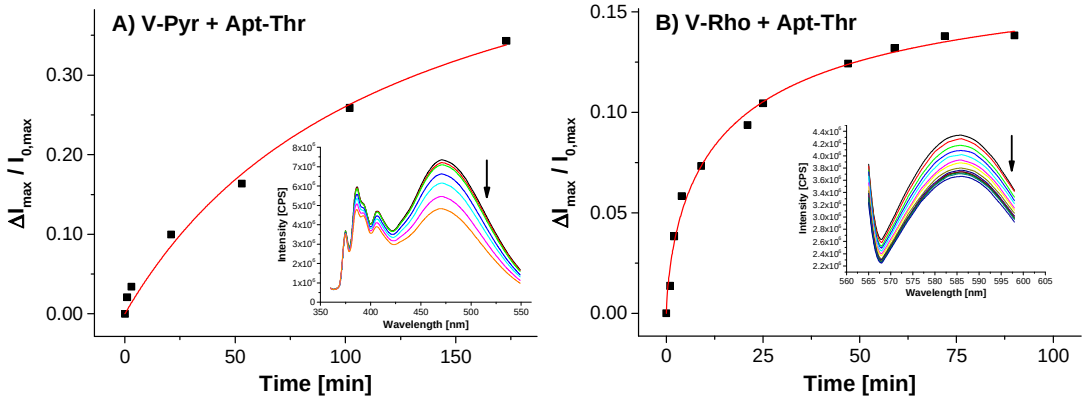

Figure 5.2: Fluorescence response monitoring the reaction progress of pyrene- (A) and rhodamine-modified (B) vesicles during surface functionalization with aptamer **Apt-Thr**.

The thrombin-binding aptamer folds into a highly compact G-quadruplex structure upon binding to thrombin.[18] This chair-like conformation is stabilized by a metal cation, particularly potassium cations. Analogously to the sensing mechanism for the membrane functionalization process, we believe that binding of the target to the surface-bound oligonucleotide, accompanied by its conformational change, has a drastic impact on the membrane structure which triggers then the dynamic emission response of the fluorophore molecules in close proximity (Figure 5.3, bottom). At last, rather the presence of the aptamer-bound analyte at the membrane–water interface causes the change of the emission signal than a defined conformation of the immobilized oligonucleotide molecules.

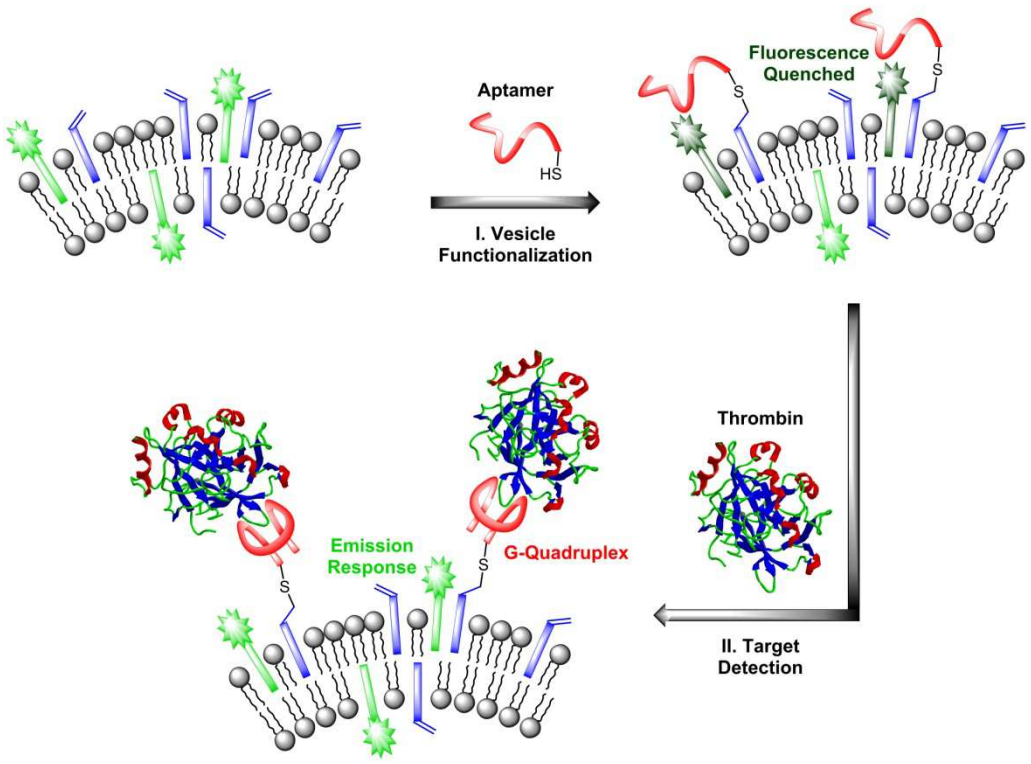

Figure 5.3: Principle of vesicle surface functionalization (I.) and fluorescence response after analyte binding (II.).

High concentrations of potassium cations are known to induce the transition of the oligonucleotide from random coil to the folded form with a reported binding constant of lg $K_a \approx 2.1$.[19] Therefore, we first tested the suitability of the thrombin aptamer-functionalized vesicles **V-Pyr-Thr** for K^+ detection. The fluorescence titration revealed an excimer signal change of almost 60 % (Figure 5.4, red squares). Due to the relatively low binding affinity of the aptamer to potassium cations, KCl concentrations of up to 140 mM were required to obtain a reasonable binding isotherm. In the same concentration range, non-functionalized vesicles showed a smaller non-specific response with linear relationship (Figure 5.4, blue dots). We explain this effect by the huge change of ionic strength in the aqueous buffer. It is well documented that high salt concentrations have a strong influence on the membrane's physical properties such as surface polarity and hydration and thus can alter the emission of membrane-embedded fluorophores.[20] Non-linear curve fitting of the obtained binding isotherm resulted in a logarithmic binding constant of 1.3 (Table 5.1). The lower value of the potassium cation binding constant compared to the reported one can be attributed to the interference of specific binding and non-specific salt effects.

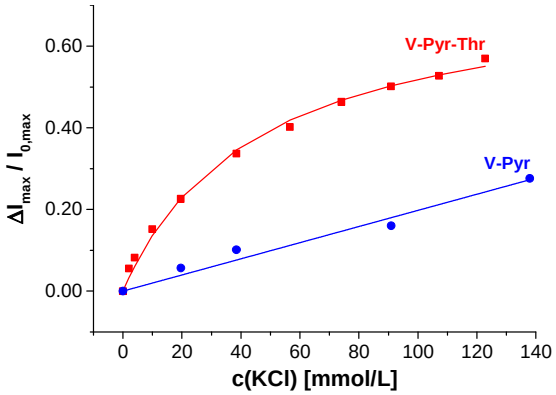

Figure 5.4: Fluorescence emission titrations of KCl versus aptamer-functionalized (red squares) and non-functionalized (blue dots) vesicles **V-Pyr**.

Next, we investigated the detection of thrombin. Pyrene-functionalized vesicles **V-Pyr-Thr** showed a relatively small fluorescence increase upon addition of thrombin (≈ 20 % at a 2.0 μM concentration of thrombin, see Figure S5.4 in Experimental Part), whereas rhodamine-modified liposomes **V-Rho-Thr** exhibited a considerable luminescence response (Figure 5.5, red squares). As expected, non-functionalized vesicles **V-Rho** did not significantly alter their emission properties upon the addition of thrombin (Figure 5.5, blue dots).

Table 5.1 summarizes the apparent binding constants of the vesicular aptasensors to different analytes. All calculations were performed by non-linear curve fitting using the equation for 1:1 binding.[21] The affinity constants of **V-Rho-Thr** to both bovine and human thrombin are in good agreement with reported literature values. The limit of detection was determined to be 25 nM (on basis of a signal to noise ratio of 3), while the sensors span a dynamic range of up to 2 μM concentration of thrombin (see Experimental Part for fluorescence titration data). The analytic results are reproducible as shown by repeated measurements. Since thrombin is a crucial enzyme in the blood coagulation cascade, its concentration in circulating blood is low and often undetectable. During clotting initiation, it becomes significantly elevated at a low nanomolar concentration level and peaks at concentrations in the low micromolar region during the propagation phase.[11b,22] Thus, the dynamic recognition range of our sensor matches the physiological concentration range.

Table 5.1: Binding affinities of fluorescent, aptamer-functionalized vesicles to different analytes.

Vesicles	Analyte	lg K_a	Reference
V-Pyr-Thr	KCl	1.3 (± 8 %)	2.1[19]
V-Pyr-Thr	Bovine thrombin	6.3 (± 3 %)	7.1[23]
V-Rho-Thr	Bovine thrombin	7.2 (± 8 %)	7.1[23]
V-Rho-Thr	Human thrombin	7.7[a]	6.7–7.6[24]

[a] Single experiment.

To demonstrate that the interaction of thrombin with the covalently membrane-attached aptamer is responsible for the change of the rhodamine emission intensity, we prepared fluorescent vesicles lacking the amphiphilic binding anchor **Mal-C_{16}** and incubated them with the thiolated thrombin-binding aptamer **Apt-Thr** leading to no significant response upon analyte addition (Figure 5.5, orange diamonds).

We tested the specificity of our aptasensors by immobilizing a non-binding control oligonucleotide **Apt-Ctrl** (Figure 5.1) with comparable length on the vesicle surface. The slight response after thrombin addition can be attributed to non-specific binding (Figure 5.5, magenta triangles). Although thrombin has a small negative overall charge in the used buffer system (pH: 7.4, isoelectric point of thrombin: 7.05[25]), its numerous negatively and positively charged residues are not distributed uniformly over the whole molecule.[26] They are clustered in a sandwich-like structure of two highly positive poles, whose electrostatic fields spread far into the extramolecular space. We suppose that the electropositive exosites are capable to displace counter ions from the negatively charged oligonucleotide backbone by electrostatic attractions.[27]

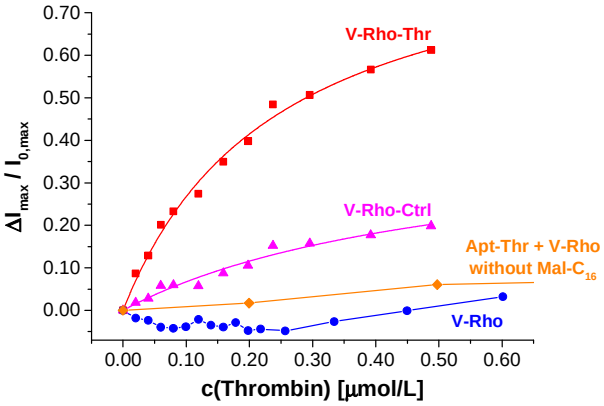

Figure 5.5: Binding isotherm of thrombin to aptamer-functionalized vesicles **V-Rho-Thr** (red squares) and fluorescence response of control experiments: non-functionalized vesicles **V-Rho** (blue dots), maleimide-lacking **V-Rho** vesicles incubated with **Apt-Thr** (orange diamonds) and vesicles **V-Rho-Ctrl** functionalized with non-binding oligonucleotide **Apt-Ctrl** (magenta triangles).

Emission titration using the protein elastase, which is besides thrombin a member of the serine proteases enzyme family, versus **V-Rho-Thr** indicates the aptamer–protein non-specific interaction. The fluorescence intensity decreases during titration (Figure 5.6), which is in contrast to the emission intensity increase observed with thrombin. Elastase has an isoelectric point of 9.5,[28] and it is assumed that its high positive net charge possibly results in strong non-specific oligonucleotide–protein interactions,[27] leading to different fluorescence emission intensity changes.

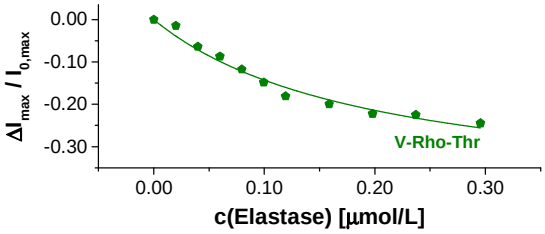

Figure 5.6: Fluorescence emission titration of control protein elastase to **V-Rho-Thr**.

V.3 Conclusion

In conclusion, we have developed a novel type of aptasensor based on self-assembled, luminescent vesicle membranes, which are functionalized with the thrombin-binding aptamer by nucleophilic thiol–maleimide addition. The high-affinity binding of the aptamer to thrombin is indicated by a dynamic response of the co-embedded fluorescent reporter molecules in the physiological concentration range. The obtained binding constants are in good agreement with the reported values. Despite of the observed non-specific interactions in

case of mismatched aptamer–protein combinations, the specific binding to thrombin can be clearly distinguished in the fluorescence output. As the reporter group is neither covalently attached nor coordinated to the aptamer, an inexpensive and easy variation of aptamer–fluorophore combinations is possible. The signaling mechanism is independent of specific conformational changes of the receptor molecules, which may allow a broader application compared to previously reported label-free aptasensors. An extension to other aptamers, enzymes or proteins and the immobilization of the vesicular aptasensors on solid supports can be readily envisaged.

V.4 Experimental Part

V.4.1 General Methods and Material

General

Commercially available solvents of standard quality were used. Starting materials were purchased from either Acros or Sigma-Aldrich and used without any further purification. Phospholipids were purchased from Avanti Polar Lipids Inc. Thrombin from bovine plasma (40–300 NIH units/mg protein) and elastase from porcine pancreas (Type IV) were obtained from Sigma-Aldrich. Human α-thrombin was available at Haematologic Technologies Inc. The thiolated aptamers were synthesized by IBA GmbH (Göttingen).

Thin layer chromatography (TLC) analyses were performed on pre-coated TLC sheets ALUGRAM Xtra SIL G/UV_{254} with 0.2 mm layer thickness from Macherey-Nagel. The detection was realized by staining with $KMnO_4$. Flash column chromatography was performed on silica gel 60 (70–230 mesh) from Macherey-Nagel.

Melting Points

Melting points were determined on a Stanford Research Systems OptiMelt MPA100 with a heating rate of 1 °C/min.

NMR Spectra

For NMR spectroscopy, a Bruker Avance 300 (^{1}H: 300.1 MHz, ^{13}C: 75.5 MHz, T = 293 K) was used. All chemical shifts are reported in δ [ppm] (multiplicity, coupling constant *J*, number of protons, assignment) relative to the solvent residual peak of $CDCl_3$ as the internal standard (^{1}H: δ = 7.26 ppm, ^{13}C: δ = 77.16 ppm). The coupling constants are given in Hertz [Hz]. Abbreviations used for signal multiplicity: ^{1}H-NMR: s = singlet, d = doublet, t = triplet, q = quartet, m = multiplet, br = broad.

Mass Spectra

Mass spectra were measured on an Agilent Q-TOF 6540 UHD mass spectrometer.

Fluorescence Measurements

Fluorescence spectroscopy was carried out on a HORIBA FluoroMax-4 fluorescence spectrophotometer with temperature control with 10 × 4 mm Hellma quartz cuvettes at 21 °C. For better comparability of the different measurements, the relative fluorescence changes

(ΔI_{max} / $I_{0,max}$) were calculated.

Dynamic Light Scattering (DLS)

Dynamic light scattering was performed on a Malvern Zetasizer Nano ZS at 25 °C using 1 cm disposable polystyrene cuvettes. Data analysis was performed using the Malvern Zetasizer software.

V.4.2 Synthesis

Compound **Rho-C_{18}**[15] was prepared according to the literature procedure. The amphiphilic maleimide **Mal-C_{16}** was synthesized by amide formation between palmitoyl chloride (**1**, Scheme S5.1) and bis-amine **2** followed by reaction of amphiphilic amine **3**[29] with maleic anhydride (**4**).

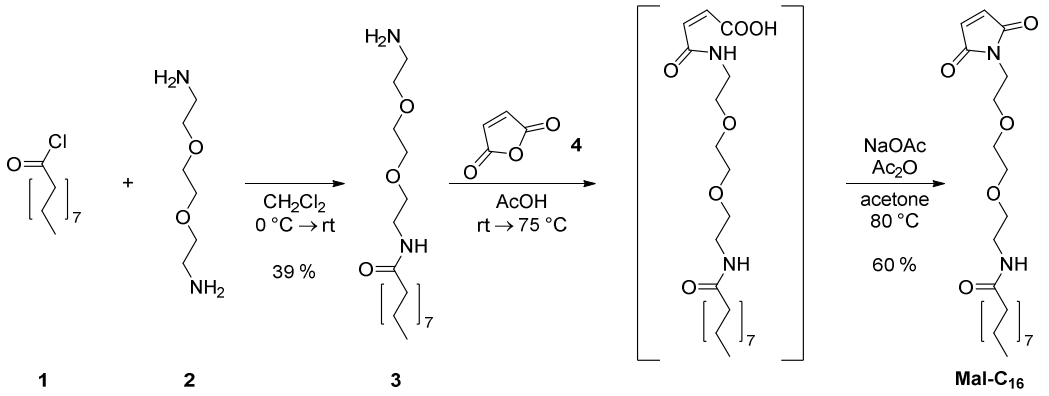

Scheme S5.1: Synthesis of amphiphilic maleimide **Mal-C_{16}**.

V.4.2.1 Synthesis of N-*(2-(2-(2-Aminoethoxy)ethoxy)ethyl)hexadecanamide (**3**)*

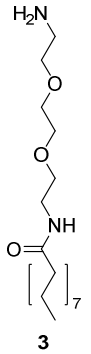

A solution of palmitoyl chloride (**1**, 3.00 g, 10.9 mmol, 1.00 eq) in CH_2Cl_2 (20 mL) was

added dropwise over 4 h to a stirred solution of 2,2′-(ethylenedioxy)bis(ethylamine) (**2**, 16.2 g, 109 mmol, 10.0 eq) in CH_2Cl_2 (40 mL) at 0 °C under nitrogen atmosphere. The reaction mixture was allowed to warm to rt (21 °C) and stirring was continued for 17 h at 25 °C resulting in the formation of a thick white precipitate. Aqueous NaOH (1.0 M, 90 mL) was added to the reaction mixture and the organic solvent was removed by rotatory evaporation under reduced pressure. The aqueous suspension was filtered and the obtained white precipitate was washed with water. After re-suspension of the solid in water (100 mL), the aqueous mixture was extracted with CH_2Cl_2 (3 × 80 mL) and the combined organic phases dried over Na_2SO_4. Evaporation of the solvent provided amide **3**[29] as white solid (1.64 g, 4.25 mmol, 39 %), which was used for the next step without any further purification.

R_f = 0.20 (MeOH/CH_2Cl_2 20:80). — ^{1}H-NMR ($CDCl_3$, 300 MHz): δ = 0.87 (t, J = 6.7 Hz, 3H, Me), 1.16–1.38 (m, 24H, $(CH_2)_{12}$), 1.54–1.67 (m, 2H, CH_2CH$_2$C=O), 1.82 (br s, 2H, NH_2), 2.16 (t, J = 7.6 Hz, 2H, CH$_2$CH_2C=O), 2.88 (t, J = 5.2 Hz, 2H, CH_2NH$_2$), 3.41–3.49 (m, 2H, CH_2NH), 3.49–3.59 (m, 4H, 2 × CH_2O), 3.59–3.64 (m, 4H, 2 × CH_2O), 6.18–6.32 (m, 1H, NH).

V.4.2.2 Synthesis of N-*(2-(2-(2-Maleimidoethoxy)ethoxy)ethyl)hexadecanamide (**Mal-C$_{16}$**)*

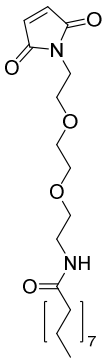

Mal-C$_{16}$

To a solution of amphiphilic amine **3** (1.60 g, 4.14 mmol, 1.00 eq) in AcOH (55 mL), maleic anhydride (**4**, 446 mg, 4.55 mmol, 1.10 eq) was added. The reaction mixture was stirred at 25 °C for 17 h and subsequently at 75 °C for 3 h. Acetic acid was distilled off under reduced pressure followed by dissolution of the obtained white residue in acetone (90 mL). Sodium acetate (1.09 g, 13.2 mmol, 3.20 eq) and acetic anhydride (55 mL) were added and the reaction mixture was stirred at 60 °C for 14 h and at 80 °C for 6 h. After removal of the solvent and excessive Ac_2O *in vacuo*, CH_2Cl_2 (50 mL) and saturated $NaHCO_3$ solution

(50 mL) were added and the aqueous layer was extracted with CH_2Cl_2 (50 mL). The combined organic phases were dried over Na_2SO_4. The crude product was obtained after evaporation of the solvent as a brownish solid. Column chromatographic purification (SiO_2, EtOAc/PE 4:6 → 7:3) provided pure compound **Mal-C_{16}** as white solid (1.29 g, 2.77 mmol, 67 %).

R_f = 0.58 (MeOH/CH_2Cl_2 10:90). — MP: 74–77 °C. — ^{1}H-NMR ($CDCl_3$, 300 MHz): δ = 0.87 (t, J = 6.7 Hz, 3H, Me), 1.16–1.36 (m, 24H, $(CH_2)_{12}$), 1.56–1.68 (m, 2H, C$H_2$$CH_2$C=O), 2.19 (t, J = 7.7 Hz, 2H, CH_2CH_2C=O), 3.38–3.46 (m, 2H, CH_2NH), 3.47–3.53 (m, 2H, CH_2N), 3.53–3.62 (m, 4H, 2 × CH_2O), 3.62–3.68 (m, 2H, CH_2O), 3.71–3.77 (m, 2H, CH_2O), 6.05–6.16 (m, 1H, NH), 6.70 (s, 2H, CH=CH). — ^{13}C-NMR ($CDCl_3$, 75 MHz): δ = 14.27 (Me), 22.83 (CH_2), 25.92 (CH_2), 29.49 (CH_2), 29.53 (CH_2), 29.66 (CH_2), 29.79 (CH_2), 29.83 (CH_2), 32.05 (CH_2), 36.88 (CH_2), 37.23 (CH_2), 39.19 (CH_2), 67.99 (CH_2O), 69.98 (CH_2O), 70.13 (CH_2O), 70.33 (CH_2O), 134.32 (CH=CH), 170.83 (CH_2N*C*=O), 173.49 (NHC=O). — HRMS (ESI$^+$): m/z = [$C_{26}H_{46}N_2O_5$ + H^+]$^+$ calculated 467.3479; found 467.3484.

*V.4.2.3 NMR Spectra of **Mal-C_{16}***

^{1}H-NMR ($CDCl_3$, 300 MHz)

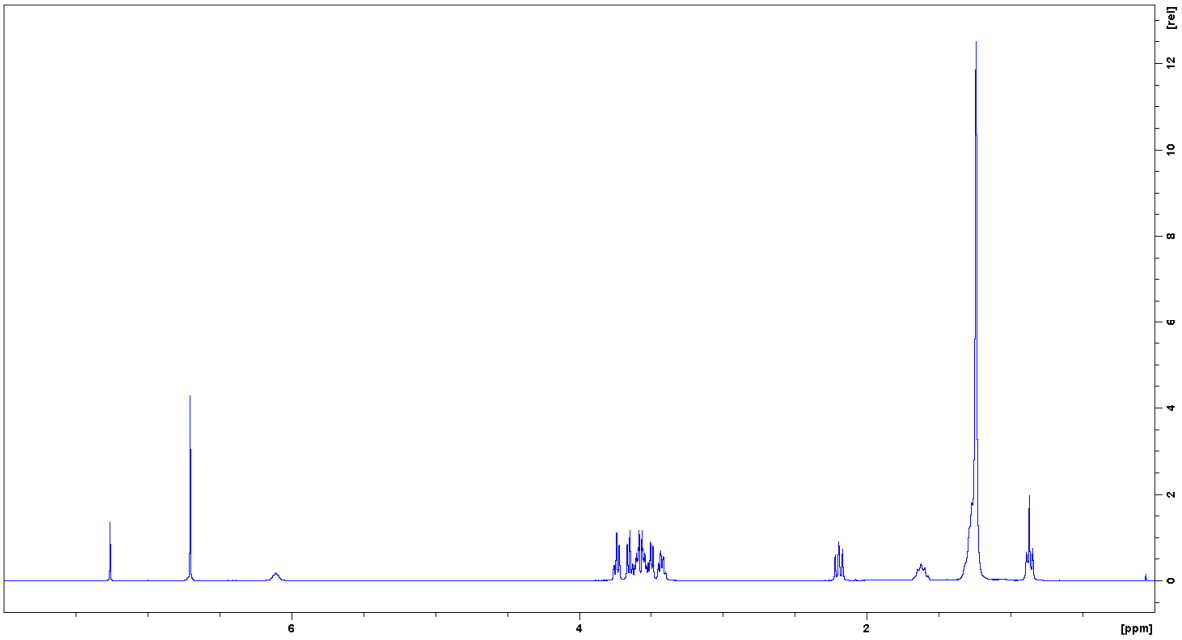

^{13}C-NMR ($CDCl_3$, 75 MHz)

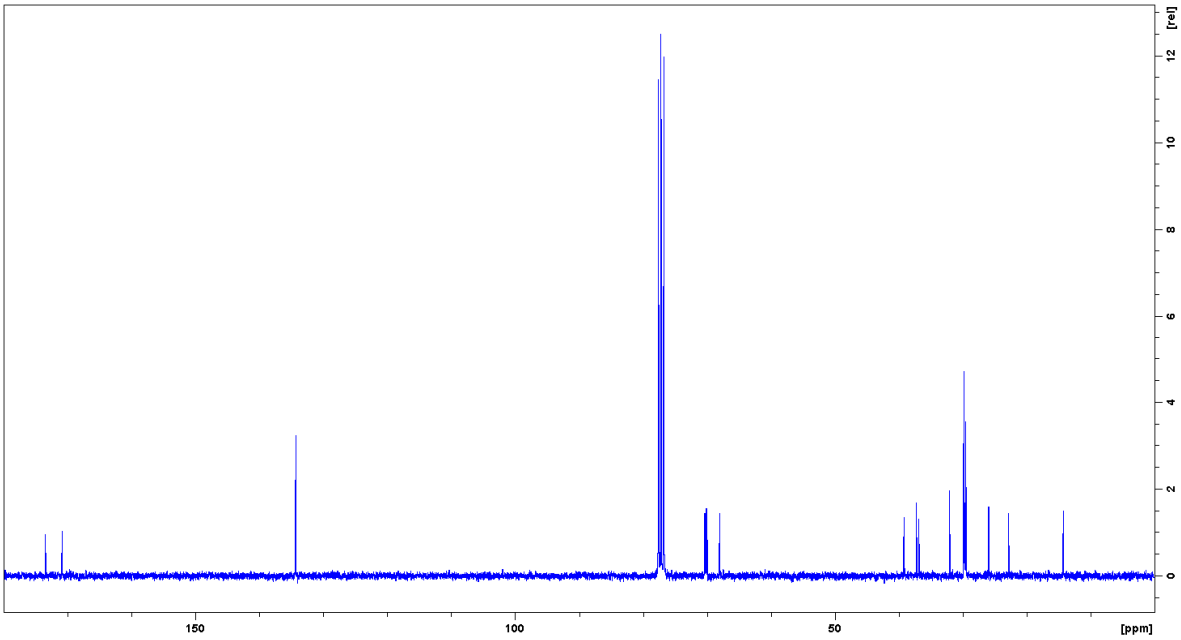

V.4.3 Preparation and Characterization of Vesicles

V.4.3.1 Preparation of Functionalizable Luminescent Vesicles

The surface-reactive luminescent vesicles were prepared analogously to formerly established protocols.[8a,9b]

Vesicles **V-Pyr**

Amphiphilic pyrene **Pyr-C_{18}** was prepared *in situ* according to Scheme S5.2 by mixing stock solutions of *N*-(1-pyrenyl)maleimide (**5**, 1.00 mM in $CHCl_3$, 100 µL) and 1-octadecanethiol (**6**, 1.00 mM in $CHCl_3$, 100 µL) in a small glass vessel followed by addition of methanol (500 µL). The reaction mixture was left at room temperature (21 °C) for 30 min and its completion was checked by TLC (EtOAc/PE 3:7). The organic solvent mixture was removed at 75 °C. Stock solutions of DSPC (2.00 mM in $CHCl_3$, 900 µL) and **Mal-C_{16}** (1.00 mM in $CHCl_3$, 100 µL) were added to the remaining residue to yield a molar ratio of DSPC / **Pyr-C_{18}** / **Mal-C_{16}** = 90:5:5. The organic solvent was evaporated under a gentle stream of nitrogen and the remaining film of amphiphiles was dried in high vacuum. Aqueous HEPES buffer solution (25 mM, pH 7.4, 1.00 mL) was added to obtain a total amphiphile concentration of 2.00 mM. The sample was sonicated for 5 min at room temperature resulting

in a slightly turbid multilamellar vesicle suspension. A dispersion of unilamellar vesicles was obtained by extrusion through 100 nm pore size polycarbonate membranes with a LiposoFast liposome extruder from Avestin at 60 °C.

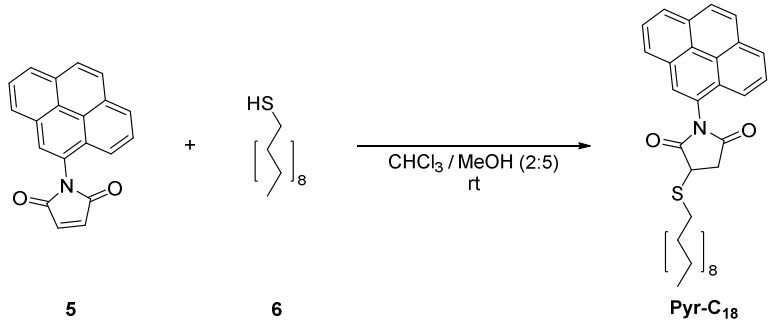

5 **6** **Pyr-C_{18}**

Scheme S5.2: *In situ* formation of **Pyr-C_{18}** by nucleophilic addition of thiol **6** to pyrene derivative **5**.

Vesicles **V-Rho**

In a small glass vessel, stock solutions of DSPC (2.00 mM in $CHCl_3$, 940 µL), **Rho-C_{18}** (1.00 mM in $CHCl_3$, 20 µL) and **Mal-C_{16}** (1.00 mM in $CHCl_3$, 100 µL) were mixed to yield a molar ratio of DSPC / **Rho-C_{18}** / **Mal-C_{16}** = 94:1:5. The organic solvent was evaporated under a gentle stream of nitrogen and the remaining film of amphiphiles was dried in high vacuum. Aqueous HEPES buffer solution (25 mM, pH 7.4, 1.00 mL) was added to obtain a total amphiphile concentration of 2.00 mM. The sample was sonicated for 5 min at room temperature (21 °C) resulting in a slightly turbid multilamellar vesicle suspension. A dispersion of unilamellar vesicles was obtained by extrusion through 100 nm pore size polycarbonate membranes with a LiposoFast liposome extruder from Avestin at 60 °C.

V.4.3.2 Aptamer-Functionalization of Vesicle Surfaces

A stock solution of thiolated aptamers **Apt-Thr** or **Apt-Ctrl** (0.10 mM, 4.0–5.0 µL) was mixed with an aqueous solution of the disulfide reducing agent tris(2-carboxyethyl)phosphine hydrochloride (1.00 mM, 2.5 µL) and left at room temperature (21 °C) for 90–120 min. This mixture was then added to 10 µL of the freshly prepared vesicle solution, diluted 20–100-fold with HEPES buffer, in a fluorescence cuvette. The reaction mixture was left at room temperature and agitated from time to time. In order to monitor the functionalization process,

fluorescence spectra of the vesicle solution were measured after certain time intervals. The surface functionalization reaction was completed after 2–4 h.

V.4.3.3 Dynamic Light Scattering of Vesicles

Vesicle size distributions were determined by dynamic light scattering. Figure S5.1 shows the typical size distribution of freshly extruded vesicles. After aptamer-functionalization of the surface and titration of thrombin, no apparent cross linking of the vesicles was observed (Figure S5.2).

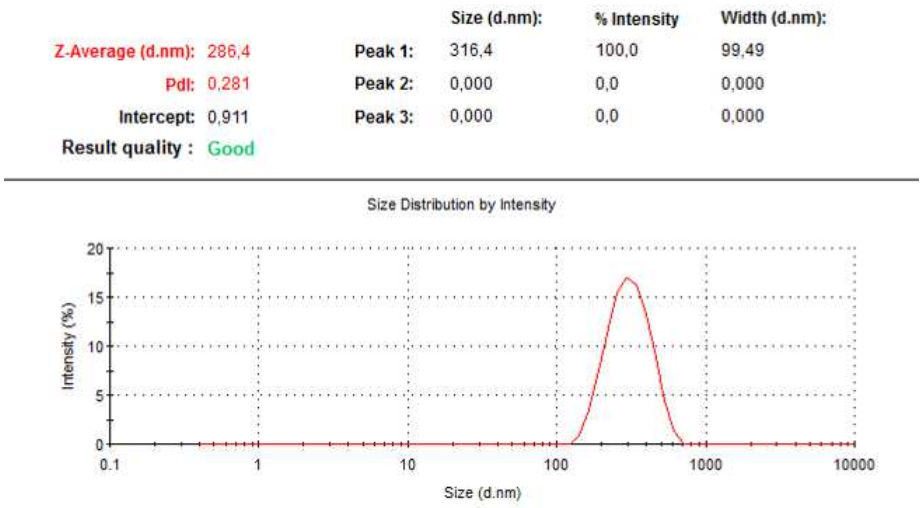

Figure S5.1: Typical size distribution of freshly prepared vesicles **V-Rho**.

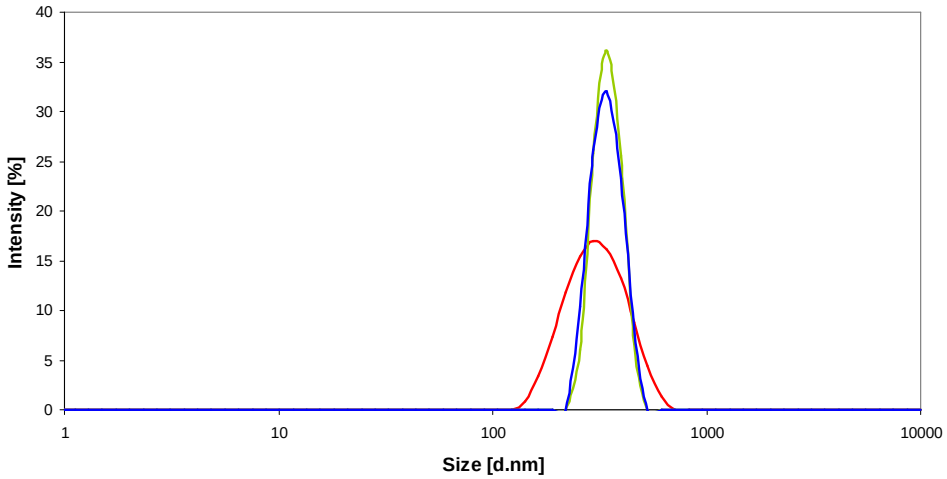

Figure S5.2: Comparison of vesicle size distribution before aptamer-functionalization (red curve), after functionalization (blue curve) and after addition of thrombin to functionalized liposomes **V-Rho-Thr** (green curve).

V.4.4 Determination of Binding Constants

A freshly prepared solution of aptamer-functionalized vesicles was diluted with HEPES buffer up to 2.5 times and filled into a fluorescence cuvette. Aliquots of the analyte solution were added and the fluorescence spectrum was measured after each addition. All fluorescence spectra were corrected for dilution. For titration of thrombin, the vesicle solution contained a 10 mM concentration of KCl. Binding constants were obtained by non-linear curve fitting (ΔI_{max} versus total concentration of added analyte) using the mathematical algorithm for 1:1 binding.[21]

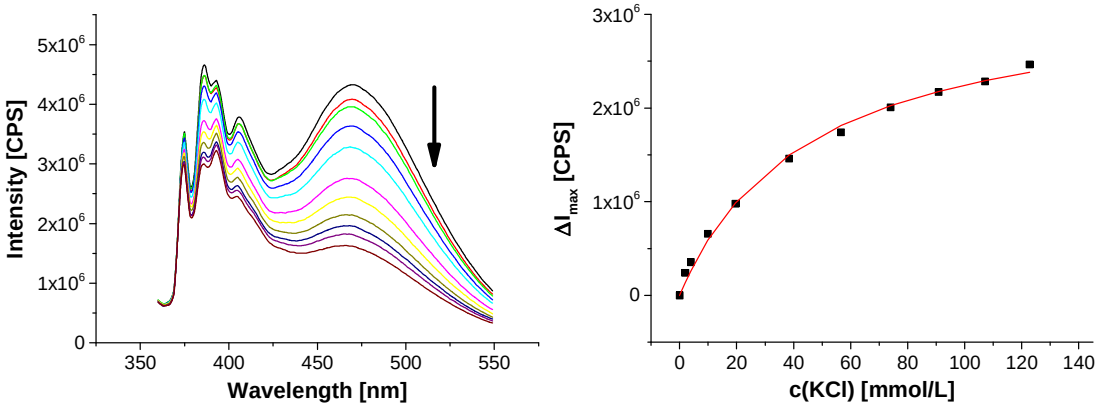

Figure S5.3: Fluorescence emission change of **V-Pyr-Thr** upon addition of KCl and non-linear curve fitting; c(**Apt-Thr**) = 2.00 µM, λ_{ex} = 345 nm, λ_{em} = 470 nm.

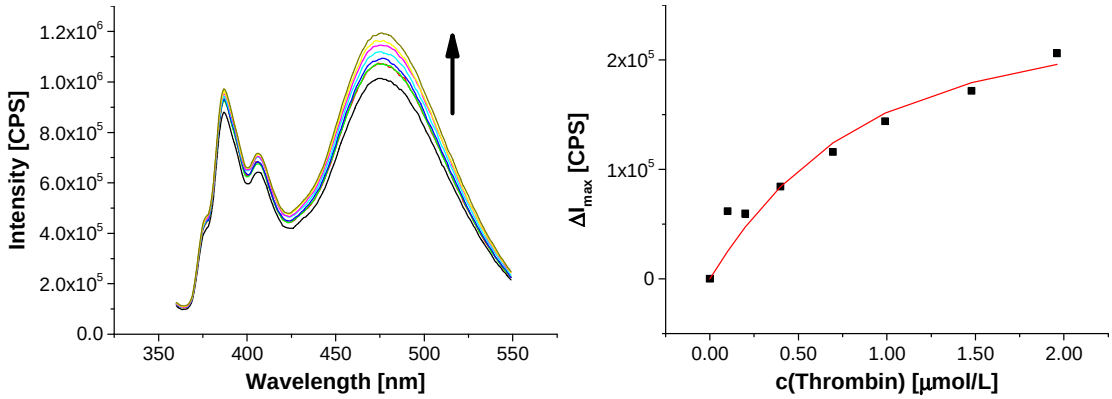

Figure S5.4: Fluorescence emission change of **V-Pyr-Thr** upon addition of bovine thrombin and non-linear curve fitting; c(**Apt-Thr**) = 0.50 µM, λ_{ex} = 345 nm, λ_{em} = 470 nm.

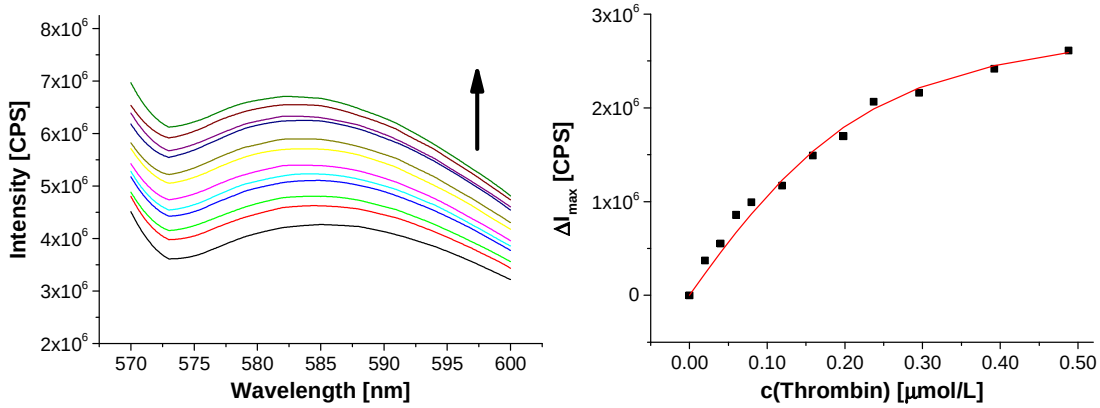

Figure S5.5: Fluorescence emission change of **V-Rho-Thr** upon addition of bovine thrombin and non-linear curve fitting; c(**Apt-Thr**) = 0.20 µM, λ_{ex} = 557 nm, λ_{em} = 585 nm.

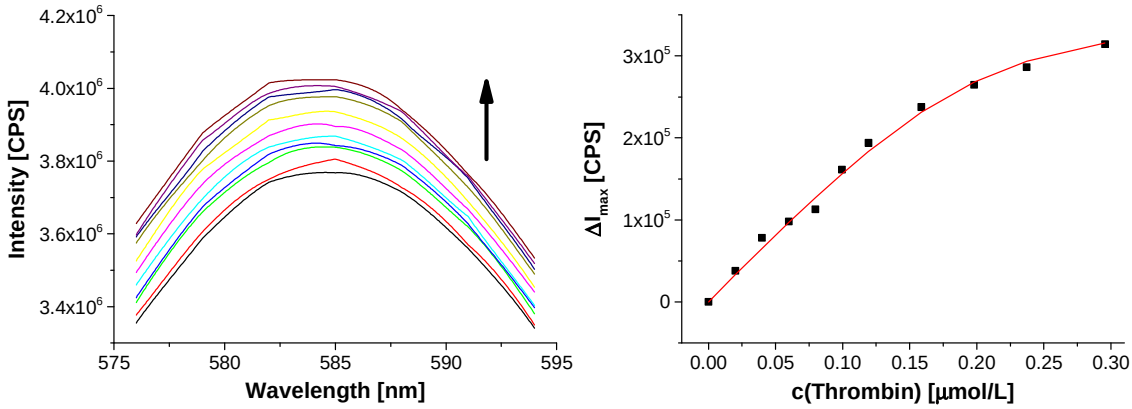

Figure S5.6: Fluorescence emission change of **V-Rho-Thr** upon addition of human thrombin and non-linear curve fitting; c(**Apt-Thr**) = 0.20 µM, λ_{ex} = 557 nm, λ_{em} = 585 nm.

V.5 Notes and Reference

[1] a) C. Tuerk, L. Gold, "Systematic Evolution of Ligands by Exponential Enrichment: RNA Ligands to Bacteriophage T4 DNA Polymerase", *Science* **1990**, *249*, 505–510; b) A. D. Ellington, J. W. Szostack, "*In vitro* selection of RNA molecules that bind specific ligands", *Nature* **1990**, *346*, 818–822.

[2] a) M. McKeague, M. C. DeRosa, "Challenges and Opportunities for Small Molecule Aptamer Development", *J. Nucleic Acids* **2012**, *2012*, 748913; b) A. D. Keefe, S. Pai, A. Ellington, "Aptamers as therapeutics", *Nat. Rev. Drug Discov.* **2010**, *9*, 537–550; c) E. Torres-Chavolla, E. C. Alocilja, "Aptasensors for detection of microbial and viral pathogens", *Biosens. Bioelectron.* **2009**, *24*, 3175–3182.

[3] a) B. Strehlitz, C. Reinemann, S. Linkorn, R. Stoltenburg, "Aptamers for pharmaceuticals and their application in environmental analytics", *Bioanal. Rev.* **2012**, *4*, 1–30; b) S. Amaya-González, N. de-los-Santos-Álvarez, A. J. Miranda-Ordieres, M. J. Lobo-Castañón, "Aptamer-Based Analysis: A Promising Alternative for Food Safety Control", *Sensors* **2013**, *13*, 16292–16311.

[4] For reviews, see: a) J. Liu, Z. Cao, Y. Lu, "Functional Nucleic Acid Sensors", *Chem. Rev.* **2009**, *109*, 1948–1998; b) B. Deng, Y. Lin, C. Wang, F. Li, Z. Wang, H. Zhang, X.-F. Li, X. C. Le, "Aptamer binding assays for proteins: The thrombin example – A review", *Anal. Chim. Acta* **2014**, *837*, 1–15.

[5] a) R. E. Wang, Y. Zhang, J. Cai, W. Cai, T. Gao, "Aptamer-Based Fluorescent Biosensors", *Curr. Med. Chem.* **2011**, *18*, 4175–4184; b) I. Willner, M. Zayats, "Electronic Aptamer-Based Sensors", *Angew. Chem. Int. Ed.* **2007**, *46*, 6408–6418; *Angew. Chem.* **2007**, *119*, 6528–6538.

[6] a) B. Li, H. Wei, S. Dong, "Sensitive detection of protein by an aptamer-based label-free fluorescing molecular switch", *Chem. Commun.* **2007**, 73–75; b) Z. Xu, K. Morita, Y. Sato, Q. Dai, S. Nishizawa, N. Teramae, "Label-free aptamer-based sensor using abasic site-containing DNA and a nucleobase-specific fluorescent ligand", *Chem. Commun.* **2009**, 6445–6447; c) M. Zayats, Y. Huang, R. Gill, C.-a. Ma, I. Willner, "Label-Free and Reagentless Aptamer-Based Sensors for Small Molecules", *J. Am. Chem. Soc.* **2006**, *128*, 13666–13667.

[7] a) L. Hu, Z. Bian, H. Li, S. Han, Y. Yuan, L. Gao, G. Xu, "$[Ru(bpy)_2dppz]^{2+}$ Electrochemiluminescence Switch and Its Applications for DNA Interaction Study and Label-free ATP Aptasensor", *Anal. Chem.* **2009**, *81*, 9807–9811; b) Z. Zhu, C. Yang, X. Zhou, J. Qin, "Label-free aptamer-based sensors for L-argininamide by using nucleic acid minor groove binding dyes", *Chem. Commun.* **2011**, *47*, 3192–3194.

[8] a) B. Gruber, S. Stadlbauer, A. Späth, S. Weiss, M. Kalinina, B. König, "Modular Chemosensors from Self-Assembled Vesicle Membranes with Amphiphilic Binding Sites and Reporter Dyes", *Angew. Chem. Int. Ed.* **2010**, *49*, 7125–7128; *Angew. Chem.* **2010**, *122*, 7280–7284; b) S. Banerjee, M. Bhuyan, B. König, "Tb(III) functionalized vesicles for phosphate sensing: membrane fluidity controls the sensitivity", *Chem. Commun.* **2013**, *49*, 5681–5683.

[9] For examples on how the modular construction principle can be utilized for the preparation of highly selective chemosensors, see: a) B. Gruber, S. Balk, S. Stadlbauer, B. König, "Dynamic Interface Imprinting: High-Affinity Peptide Binding Sites Assembled by Analyte-Induced Recruiting of

Membrane Receptors", *Angew. Chem. Int. Ed.* **2012**, *51*, 10060–10063; *Angew. Chem.* **2012**, *124*, 10207–10210; b) S. Banerjee, B. König, "Molecular Imprinting of Luminescent Vesicles", *J. Am. Chem. Soc.* **2013**, *135*, 2967–2970.

[10] L. C. Bock, L. C. Griffin, J. A. Latham, E. H. Vermaas, J. J. Toole, "Selection of single-stranded DNA molecules that bind and inhibit human thrombin", *Nature* **1992**, *355*, 564–566.

[11] a) K. A. Edwards, A. J. Baeumner, "Optimization of DNA-tagged liposomes for use in microtiter plate analyses", *Anal. Bioanal. Chem.* **2006**, *386*, 1613–1623; b) K. A. Edwards, Y. Wang, A. J. Baeumner, "Aptamer sandwich assays: human α-thrombin detection using liposome enhancement", *Anal. Bioanal. Chem.* **2010**, *398*, 2645–2654.

[12] a) P. A. Beales, T. K. Vanderlick, "Specific Binding of Different Vesicle Populations by the Hybridization of Membrane-Anchored DNA", *J. Phys. Chem. A* **2007**, *111*, 12372–12380; b) Y.-H. M. Chan, B. van Lengerich, S. G. Boxer, "Effects of linker sequences on vesicle fusion mediated by lipid-anchored DNA oligonucleotides", *Proc. Natl. Acad. Sci. U. S. A.* **2009**, *106*, 979–984.

[13] a) Z. Cao, R. Tong, A. Mishra. W. Xu, G. C. L. Wong, J. Cheng, Y. Lu, "Reversible Cell-Specific Drug Delivery with Aptamer-Functionalized Liposomes", *Angew. Chem. Int. Ed.* **2009**, *48*, 6494–6498; *Angew. Chem.* **2009**, *121*, 6616–6620; b) H. Kang. M. B. O'Donoghue, H. Liu, W. Tan, "A liposome-based nanostructure for aptamer directed delivery", *Chem. Commun.* **2010**, *46*, 249–251.

[14] a) C. Wang, Z. Ma, "Colorimetric detection of oligonucleotides using a polydiacetylene vesicle sensor", *Anal. Bioanal. Chem.* **2005**, *382*, 1708–1710; b) J. Lee, H.-J. Kim, J. Kim, "Polydiacetylene Liposome Arrays for Selective Potassium Detection", *J. Am. Chem. Soc.* **2008**, *130*, 5010–5011; c) J. Lee, H. Jun, J. Kim, "Polydiacetylene–Liposome Microarrays for Selective and Sensitive Mercury(II) Detection", *Adv. Mater* **2009**, *21*, 3674–3677; d) Y. K. Jung, T. W. Kim, H. G. Park, H. T. Soh, "Specific Colorimetric Detection of Proteins Using Bidentate Aptamer-Conjugated Polydiacetylene (PDA) Liposomes", *Adv. Funct. Mater.* **2010**, *20*, 3092–3097; e) W. Wu, J. Zhang, M. Zheng, Y. Zhong, J. Yang, Y. Zhao, W. Wu, W. Ye, J. Wen, Q. Wang, J. Lu, "An Aptamer-Based Biosensor for Colorimetric Detection of *Escherichia coli* O157:H7", *PLOS ONE* **2012**, *7*, e48999.

[15] P. M. Keller, S. Person, W. Snipes, "A fluorescence enhancement assay of cell fusion", *J. Cell. Sci.* **1977**, *28*, 167–177.

[16] M. Manoharan, K. L. Tivel, M. Zhao, K. Nafisi, T. L. Netzel, "Base-Sequence Dependence of Emission Lifetimes for DNA Oligomers and Duplexes Covalently Labeled with Pyrene: Relative Electron-Transfer Quenching Efficiencies of A, G, C, and T Nucleosides toward Pyrene*", *J. Phys. Chem.* **1995**, *99*, 17461–17472.

[17] S. A. E. Marras, F. R. Kramer, S. Tyagi, "Efficiencies of fluorescence resonance energy transfer and contact-mediated quenching in oligonucleotide probes", *Nucleic Acids Res.* **2002**, *30*, e122.

[18] a) R. F. Macaya, P. Schultze, F. W. Smith, J. A. Roe, J. Feigon, "Thrombin-binding DNA aptamer forms a unimolecular quadruplex structure in solution", *Proc. Natl. Acad. Sci. U. S. A.* **1993**, *90*, 3745–3749; b) K. Y. Wang, S. McCurdy, R. G. Shea, S. Swaminathan, P. H. Bolton, "A DNA Aptamer Which Binds to and Inhibits Thrombin Exhibits a New Structural Motif for DNA", *Biochemistry* **1993**, *32*, 1899–1904;

c) K. Padmanabhan, K. P. Padmanabhan, J. D. Ferrara, J. E. Sadler, A. Tulinsky, "The Structure of α-Thrombin Inhibited by a 15-Mer Single-stranded DNA Aptamer", *J. Biol. Chem.* **1993**, *268*, 17651–17654.

[19] S. Nagatoishi, T. Nojima, B. Juskowiak, S. Takenaka, "A Pyrene-Labeled G-Quadruplex Oligonucleotide as a Fluorescent Probe for Potassium Ion Detection in Biological Applications", *Angew. Chem. Int. Ed.* **2005**, *44*, 5067–5070; *Angew. Chem.* **2005**, *117*, 5195–5198.

[20] a) G. Cevc, "Membrane electrostatics", *Biochim. Biophys. Acta, Rev. Biomembr.* **1990**, *1031*, 311–382; b) Y. Zhang, P. S. Cremer, "Interactions between macromolecules and ions: the Hofmeister series", *Curr. Opin. Chem. Biol.* **2006**, *10*, 658–663.

[21] A. E. Hargrove, Z. Zhong, J. L. Sessler, E. V. Anslyn, "Algorithms for the determination of binding constants and enantiomeric excess in complex host : guest equilibria using optical measurements", *New J. Chem.* **2010**, *34*, 348–354.

[22] M. Lee, D. R. Walt, "A Fiber-Optic Microarray Biosensor Using Aptamers as Receptors", *Anal. Biochem.* **2000**, *282*, 142–146.

[23] M. C. R. Buff, F. Schäfer, B. Wulffen, J. Müller, B. Pötzsch, A. Heckel, G. Mayer, "Dependence of aptamer activity on opposed terminal extensions: improvement of light-regulation efficiency", *Nucleic Acids Res.* **2010**, *38*, 2111–2118.

[24] P. Baaske. C. J. Wienken, P. Reineck, S. Duhr, D. Braun, "Optical Thermophoresis for Quantifying the Buffer Dependence of Aptamer Binding", *Angew. Chem. Int. Ed.* **2010**, *49*, 2238–2241; *Angew. Chem.* **2010**, *122*, 2286–2290.

[25] P. G. Righetti, G. Tudor, K. Ek, "Isoelectric points and molecular weights of proteins: A new table", *J. Chromatogr. A* **1981**, *220*, 115–194.

[26] W. Bode, D. Turk, A. Karshikov, "The refined 1.9-Å X-ray crystal structure of D-Phe-Pro-Arg chloromethylketone-inhibited human α-thrombin: Structure analysis, overall structure, electrostatic properties, detailed active-site geometry, and structure–function relationships", *Protein Sci.* **1992**, *1*, 426–471.

[27] P. L. Privalov, A. I. Dragan, C. Crane-Robinson, "Interpreting protein/DNA interactions: distinguishing specific from non-specific and electrostatic from non-electrostatic components", *Nucleic Acids Res.* **2011**, *39*, 2483–2491.

[28] U. J. Lewis, D. E. Williams, N. G. Brink, "Pancreatic elastase: purification, properties, and function", *J. Biol. Chem.* **1956**, *222*, 705–720.

[29] a) N. Weiner, "Mono-Acyl Ethylene Diamines", US Patent 2,387,201, Oct. 16, 1945; b) CN Patent 103739510 A, Apr. 23, 2014.

SUMMARY

Within the scope of this thesis, a method for the quick and versatile functionalization of preformed liposomes was developed. Further investigations demonstrated the applicability of the obtained vesicular sensors in analytics.

Chapter I briefly introduces the concept of functionalized vesicles and its use for analytical applications. In this context, some established assay formats for the quantification of receptor–target binding at vesicular membranes are highlighted.

Chapter II deals with hydrogen bonding at phospholipid membranes. Those interactions were initially intended to be utilized for the non-covalent attachment of receptors at vesicles surfaces. Studies on basis of melamine–barbiturate pairs demonstrated that the supposed unique physico-chemical properties at the lipid–water interface are not sufficient to result in stable monovalent complexes. However, cooperative hydrogen bonding at vesicular membranes could be achieved by exploiting concentration-dependent phase separation processes in gel phase phospholipid bilayers. The resulting densely packed clusters of membrane-embedded amphiphilic melamines allowed multisite binding to complementary hexavalent thymidine oligonucleotides.

Due to the observed inefficiency of hydrogen bonding at liposomal surfaces, the focus of research was shifted towards a covalent modification of phospholipid membranes by employing thiol-based click reactions. **Chapters III** and **IV** illustrate the development of that technique. Initial studies in view of utilizing a radical thiol–ene coupling are summarized in **Chapter IV**. This UV light-induced reaction would provide a possibility to temporally control the functionalization process. It was found that radical thiol–ene additions are not efficient in the micromolar concentration range in aqueous solution and thus, their applicability for the post-functionalization of vesicle surfaces is very limited. The nucleophilic version employing a thiol–maleimide system, however, turned out to fulfill the requirements for the intended strategy. Based on this, surface-reactive luminescent vesicles were prepared by self-assembly of phospholipids, amphiphilic maleimides and fluorophores in aqueous solution (**Chapter III**). Those preformed liposomes were functionalized with

various thiolated receptor units such as a bis-Zn^{2+}-cyclen derivative for the detection of phosphate moieties or a DNA aptamer for specific interactions with the antibiotic ampicillin. The obtained receptor-modified vesicles indicated the binding of the targets to their surface by changes of the fluorescence emission properties of the membrane co-embedded carboxyfluorescein dyes. The post-functionalization concept could also be used for molecular imprinting of vesicle surfaces. The template-guided patterning of receptors based on bis-Zn^{2+}-cyclen resulted in fluorescent sensors suitable for the specific recognition of a bivalent peptide.

In **Chapter V**, the versatile applicability of the post-functionalization strategy of vesicles is demonstrated by extension to a thrombin-binding aptamer as further recognition element. The resulting aptasensors signaled the high-affinity binding of the analyte to the liposome surface again by dynamic changes of the emission properties of membrane-embedded fluorescent reporter dyes. Here, the sensing of thrombin was achieved within its physiological concentration range.

In conclusion, the presented functionalization method of preformed liposomes allows an easy, fast and inexpensive access to various supramolecular sensors. Due to the highly modular approach, a simple variation of the receptor–fluorophore combinations can be accomplished. An extension of that technique to recognition elements such as peptides, other oligonucleotides or complex macromolecules may be envisaged, which could facilitate the development of novel customized devices for bioanalytical applications.

ZUSAMMENFASSUNG

Im Rahmen der vorliegenden Doktorarbeit wurde eine Methode zur schnellen und vielseitigen Funktionalisierung von „Liposomenrohlingen“ entwickelt. Weitere Untersuchungen veranschaulichten die Eignung der so erzeugten Sensorvesikel in der Analytik.

Kapitel I liefert eine kurze Einführung in das Konzept der funktionalisierten Vesikel und erläutert dessen Einsatzmöglichkeit im Rahmen von analytischen Anwendungen. In diesem Zusammenhang werden einige etablierte Assayformate beleuchtet, mit welchen sich Rezeptor–Analyt-Bindungen an Vesikelmembranen quantifizieren lassen.

Kapitel II beschäftigt sich mit Wasserstoffbrückenbindungen an Phospholipidmembranen. Diese Art der Wechselwirkung sollte ursprünglich genutzt werden, um Rezeptoren nichtkovalent an Vesikeloberflächen anzubringen. Untersuchungen anhand von Melamin–Barbiturat-Paaren zeigten, dass die vermuteten außergewöhnlichen physikalisch-chemischen Eigenschaften an der Lipid–Wasser-Grenzfläche nicht ausreichen, um stabile monovalente Komplexe zu ermöglichen. Kooperative Wasserstoffbrückenwechselwirkungen an Vesikelmembranen konnten jedoch unter Ausnutzung von konzentrationsabhängigen Phasentrennungsprozessen in gelartigen Phospholipid-Doppelschichten induziert werden. Die resultierenden dicht gepackten Aggregate der in die Membran eingelagerten amphiphilen Melamine ermöglichten die Interaktion mit komplementären hexavalenten Thymidin-Oligonukleotiden über mehrere Bindungsstellen.

Aufgrund der beobachteten zu geringen Stärke von Wasserstoffbrückenbindungen an der Oberfläche von Liposomen wurde der Forschungsschwerpunkt in Richtung einer kovalenten Modifizierung von Phospholipidmembranen mittels Thiol-basierten Klick-Reaktionen verschoben. **Kapitel III** und **IV** zeichnen die Entwicklung dieser Methode nach. Anfängliche Untersuchungen hinsichtlich der Eignung einer radikalischen Thiol–En-Kupplung werden in **Kapitel IV** zusammengefasst. Diese durch UV-Licht induzierte Reaktion würde die Möglichkeit eröffnen, den Funktionalisierungsprozess zeitlich zu steuern. Es wurde festgestellt, dass radikalische Thiol–En-Additionen im mikromolaren

Konzentrationsbereich in wässriger Lösung nicht effizient ablaufen und daher ihre Anwendbarkeit für die nachträgliche Funktionalisierung von Vesikeloberflächen stark eingeschränkt ist. Die nukleophile Variante auf der Basis eines Thiol–Maleinimid-Systems erwies sich im Hinblick auf die geplante Strategie allerdings als geeignet. Darauf aufbauend wurden Oberflächen-reaktive lumineszente Vesikel durch Selbstanordnung von Phospholipiden, amphiphilen Maleinimiden und Fluoreszenzfarbstoffen in wässriger Lösung hergestellt (**Kapitel III**). Diese vorgeformten Liposomen wurden mit einer Reihe von Thiol-haltigen Rezeptoreinheiten funktionalisiert, wie zum Beispiel einem Bis-Zn^{2+}-Cyclen Komplex zur Detektion von Phosphaten oder einem DNA-Aptamer, welches das Antibiotikum Ampicillin spezifisch bindet. Die erhaltenen Rezeptor-modifizierten Vesikel zeigten die Bindung der Zielmoleküle an ihre Oberfläche durch eine Änderung der Fluoreszenzeigenschaften von in die Membran eingebetteten Carboxyfluorescein-Farbstoffen an. Das Konzept der nachträglichen Funktionalisierung konnte auch für das molekulare Prägen von Vesikeloberflächen genutzt werden. Die Templat-gesteuerte Strukturierung von Bis-Zn^{2+}-Cyclen-Rezeptoren erzeugte fluoreszente Sensoren, die ein bivalentes Peptid spezifisch detektieren konnten.

In **Kapitel V** wird die vielseitige Verwendungsmöglichkeit der Post-Funktionalisierungsstrategie durch deren Erweiterung auf ein Thrombin-bindendes Aptamer als Rezeptoreinheit veranschaulicht. Die hergestellten Aptasensoren signalisierten die starke Bindung des Zielmoleküls an die Liposomenoberfläche wiederum durch dynamische Veränderungen der Emissionseigenschaften von fluoreszenten Reporterfarbstoffen, die in die Membran eingelagert wurden. Die Detektion von Thrombin wurde hierbei innerhalb seines physiologischen Konzentrationsbereichs erzielt.

Alles in allem ermöglicht die vorgestellte Methode der nachträglichen Funktionalisierung von Liposomen einen einfachen, schnellen und günstigen Zugang zu verschiedenartigen supramolekularen Sensoren. Wegen des höchst modularen Konstruktionsprinzips kann eine Variation der Rezeptor–Fluorophor-Kombinationen leicht bewerkstelligt werden. Eine Erweiterung dieser Strategie auf Rezeptorelemente basierend auf Peptiden, anderen Oligonukleotiden oder komplexen Makromolekülen ist vorstellbar, wodurch die Entwicklung neuer maßgeschneiderter Sensoren für bioanalytische Anwendungen ermöglicht werden könnte.

ABBREVIATIONS

A	hydrogen bond acceptor
Abs	absorbance
Ac	acetyl
Ac_2O	acetic anhydride
AcOH	acetic acid
AFM	atomic force microscopy
Boc	*tert*-butyloxycarbonyl
BP	benzophenone
c	concentration
CMS	coumarin methyl sulfonate
Cyclen	1,4,7,10-tetraazacyclododecane
Cys	cysteine
D	hydrogen bond donor
DEPT	distortionless enhancement by polarization transfer
DLS	dynamic light scattering
DMF	dimethylformamide
DMPA	2,2-dimethoxy-2-phenylacetophenone
DMSO	dimethyl sulfoxide
DNA	deoxyribonucleic acid
DOPC	1,2-dioleoyl-*sn*-glycero-3-phosphocholine
DPPC	1,2-dipalmitoyl-*sn*-glycero-3-phosphocholine
DSPC	1,2-distearoyl-*sn*-glycero-3-phosphocholine
DTNB	5,5’-dithiobis(2-nitrobenzoic acid)
eq	equivalents
ESI	electrospray ionization
Et_2O	diethyl ether
ETG	ethyl thioglycolate
EtOAc	ethyl acetate
EtOH	ethanol

Fmoc	fluorenylmethyloxycarbonyl
FRET	Förster resonance energy transfer
FT-IR	Fourier transform infrared spectroscopy
HEPES	4-(2-Hydroxyethyl)piperazine-1-ethanesulfonic acid
HRMS	high-resolution mass spectrometry
IDA	indicator-displacement assay
I_{max}	maximum intensity
K_a	complex association constant
k_{obs}	apparent rate constant
LAP	lithium phenyl-2,4,6-trimethylbenzoylphosphinate (abbreviated for lithium acylphosphinate)
lg	common logarithm
M	mol/L
MeCN	acetonitrile
MeOH	methanol
mol-%	percentage by mole
MP	melting point
MS	mass spectrometry
NMR	nuclear magnetic resonance
PCDA	10,12-pentacosadiyonic acid
PDI	polydispersity index
PE	petroleum ether
PET	photoinduced electron transfer
pk_a	acid dissociation constant
PP_i	pyrophosphate
QCM	quartz crystal microbalance
R_f	retention factor
RNA	ribonucleic acid
rpm	revolutions per minute
rt	room temperature
SATA	*N*-succinimidyl *S*-acetylthioglycolate
SEC	size-exclusion chromatography
SPR	surface plasmon resonance

TCEP	tris(2-carboxyethyl)phosphine hydrochloride
TFA	trifluoroacetic acid
THF	tetrahydrofuran
TLC	thin layer chromatography
TRIS	tris(hydroxymethyl)aminomethane
Trp	tryptophan
Trt	triphenylmethyl / trityl
UV	ultraviolet
Vis	visible
vol-%	percentage by volume
Z-Average	intensity-weighted harmonic mean of particle diameters